Journal of Environmental Chemical Engineering 11 (2023) 109356

Contents lists available at ScienceDirect

Journal of Environmental Chemical Engineering

journal homepage: www.elsevier.com/locate/jece

Critical parameters and essential strategies in designing photoanodes to overcome the sluggish water oxidation reaction

Hairus Abdullah [a,b,*], Hardy Shuwanto [b], Jenni Lie [c], Mika Sillanpää [d,e,f,g]

[a] Department of Materials Science and Engineering, National Taiwan University of Science and Technology, No. 43, Section 4, Keelung road, Taipei 10607, Taiwan
[b] Department of Industrial Engineering, Universitas Prima Indonesia, Medan, North Sumatera, Indonesia
[c] Department of Chemical Engineering, Widya Mandala Surabaya Catholic University, Kalijudan 37, Surabaya 60114, Indonesia
[d] Department of Chemical Engineering, School of Mining, Metallurgy and Chemical Engineering, University of Johannesburg, P. O. Box 17011, Doornfontein 2028, South Africa
[e] International Research Centre of Nanotechnology for Himalayan Sustainability (IRCNHS), Shoolini University, Solan 173212, Himachal Pradesh, India
[f] Zhejiang Rongsheng Environmental Protection Paper Co. LTD, NO. 588 East Zhennan Road, Pinghu Economic Development Zone, Zhejiang 314213, PR China
[g] Department of Civil Engineering, University Centre for Research & Development, Chandigarh University, Gharuan, Mohali, Punjab, India

ARTICLE INFO

Keywords:
Photoanode
Nanostructuring
Heterojunction
Doping
Co-catalyst
And gradient doping

ABSTRACT

Photoelectrochemical (PEC) water splitting is a promising technology to generate green hydrogen energy from solar light. However, the water oxidation process limits the efficiency of overall water splitting. To overcome the limitation, it needs to understand some critical parameters in a PEC water-splitting process and precise strategies to select, design, prepare, and modify the materials for photoelectrode. A fundamental consideration in selecting materials for a PEC cell should include a thermodynamic requirement, appropriate band structure, high crystallinity and surface area, high stability, and low cost. The interested photoanode semiconductors with low cost and toxicity are discussed with various modification strategies, such as surface modification with nanostructuring, co-catalyst, and surface passivation. The strategies with heterojunction, Z-scheme charge transfer, and gradient doping with cations and anions are also presented to improve the charge transfer and lower its recombination rate. In addition, the recent application of ternary oxide-based photoanodes is briefly reviewed. Finally, the challenges and prospects for the future development of photoanodes are presented.

1. Introduction

Presently, global energy demands has been excruciatingly increasing, with nearly 83% of total energy still based on traditional fossil fuels, such as coal and petroleum [1]. It is predicted to be more than 30 – 50 TW by 2050 to accommodate the rapid economic growth because of global population inflation. However, the diminishing fossil-fuel reserves that were ample and easy to obtain are no longer support current production and living needs. [2] Simultaneously, the massive carbon-based fuel consumption considerably harms our environment. Therefore, it is urgent to seek sustainable clean energy to relieve the environmental pollution and status quo of the energy crisis. Harnessing solar light energy is preferable as the total energy of irradiated solar light on land per year (3.6×10^5 TW) far exceeds the predicted global energy (50 TW). One of the methods is converting solar-light energy into chemical energy with hydrogen as the energy carrier. Hydrogen energy is considered an excellent sustainable resource since its combustion product is only water. Therefore, solar-derived hydrogen energy can be utilized to simultaneously solve energy and environmental issues due to its high energy density, as shown in Fig. 1. However, most of the hydrogen production is currently done with non-renewable methods, such as natural gas and coal reformation, coke ovens, chlor-alkali process, and propane dehydrogenation [3]. All the hydrogen production methods with advantages and disadvantages are indicated in Table 1. A green hydrogen gas generation method should be conducted with a water-splitting process. There are several ways to generate hydrogen from water, such as photocatalysis, electrolysis, and photoelectrocatalysis. Among those methods, photoelectrochemical water splitting (PEC-WS) is promising to be scaled up. The reason is that mimicking the natural photosynthesis process in which the photoelectrode cells of PEC-WS play similar roles in a photoreaction in the leaf is sustainable, as shown in Fig. 2a. During the PEC-WS process, the PEC

* Corresponding author at: Department of Materials Science and Engineering, National Taiwan University of Science and Technology, No. 43, Section 4, Keelung road, Taipei 10607, Taiwan.
E-mail address: hairus@unprimdn.ac.id (H. Abdullah).

https://doi.org/10.1016/j.jece.2023.109356
Received 26 November 2022; Received in revised form 17 January 2023; Accepted 20 January 2023
Available online 21 January 2023

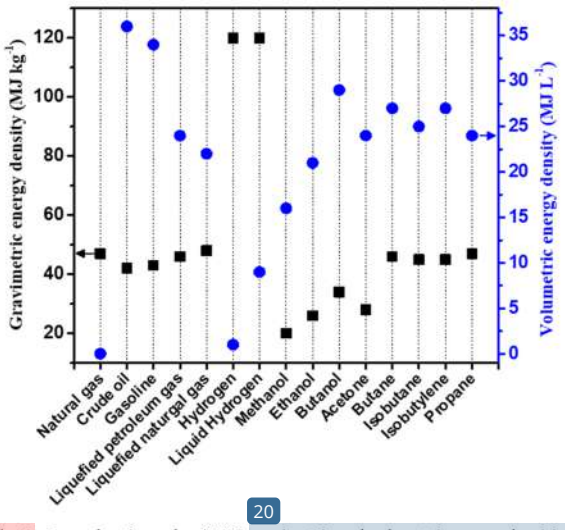

Fig. 1. Lower heating value (LHV) gravimetric and volumetric energy densities of standard fuels.
Reproduced from Ref. [1] with permission from the Royal Society of Chemistry.

cells should efficiently harness the solar light energy to generate hydrogen as the energy carrier. Many works in the PEC-WS field study the cathodic and anodic cells separately, which allows for better screening and rational development of catalysts. Some reported that the PEC hydrogen evolution coupled with organic degradation required an external bias with low photocurrent densities [4–8]. However, mimicking natural photosynthesis requires high performances of photoanode and photocathode with a free external bias during the photo reactions [9–14]. Therefore, it is crucial to understand the current strategies for improving the PEC-WS process.

As the water oxidation process requires four electrons in the reaction, the mechanism to evolve oxygen gas is more sluggish than the proton reduction reaction with only two electrons. Therefore, more work has been done to improve photoanodes than photocathodes in a water-splitting process, as indicated in Fig. 2b. Following the pioneering work of Fujishima and Honda in 1972 [16], numerous research efforts have been conducted to increase the solar-to-hydrogen (STH) conversion yield [17–19]. STH conversion efficiency depends on some critical factors in the PEC-WS processes, including light absorption, separation degree of photocarriers, and chemical stability [20–22]. Nanostructuring the photoanodes can enhance solar light harvesting, increase the contact area, and reduce the diffusion length of photocarriers, leading to higher STH conversion efficiency. Different nanostructures such as 3D inverse opals [23,24], 2D nanosheets [25,26], 1D nanorods [27,28], and nanowires [29] demonstrate high performances. However, a single semiconductor is challenging to satisfy all the critical factors in the PEC-WS process. For instance, low-bandgap α-Fe_2O_3 [30] and $BiVO_4$ [31] can be sensitizers for wide-bandgap semiconductors, such as ZnO, SnO_2, and WO_3 [32,33]. As a result, the heterojunction formation between them can increase the light absorbance, photocarrier separation, and STH conversion efficiency [34,35].

The present review highlights the promising PEC-WS process for overcoming energy and environmental issues and essential strategies in developing photoanodes. Common semiconductors with low cost and toxicity are discussed for various modification strategies, such as surface modification with nanostructuring, co-catalyst, and surface passivation. Furthermore, the cocatalysts with MOF, LDH, oxyhydroxide, CoOx, and CoPi, oxygen vacancy-based metal oxides, are also elucidated. In addition, the strategies with heterojunction, Z-scheme charge transfer, and gradient doping with cations and anions are also presented to improve

Table 1
Various methods of hydrogen production with their advantages and disadvantages [10,15].

Methods of hydrogen production	Advantages	Disadvantages	Efficiency	Cost [$/Kg]
Thermal reforming	Well-established technology and existing infrastructure	CO_2 as a byproduct due to the fossil fuels	60 – 75	1.48
Steam reforming	Well-developed technology with existing infrastructure	Generating CO and CO_2	74 – 85	2.27
Partial oxidation	Well-established technology	Producing heavy oils and petroleum coke	60 – 75	1.48
Photo fermentation	Abundant, cheap feedstock and neutral CO_2	The necessity of a considerable volume of reactor, O_2–sensitivity, fluctuating H_2 yields because of feedstock impurities, seasonal availability, and formation of tar	30 – 40	1.77–2.05
Biophotolysis	Consumed CO_2, produced O_2 as a byproduct, working under mild conditions	Low yields of H_2, sunlight needed, large reactor required, O_2 sensitivity, high cost of material	10 – 11	2.13
Dark fermentation	Simple method, H_2 produced without light	Fatty acids elimination, low yields of H_2, low efficiency	60 – 80	2.57
Gasification	Organic waste waters, CO_2 -neutral. Abundant, cheap feedstock and neutral CO_2	The necessity of a considerable volume of reactor, O_2–sensitivity, fluctuating H_2 yields because of feedstock impurities, seasonal availability, and formation of tar	30 – 40	1.77–2.05
Electrolysis	Established technology, zero-emission, existing infrastructure, O_2 as a byproduct	Storage and transportation problem	60 – 80	10.30
Photolysis	O_2 as a byproduct, abundant feedstock, no emissions	Low-efficiency photocatalytic material	8 – 10	0.06
Pyrolysis	Abundant, cheap feedstock and CO_2 -neutral	Tar formation, fluctuating H_2 amount because of feedstock impurities, and seasonal availability	35 – 50	1.59–1.70
Thermolysis	Clean and sustainable, O_2 byproduct, copious feedstock	High capital costs, elements toxicity, corrosion problems	20 – 45	7.98–8.40

the charge transfer and lower its recombination rate. Furthermore, the ternary oxide-based photoanodes as the alternative design of photoanode materials are briefly discussed. Recent works with different reaction conditions and promising electrolytes to optimize the oxidation capability of photoanode are also listed in tables to indicate the material development in photoanode. Finally, the challenges and prospects for the future development of photoanodes are presented.

2. Critical parameters of PEC-WS processes

2.1. General requirements in photoredox reactions

A PEC cell consists of a photoanode, photocathode, and electrolyte. The photoanode is connected to the photocathode for electron transfer with or without external bias, depending on the light absorbance, favorable charge carrier dynamics, and tunable band structure [36]. Common PEC cells have a configuration of an n-type semiconductor for photoanode and a p-type semiconductor for photocathode due to their band bending during light illumination, as shown in Fig. 3a [37,38]. An energetic photoanode and photocathode conduct water oxidation and reduction reactions, respectively. To allow the surface redox reaction, the photogenerated electron and hole should comply with the minimum thermodynamic energy required for oxidation and reduction reactions. Generally, the position of a conduction band (CB) of semiconductor must be more negative than that of the reduction potential of a particular species to proceed with the reduction reaction. Meanwhile, the position of a valence band (VB) of semiconductor must be more positive than that of the oxidation potential of a species to conduct the oxidation reaction. Ideally, the photocarriers will diffuse to electrode surfaces for chemical reaction; Otherwise, they would be lost through the charge recombination process. As a result, some semiconductors are incapable of evolving hydrogen due to the negative CB position. Fig. 3b indicates single semiconductors with different VB and CB positions relative to the standard water oxidation and reduction potentials. As the CB position is more positive than that of the water reduction potential, the single phases of SnO_2, WO_3, Fe_2O_3 and ternary oxides such as $CuWO_6$, $ZnFe_2O_4$, $BiFeO_3$, Fe_2WO_6 can not evolve hydrogen. However, those single-phase semiconductors are reliable for oxygen evolution catalysts due to the appropriate VB position relative more positive to the water oxidation potential. Therefore, many works provide efforts to overcome the drawbacks of those materials as photocells [12,39–41]. On the other hand, those materials with CB positions higher than hydrogen reduction potential, such as TiO_2, ZnO, $FeVO_4$, $CuFe_2O_4$, $MgFe_2O_4$ and CdS are suitable for photocathodes [42–44].

The specific WS reactions on photoanode and photocathode after photoexcitation are as follows:

Photocathode: $2H^+ + 2e^- \rightarrow H_2$ (acid)

$$2H_2O + 2e^- \rightarrow H_2 + 2OH^- \text{ (alkaline)} \quad (1)$$

Photoanode: $2H_2O + 4h^+ \rightarrow O_2 + 4H^+$ (acid)

$$4OH^- + 4h^+ \rightarrow O_2 + 2H_2O \text{ (alkaline)} \quad (2)$$

Overall reaction: $2H_2O \rightarrow 2H_2 + O_2$ (3)

2.2. Essential steps in a PEC-WS process

The basic process of PEC-WS could be divided into three main steps. The first step is induced by light illumination, in which electron and hole pairs are generated if the photon energy is larger than the bandgap of electrode materials. After the photoexcitation process, the second step is the photocarriers would be separated or recombined depending on many factors, such as carrier lifetime, conductivity, temperature, surface defects, etc. The third step is the surface redox reactions on electrodes [51,52]. Light absorption can be tuned by modifying the electrode morphology, thickness, and bandgap [53–55]. Photocarrier separation process after the photoexcitation is crucial and can be ruled by element doping [56,57], incorporating defects [58,59], and heterojunction formation [60–62]. As compared to the hydrogen evolution reaction (HER) on the photocathode, the oxygen evolution reaction (OER) on the photoanode is a sluggish reaction that utilizes a four-electron and four-proton transfer process. The slow reaction can be significantly alleviated by loading a cocatalyst [63–65]. During the PEC-WS process, separation and recombination between photogenerated electrons and holes are competitive. Appropriate amounts of doping and defects could change the conductivity of the electrode materials to promote charge transfer [66,67].

2.3. Basic consideration in selecting electrode materials

A fundamental consideration in selecting materials for water splitting should include several factors: potential requirement, appropriate band structure, high crystallinity and surface area, high stability, and low cost. Under a standard condition, the WS reaction would only occur if the potential difference between the electrodes exceeds 1.23 eV with $\Delta G^\circ = 237.1$ Kj/mol. It is why the combined bandgap of semiconductors should be larger than 1.23 eV. The energy loss is considered as overpotential at electrodes and ionic conductivity loss in electrolytes. The current density also increases with the increasing applied voltage, higher than 1.23 V. The excess voltages shown with linear sweep voltammetry (LSV) curves in Fig. 4a are higher than oxidation and reduction potentials called overpotentials (η_{HER} or η_{OER}). The overpotential

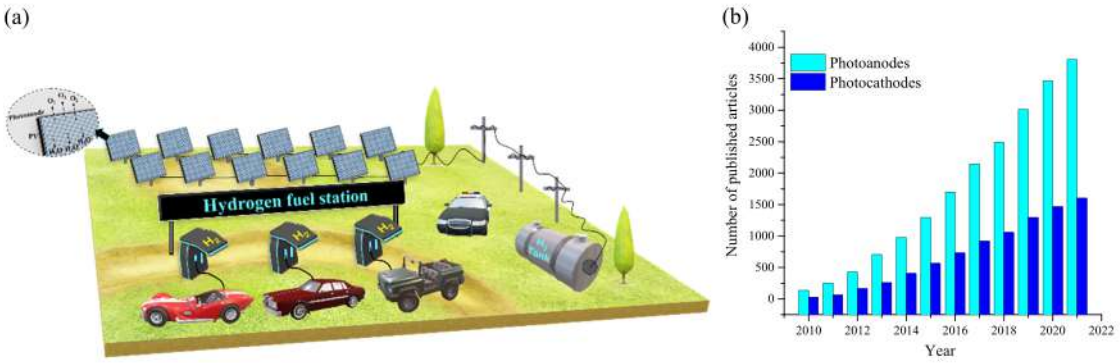

Fig. 2. (a) Application of PEC WS cells to support hydrogen fuel station and (b) numbers of published research articles indexed by Scopus with the search keywords of photoanodes or photocathodes water splitting.

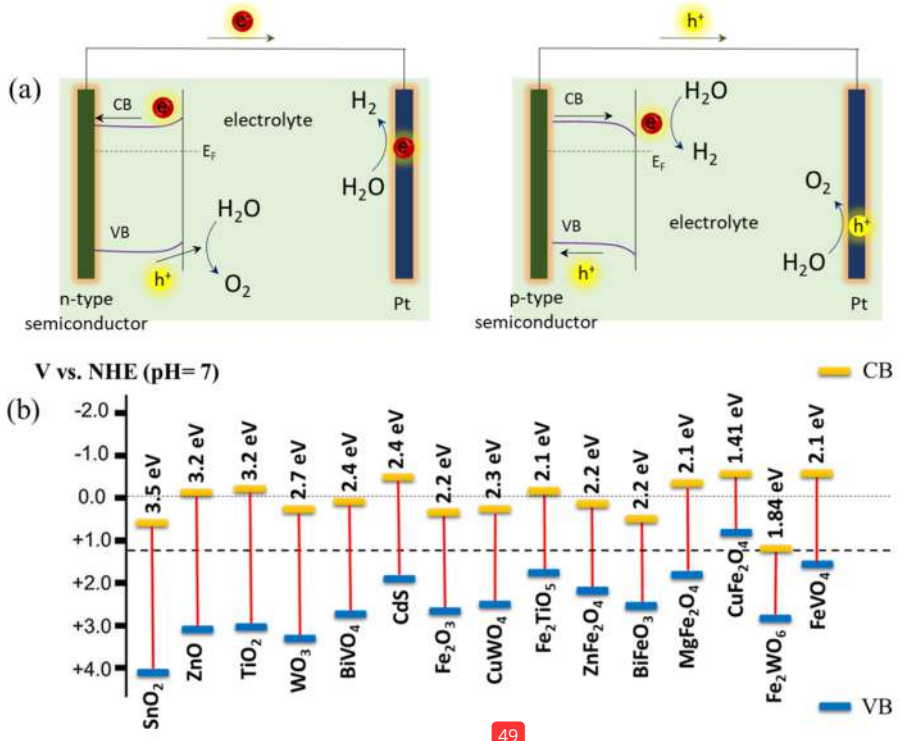

Fig. 3. (a) Schematic drawing of n- and p-type semiconductors for PEC half-cells under light illumination with Pt as a counter electrode, in which it is assumed that their CB and VB positions are more negative than that of water reduction potential and more positive than that of water oxidation potential, respectively. (b) CB and VB positions of common semiconductors used for PEC-WS process [45–50].

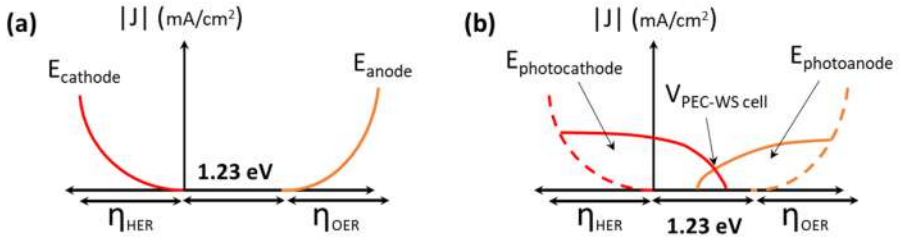

Fig. 4. Polarization LSV curves for (a) anode and cathode in electrocatalysis and (b) photoanode and photocathode in PEC-WS with simulated solar-light illumination.

values are crucial indicators to determine the performances of water-splitting cells. In this case of the water-splitting process, if the electrodes are photoactive materials, the overpotentials will be reversely shifted. The onset potential of a light-illuminated cathode will be more positive than 0 V_{RHE} and that of an anode will be less than 1.23 V_{RHE}. The early onset potential indicates that the light has been harnessed for a water-splitting process with lower electrical potential. Fig. 4b shows typical LSV curves of photoanode and photocathode, in which the onset potentials of photocathode and photoanodes are positively and negatively shifted, respectively. As a result, the photoanode and photocathode will generate the areas in Fig. 4b, indicating a similar fill factor (FF) in solar-cell work to determine the efficiency of a PEC cell. In addition, the intercept point between the photocathode and photoanode polarization curves is an operational voltage of the PEC cell during the water-splitting process.

2.4. Metrics as the indicators of PEC cell performances

The performances of PEC cells are determined with different metrics of electrochemical measurements. Most of the metric indicators related to photoanode as the rate-determining electrode are to assess water oxidation reaction. Generally, the cell efficiency is evaluated with incident photo-to-electron conversion efficiency (IPCE), solar-to-hydrogen conversion efficiency (STH), applied bias photon-to-current efficiency (ABPE), Faradaic efficiency, onset potentials, and the stability of photoelectrodes. A measurement of a PEC cell should be built with a three-electrode system consisting of work, reference, and counter electrodes in a particular electrolyte under a solar-light simulator to examine the electrochemical properties of photoelectrodes. IPCE and ABPE are the most crucial metrics for photoanode performances. IPCE is to measure the quantum efficiency of photoanode at different wavelengths. It is related not only to light absorption but also to charge separation,

transport, and transfer at photoanode/electrolyte. During the IPCE measurement, a certain monochromatic light with a particular wavelength is used to excite the electron from VB. Simultaneously, the external bias is applied to a cell to measure the passing photocurrent, which is facilitated with LSV measurement (*J–V* curves). However, the IPCE photocurrent is observed with external bias at 1.23 V_{RHE}. The IPCE can be simply calculated based on Eq. (1). Furthermore, to indicate how efficient the applied external bias on photoanode below 1.23 V in the presence of light illumination, ABPE is calculated based on Eq. (2). The calculation is done by assuming a 100% Faradaic efficiency on the photoanode. ABPE can be directly calculated from $J - V$ curves by substituting the photocurrent during the light illumination with corresponding external potential bias.

$$\mathrm{IPCE} = \frac{\left[\left(\frac{1240}{\lambda}\right) x \left(I_{light} - I_{dark}\right)\right]}{P} x\ 100\% \quad (1)$$

$$\mathrm{ABPE} = \frac{\left|I_{light}\right| x\ (1.23 - V)}{P} x\ 100\% \quad (2)$$

In which λ is the wavelength of light illumination, I_{light} is the photocurrent under illumination, I_{dark} is the photocurrent without light illumination, and P is the incident light power density (for example, a simulated solar light AM 1.5 G, 100 mW/cm^{-2}). The released gases (H_2 and O_2) from electrodes can be measured to determine the Faradaic efficiency to prove the water-splitting process has occurred on a PEC cell. The Faradaic efficiency in PEC cell is mainly to compare the experimental and theoretical gas evolution from photoanode and calculated with Eq. (3).

$$\mathrm{Faradaic}\mathit{efficiency} = \frac{Oxygen\ \ evolution\ \ amount}{\left[\frac{J_{photo} x A x T}{4e x N_A}\right]} x\ 100\% \quad (3)$$

In which oxygen evolution amount is obtained in a molar unit, J_{photo} is the photocurrent density in the light illuminated condition, A is the area of photoanode, T is the reaction time (s), e is the charge of an electron (1.6×10^{-19} C), and N_A is the Avogadro number. The critical event in the gas evolution experiment is the coverage of evolved gases on photoelectrodes. It should be removed immediately to minimize the ionic conductivity loss due to lower mass transport and eliminate the light blocking by bubbles. One of the appropriate ways is increasing the electrolyte concentration. However, the high electrolyte concentration will cause photo corrosion at extremely high or low pH. To briefly check the performances of photoanodes, it can be observed based on the following factors: [68].

1. If the photocurrent onset is cathodically shifted;
2. If a high photocurrent density plateau is obtained;
3. If the greater fill factor area is observed;
4. If long-time stability is noticed

In addition, the STH efficiency is a conversion measure by comparing the energy to evolve hydrogen and the energy of incident light on photocathodes. By assuming the PEC-WS process delivers a stoichiometric water splitting, the STH efficiency can be calculated, as expressed in Eq. (4).

$$\mathrm{STH} = \frac{amount\ \ of\ \ H_2\ per\ \ second\ \ x\ \ 237\frac{Kj}{mol}}{P\ \ x\ \ Area} x\ 100\% \quad (4)$$

In which the amount of H_2 per second is the rate of H_2 production, the Gibbs Free energy is 237 Kj/mol, P is the incident light intensity with AM 1.5 G at 100 mW/cm^2, and the area is the immersed surface of photoanode in the electrolyte during the WS process. Furthermore, one of the critical parameters in PEC cell is the band structure positions of photoanodes and photocathodes that provide a suitable photovoltage to straddle the water redox potentials, as shown in Fig. 5a. After photon energy excites the electron to CB on photoanode, the accumulated electrons will transfer to the photocathode, which induces the Fermi level pins to water oxidation potential due to the hole as the majority carrier at the interfaces. The pinned Fermi level on photoanode surfaces facilitates the hole transfer for water oxidation. On the other hand, the Fermi level in photocathode will pin to water reduction potential to facilitate the electron for HER. Some semiconductors that used for photoanodes and photocathodes are indicated in Fig. 5b. The diagram shows the utilization of photovoltages with different photoelectrodes close to the Shockley-Queisser (SQ) limit in the interfaces of semiconductor/liquid. Photovoltage benchmarks for photoelectrochemical and solar-cell materials as a function of the optical bandgap. Photovoltage values for PEC electrodes are taken from published onset potentials, with photocathodes referenced to E_{HER}° (0 V_{RHE}), and photoanodes referenced to E_{OER}° (1.23 V_{RHE}). The diagonal lines represent the material bandgap, the SQ photovoltage limit, and the SQ limit at − 1 V.

2.5. Stability of photoanodes

The essence of photoanode stability depends on the semiconductor materials. The photoanode materials have been explored, including metal nitrides, metal sulfides, metal oxides, and other organic materials [70–72]. When the photoanode material oxidizes during a PEC-WS

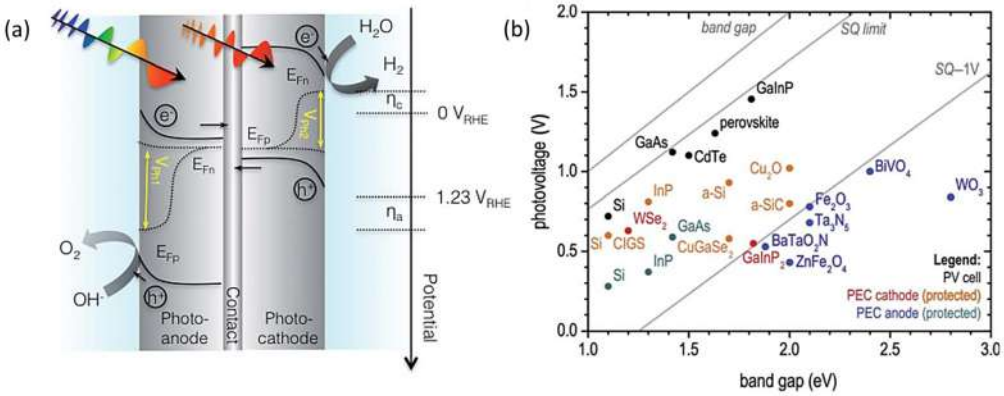

Fig. 5. (a) Appropriate bandgap positions of photoanodes and photocathodes to provide sufficient photovoltage ($V_{ph1} + V_{ph2}$) to drive the WS process. (b) Photovoltages of different semiconductors as a function of bandgap with the Shockley-Queisser (SQ) limit in a semiconductor/liquid junction type device. Reproduced from Ref. [69] with permission from the Royal Society of Chemistry.

process, the stability of photoanode will be degraded. The photoanode material in a PEC-WS process experiences three main steps such as light absorption, bulk separation, and surface catalytic processes. In this condition, there are common points in the degradation of photoanode materials, regardless of the types of semiconductor materials. The major issues that cause the instability of photoanodes during the PEC test are written as follows: Firstly, the photogenerated holes dissolve or oxidize the photoanode materials. It is related to the existing holes on photoanode surfaces with an equivalent of the loss of electrons in the bonding orbital of VB. This phenomenon indicates a weakening of chemical bonds between atoms, making these related atoms easily dissolve through interaction with a reagent in solution. As a result, a low bandgap material has a higher carrier concentration, making them susceptible to photo corrosion during the water-splitting process [29, 73]. That is why narrow-bandgap photoanodes are very unstable compared to wide-bandgap photoanodes [74,75]. Therefore, selecting materials with a particular bandgap and light absorption capability is essential to achieve a stable photoanode. Secondly, the photoanode materials should be chemically stable in electrolytes as the photoanode always contacts with electrolytes during the PEC test. Most semiconductors are unstable in acid electrolytes; thus, selecting an electrolyte for a PEC system is essential for cell stability [76]. Relatively stable electrolytes such as KOH, Na_2SO_4, borate, and phosphate buffers have been applied in the PEC test. Thirdly, the stability of photoanodes is related to the self-oxidation potential with a relative position to the oxidation potential (Φ_{ox}) of a photoanode. In a particular condition, after band alignment, the photo corrosion of semiconductors depends on the reduction and oxidation potentials relative to the conduction band minimum (CBM) and valence band maximum (VBM) of the material, respectively [77]. Consequently, only a specific semiconductor has an appropriate energy band position that has a better stability performance. Fourthly, during the PEC testing, the generated holes are used to oxidize water molecules at the catalyst surfaces. However, suppose these holes are not utilized in time and accumulate at the interfaces due to some reasons (surface states), the photoanode will be oxidized by the accumulated holes, causing deactivation of the photoanode [78]. The photo corrosion of semiconductor materials is regardless of metal oxide or sulfide, as the example: the instability $BiVO_4$ during the PEC test is also occurred when V is dissolved [79].

There are some instability test methods in a PEC process. The most direct examination is applying the photoanode in a long-term PEC test to observe if there is a significant change in the photocurrent density. Some attributes can be observed after and before a PEC process: (1) The photocurrent density (J) – potential (V) or J vs. V curve of a stable photoanode will not change after a long-term test; (2) During the testing of constant current or voltage, the curves of J vs. t (time) and J vs. t (time) will be constant for a long time test; (3) Simultaneously, the generated hydrogen and oxygen rates are not altered; (4) Surface morphology, crystal structure, chemical states, and element contents of photoanode do not significantly change. The excellent stability of photoanodes indicates all the above characteristics during a PEC test. Besides comparing the J values before and after a PEC test, HER and OER performances should be unaltered to indicate favorable stability.

2.6. Standard examination of photoanode stability

Various kinds of characterization methods have been reported. Moreover, the characterization with electrochemical (EC) techniques has been widely used in this field [80]. Bisquert et al. utilized EC characterization to study the surface states of Fe_2O_3 photoelectrode in detail [81]. Materials identification with scanning electron microscopy (SEM), transmission electron microscopy (TEM), X-ray diffraction (XRD), Raman spectroscopy, X-ray photoelectron spectroscopy (XPS), and inductively coupled plasma spectroscopy (ICP) are commonly conducted for photoelectrode. Meanwhile, the performance test is done with J–V curves, I–t curves, electrochemical impedance spectroscopy (EIS), IPCE, and ABPE.

In general, the stability of PEC devices is determined by photocurrent density, solar-to-hydrogen efficiency, and the onset potential of photoelectrodes before and after long-term test [82]. More specific or direct evidence can be expressed with I-t curve or chronoamperometric plot. Scheme 1a indicates a particular example of I-t curve after a PEC test. The figure shows samples A and B with different stability properties. After a period of time, sample A exhibits a constant current density and sample B decays rapidly, indicating its stability is not good. However, the stability of a photoanode may be influenced by the applied external potential during the PEC test [83]. As a result, the I-t curve will be smoother if the applied bias is smaller. In this regard, the influence of external bias should be noted when investigating the photoanode stability. Generally, the I–t curves will be done at 1.23 V_{RHE} for a PEC-WS process [84,85]. In addition, the stability also can be observed with a J-V test on the photoanode by comparing the curves before and after a long-term PEC process [86]. The onset potential, current density (J), and the curve states of photoanodes before and after the PEC test are crucial with this J-V measurement. A stable photoanode will exhibit consistent J-V curves. Scheme 1b shows an example for samples A, B, A′, and B′ after a long-term PEC test. Samples A and A′ indicate a similar J–V curves, implying that sample A is stable. In another case for samples B and B′, there is a different trend of curves after a long-term test. The phenomena may be caused by photocorrosion of the sample. Some characterizations with EC techniques can corroborate the photoanode stability, such as ABPE and IPCE tests. Nevertheless, the EC test can also deliver a wrong message to us with a stable J-V curve since the morphology of photoanode may be changed; however, it is not revealed with the EC test. For instance, the morphology may change to porous after a long-term use and the performance of a photoanode is stable, indicating the actual performance of the photoanode should be degraded as the porous property should enhance the performance. If the J-V curve of the photoanode remains unchanged, it will result in a misjudgment of photoanode stability. As a result, the characterization with different measurements are required to ensure the stability of a photoanode after a long-term PEC test.

3. Essential strategies to design photoanodes

As the material selection for photoanodes is limited by the band structure position, not too many semiconductor materials can comply with the requirements. Some modifications and treatments are considerably needed to improve the existing photoanodes. The current strategies for improving photoanodes involve surface modification, light trapping efficiency, heterojunction formation, and doping. The major purpose of the different strategies is to enhance charge separation and transfer after photoexcitation.

A fast OER kinetics is of equal importance besides the photocarrier separation. Surface modification on the main photoanode using promising electrocatalysts such as IrO_x, CoO_x, NiO_x, spinel structures ($NiFe_2O_4$, Co_3O_4, etc.), and amorphous Co-Pi can improve OER kinetics [88–94]. The purpose of surface modification is to suppress the charge recombination in the bulk and energy loss attributed to the surface-trapped states. One of the simple ways is to create a buried p/n junction at the photoanode surface. This method is helpful for thermodynamically removing photogenerated holes from the bulk photoanode material and storing them in the surface p-type material for a prolonged period. A conformal deposit of an ultrathin p-type layer can also effectively passivate the surface-trapped electrons to reduce the likelihood of surface charge recombination. Furthermore, the ultrathin p-type layer deposited on the electrode allows holes to migrate efficiently to the electrolyte with a slight resistive loss within the electrode. The NiO material is particularly auspicious among various p-type materials due to its appropriate valence band position [95]. Some current strategies, such as nanostructuring, co-catalyst, and surface passivation, are observed to efficiently make the charge separation. In addition, material

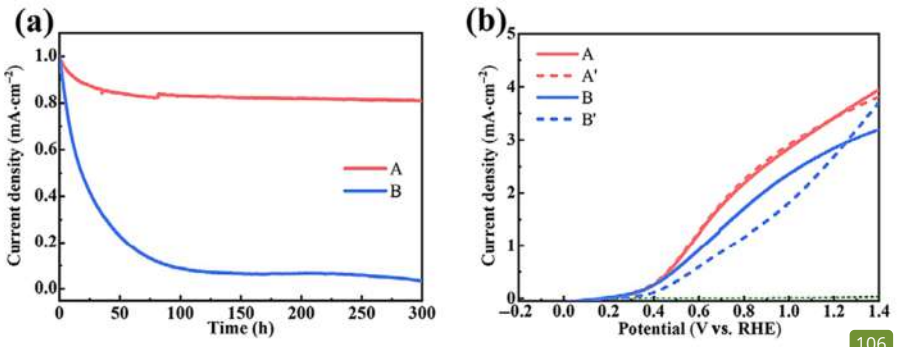

Scheme 1. Examples of linear sweep voltammetry (LSV) data of (a) J-t curves of samples A (be stability) and B (poor stability) and (b) J-V curves of samples A and B after a PEC test (A and B indicate the initial sample and A′ and B′ indicate after a PEC test). Reproduced with permission from Ref. [87] based on the term of CC by 4.0 license.

modification with heterojunction and gradient doping is critical for charge transfer.

3.1. Nanostructuring

One of the main issues in charge separation is the short-length diffusion that suppresses the development of a thick layer of photoanode material, especially for hematite (2–3 nm) [96]. Besides overcoming the short-length diffusion, the surface area of nanostructured porous particles or grain size of anode materials will also enhance the charge separation. As seen in Fig. 6, the nanostructured α-Fe_2O_3 thin films have some appropriate advantages over planar α-Fe_2O_3 thin films: (1) Increasing the light pathway for completing light absorption; (2) Holes can be facilitated to reach the electrolyte interface with a tiny diameter of a porous 1D nanostructure; (3) The tiny nanostructure will provide an enormous specific surface area for water adsorption and activation [97,98].

The thickness of a planar thin film should be in the range of space charge region width (W_{sc}). If the holes are generated far from the surface, they prefer recombining with electrons rather than oxidizing water. The space charge region also depends on the impurity of semiconductor materials, as defined in Eq. (5).

$$W_{sc} = (2 \quad x \quad \Delta\varphi_{SC} \quad x \quad \varepsilon \quad x \quad \frac{\varepsilon_o}{qN})^{1/2} \tag{5}$$

In which, $\Delta\varphi_{SC}$ is the potential drop of space-charge region and N is the doping density. When the doping density decreases, W_{sc} increases from nanometer to microns and the degree of band bending also increases, as indicated in Fig. 7. The intrinsic electric field facilitates a more facile charge-carrier due to the charge-separation effects [99]. Fig. 7a shows the band bending before and after contact with electrolyte due to adsorbed charged species or surface states at the interfaces. During light irradiation, electrons are excited from VB to CB. However, the change of majority carrier in an n-type semiconductor is relatively small to induce no change in the Fermi level. The magnitude of Fermi level separation is defined as photovoltage (V_{ph}) in Fig. 7b. In an equilibrium condition, the Fermi level is aligned with that of electrolyte; Therefore, the generated hole will readily oxidize water molecules at the interfaces. In a natural condition, the surface states induce a reverse effect on water oxidation due to the reduction of a built-in electric field, which decreases the photovoltages. Surface states can be the termination of lattice periodicity, adsorption of chemical species, and the recombination center, which potentially quench the photocarriers and lower the water oxidation efficiency.

Effective charge separation can be further improved by increasing the aspect ratio (a ratio between the length and diameter of nanostructure) of nanowires or nanorods. A higher aspect ratio determines a shorter hole diffusion length and makes the charge separation effective. The light absorption is ensured by the micrometer scale length of nanorods or nanowires, while the charge separation is supported with a higher aspect ratio. As the dimension of nanomaterial is crucial for charge transfer and separation, novel 2D materials have recently emerged for energy storage and conversion since their optoelectronic

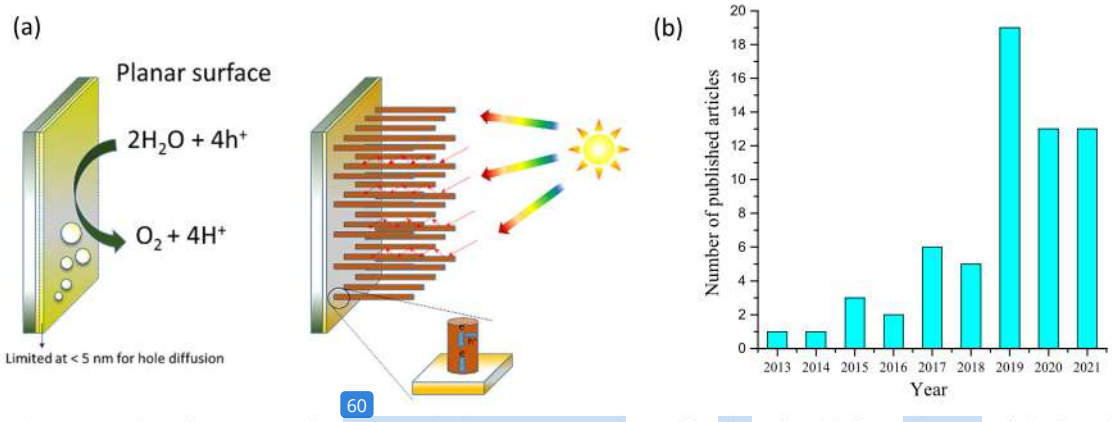

Fig. 6. (a) Nanostructuring a planar Fe_2O_3 surface to improve the charge separation and extend the light pathway for better absorption and (b) the number of publications using 2D photoanodes with Scopus index.

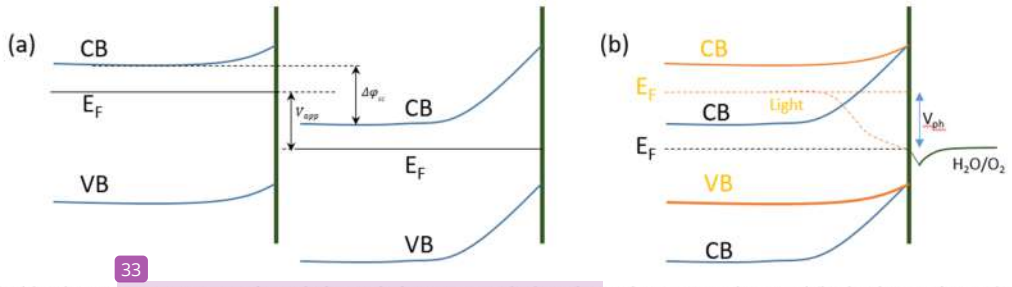

Fig. 7. (a) Band bending in an n-type semiconductor before and after contact with electrolyte to form a space charge and (b) the change of Fermi level after light illumination.

properties depend on thickness [100,101], large surface areas [102], and charge mobilities [103–105]. Therefore, 2D materials with a unique morphology offer a promising alternative for photoanode design. Consistently, the number of published articles on 2D photoanodes is also increased, as indicated in Fig. 6b. Some recent works utilizing 2D materials are summarized in Table 2.

Integrating 2D materials with metal oxides (MOs) is an exciting solution to overcome their drawbacks of narrow light absorption, short charge lifetime, high charge recombination rate, and poor structural stability. The nanoscale 2D materials with MOs heterostructures provide some beneficial aspects for PEC water splitting in several ways. Firstly, nanoscale MOs with high surface area tend to aggregate to form larger clusters with decreased surface area [129,130]. The issue can be overcome by immobilizing the tiny MOs on 2D material surfaces with a good interaction to provide facile charge transfer between them and reduce agglomeration. Secondly, Facile charge transfer is possible since the interfaces with different band positions between MOs and 2D materials could be engineered to provide an electron migration with a built-in electric field and spatially separate the charge carriers with longer lifetime [131–133]. Thirdly, the interface between the MOs and 2D materials could contribute to the bandgap tuning due to the surface strains near the interfaces. It provides an enhancement in the light absorption range [134,135]. Fourthly, the high aqueous stability of 2D materials can be a protective layer for unstable MOs to avoid decomposition [136]. Finally, as the electrons are transferred from one phase to another, those two materials can synergistically perform the PEC-WS process. In addition, most MOs and 2D materials can serve as photoactive sites to increase the amount of electron and hole pairs and boost the surface reaction by reducing the activation energy. However, if the 2D materials are non-photoactive, they can serve as support for the MOs. As a result, synergistic between these materials may show good light absorption and high catalytic activity compared to their pristine counterparts [137].

3.2. Co-catalyst

After photoexcitation, the charge carriers diffuse to the electrode surface for redox reactions. However, many factors, such as surface states, defects, and long diffusion pathways, induce a higher surface recombination rate. Suitable co-catalysts are required to improve the redox activities on the electrode, reduce the reaction energy barrier, and accelerate the charge transfer for boosting surface chemical reactions [138–140]. For instance, an approach with surface modification to decrease the charge recombination in hematite-based photoanodes can control the surface irregularities by passivation of surface states and applying a metal-oxide layer or deposition of co-catalysts [141–145]. Some co-catalysts such as IrO_2, NiOOH, Ni-Pi, Co-Pi, Pt, $FeNiO_x$, graphene, and molecular catalysts are promising for surface modification to overcome sluggish water oxidation. [146–152] Recently, transition metals, such as Ni, Co, Fe, and Mo hydroxides and oxides and their

Table 2
Recent works on 2D nanostructure photoanodes for effective charge separation.

Photoanode materials	OER onset potential (V_{RHE})	J_{ph} at 1.23 V (mA/cm^2)	IPCE at 400 nm (%)	Electrolyte	Light intensity (mW/cm^2)	Ref.
ZnO/MoS_2	0.4	2.0		0.5 M Na_2SO_4	100	[106]
$TiO_2/MoSe_2$	0.1	0.9	N.A.	1.0 M NaOH	100	[107]
α-Fe_2O_3/C_3N_4	1.0	0.4	N.A.	0.5 M Na_2SO_4	100	[108]
Bi-doped Fe_2O_3	0.43	0.6	2.5	M $Na_2B_4O_7$	100	[39]
ZnO/Graphene	0.2	0.6	1.8	1.0 M NaOH	100	[109]
ZnO/Graphene	0.4	0.3	N.A.	0.5 M Na_2SO_4	150	[110]
WO_3/h-BN	0.8	1.6	15.0	0.1 M Na_2SO_4	100	[111]
$BiVO_4$/rGO	0.2	1.1	32.3	d phosphate buffer	100	[112]
α-Fe_2O_3/ZIF-67	0.7	0.9	20.0	1.0 M KOH	100	[113]
TiO_2/NH_2-MIL-125	0.4	0.8	36.0	0.5 M Na_2SO_4	100	[114]
TiO_2/NiFe-MOF	0.3	0.8	25.0	0.5 M Na_2SO_4	100	[115]
$BiVO_4$/CoNi-MOF	0.6	3.2	32.0	0.5 M Na_2SO_4	100	[116]
$BiVO_4/Ti_3C_2T_x$	0.6	0.9	N.A.	1.0 M $K_2B_4O_7$	100	[117]
In_2S_3/TiO_2	0.1	2.73		1.0 M NaOH	100	[118]
In_2S_3/ In_2O_3	0.2	0.15	N.A.	M NaOH	100	[119]
$Fe_2O_3/BiVO_4/WO_3$	0.3	2.75	N.A.	0.5 M Na_2SO_4/0.5 M Na_2SO_3	100	[120]
$BiVO_4/TiO_2$	0.2	1.70		0.5 M KPi/1 M Na_2SO_3	100	[121]
NiO/g-C_3N_4	1.2	0.1	N.A.	0.1 M KOH	N.A.	[122]
$BiVO_4$/Black P	0.6	1.7	N	0.5 M KPi	100	[123]
$CuWO_4$/CdS	0.2	N.A.	N.A.	0.1 M Na_2SO_4	100	[124]
CdS/$ZnFe_2O_4/Cu_2O$	0.1	2.0	N.A.	M Na_2SO_4	100	[125]
α-Fe_2O_3/Ni-MOF-74	0.6	0.9	6.2	1.0 M KOH	100	[126]
ZnO/ZnNi-MOF	0.3	1.4	N.A.	0.5 M Na_2SO_4	100	[127]
α-Fe_2O_3/h-BN	0.7	1.1	45.0	1 M NaOH	100	[128]

oxyhydroxides and phosphates, have been used as co-catalysts for oxygen evolution reactions (OERs) [153–156]. Although all those co-catalysts suffer from low electrical conductivity [157], their low cost, abundant earth reserve properties, and capability to work under benign conditions are advantageous for material development. In addition, transition-metal phosphides (TMPs), namely NiP. FeP, MoP, and CoP are excellent co-catalysts with comparable OER performance as precious metals (Ir, Ru) and metal oxides (RuO_2, IrO_x) catalysts [158–162]. Among the TMPs, NiP have been widely applied for different kinds of electrochemical uses [163,164]. It is considered that phosphor induces stable structure and a crucial part in the electrochemical features. [165] Nevertheless, incorporating TMP-based co-catalyst to oxide electrodes is still required for industrial applications. Liu and Bu et al. successfully applied Co_2P and Ni_2P co-catalysts on Fe_2O_3 electrodes to enhance the WS process [166,167]. However, the exact mechanism of phosphide-based catalytic materials for water oxidation is still not clear and requires more research efforts. Ruifeng et al. investigated a Ni-Pi-modified Fe_2O_3 photoanode that exhibited improved photoelectrochemical activity toward glycerol oxidation. The catalytic activities were enhanced twofold at 1.5 V_{RHE} after incorporating Ni-Pi to form Pi-Fe_2O_3 [168]. Schipper et al. also confirmed the utilization of bimetallic phosphide FeMnP co-catalyst on rutile TiO_2 for PEC-WS reactions [169]. Furthermore, Cao et al. modified α-Fe_2O_3 with Ta doping and Ni_2P and successfully reached a photocurrent density of 2.98 mA/cm^2 at 1.23 V_{RHE}, which is 2.76-fold higher than that of pristine α-Fe_2O_3, as shown in Fig. 8a [170]. The onset potentials and chronoamperometric OER stability also enhanced, as indicated in Fig. 8b and c after spin coating of Ni_2P quantum dots (Fig. 8f). It is also shown that the surface activation of NiOOH induces lower Gibbs free energy during the steps of OER mechanism in Fig. 8d and e. This work shown that the incorporation of Ni_2P and NiOOH on α-Fe_2O_3 reduces the reaction energy barrier and accelerates the charge transfer to boost the water oxidation reaction in Fig. 8g.

In addition, some works on $BiVO_4$ photoanodes with co-catalyst modification to overcome the severe charge recombination and slow kinetics in PEC performance [171]. It was found that suitable co-catalysts can capture the charge carriers and accelerate the surface reactions to provide oxidation sites as well as protect $BiVO_4$ from photocorrosion. Table 3 indicates the critical results in PEC water oxidation with different co-catalysts on $BiVO_4$ in recent years.

3.3. Surface passivation

The stability of photoanode materials, including metal oxides, metal sulfides, metal nitrides, and other organic materials [29,71,72] depends on the properties of semiconductor materials. If the photoanode materials oxidize during the PEC-WS process (light absorption, bulk separation, and surface catalytic activities), the stability will be poor. There are primary causes of photoanode instability under these circumstances. Firstly, oxidation is indicated with a dissolution rate of photoanode materials during the PEC test, which is related to the photogenerated holes. Holes on the electrode surface are equivalent to losing electrons and weakening chemical bonds among atoms. If affinity reagents exist in the solution, the bond-weakened particles will dissolve easily due to the strong coloumbic interaction. Based on the observed phenomenon, narrow-bandgap materials have more photogenerated carriers.

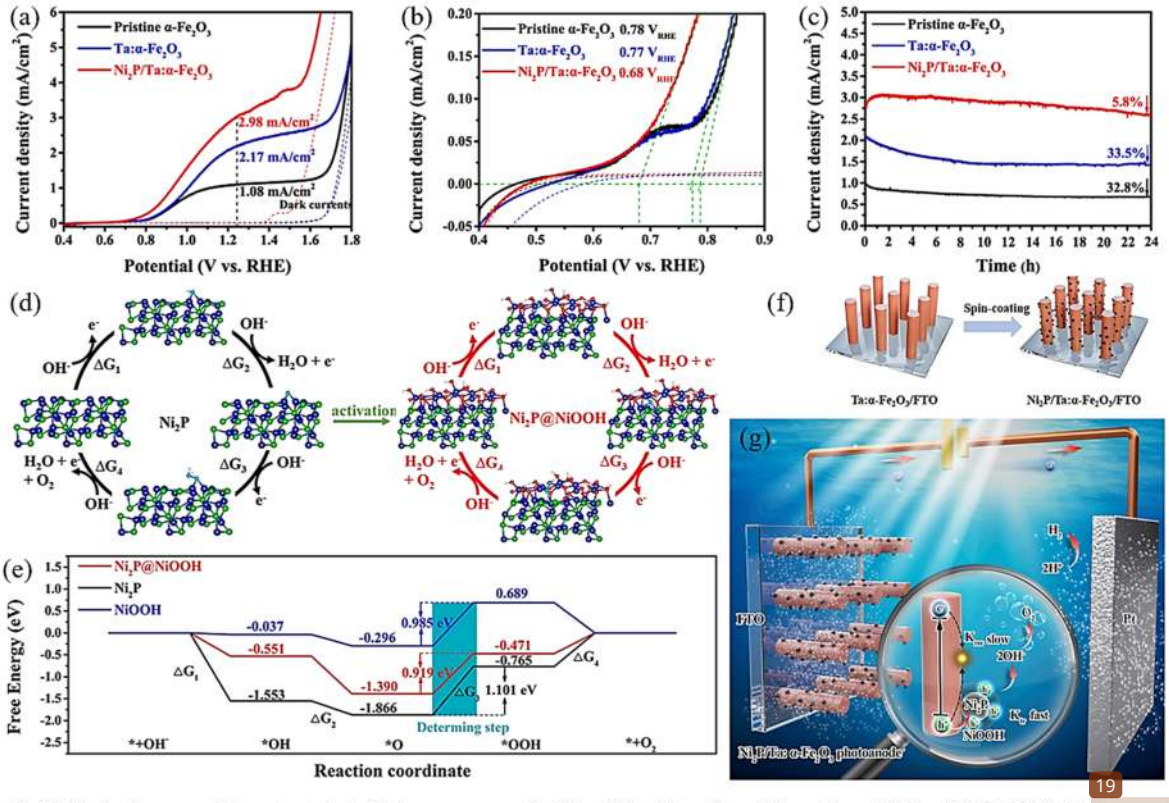

Fig. 8. (a) Polarization curves, (b) onset potentials, (c) chronoamperometric OER stability, (d) multistep-OER reactions of Ni_2P and Ni_2P@NiOOH, (e) the oxygenic adsorbates were represented by cyan groups, (e) Free-energy graph of OER reaction of Ni_2P and Ni_2P@NiOOH, and (f) schematic drawing of Ni_2P/Ta:α-Fe_2O_3 photoanode with reduced the reaction energy barrier to boost the water oxidation reaction.
Reproduced from Ref. [170] with permission from Chemical Engineering Journal.

Table 3
Specific co-catalysts on $BiVO_4$ photoanodes with the synthesis methods, reaction conditions, and photocurrents at 1.23 V_{RHE}.

Cocatalyst	Synthesis methods	Reaction conditions	Photocurrent at 1.23 V_{RHE}	Ref.
H-CoAl-LDH	plasma etching	M Na_2SO_4, illumination (100 mW/cm^2)	3.5 mA/cm^2	[172]
H-Co-Ci	plasma etching	M Na_2SO_4, illumination (100 mW/cm^2)	3.95 mA/cm^2	[173]
LDH@QD	hydrothermal method	PBS (pH 7), illumination (100 mW/cm^2)	2.23 mA/cm^2	[174]
FeOOH	photodeposition	M KH_2PO_4 (pH 7), illumination (100 mW/cm^2)	1.0 mA/cm^2	[175]
U-CoOOH	Ar-plasma treatment	M Na_2SO_4 (pH 7), illumination (100 mW/cm^2)	4.9 mA/cm^2	[176]
Ni_4O_4	hydrothermal method	M phosphate buffer (pH 7), illumination (100 mW/cm^2)	3.9 mA/cm^2	[177]
CoPi	electrodeposited	M KPi buffer (pH 7), illumination (4 mW/cm^2)	0.99 mA/cm^2	[178]
Co-Sil	photoelectrophoretic deposition	M $K_2B_4O_7$ (pH 9.5), illumination (100 mW/cm^2)	5.0 mA/cm^2	[179]
CoFe-PA	solvothermal	M NaBi (Ph 8.5), illumination (100 mW/cm^2)	4.5 mA/cm^2	[180]
TiO_{2-x}	atomic layer deposition	M KBi (pH 7), illumination (100 mW/cm^2)	6.1 mA/cm^2	[181]
$Fe_xNi_{1-x}OOH$	Ph modulated immersion	m K_3BO_3 (pH 9.5), illumination (100 mW/cm^2)	5.8 mA/cm^2	[64]
NiB	chemical reduction	M KBi (pH 9.2), illumination (100 mW/cm^2)	3.47 mA/cm^2	[182]
β-FeOOH	solution impregnation	M Na_2SO_4 (pH 7), illumination (100 mW/cm^2)	4.3 mA/cm^2	[183]
CMs	immersion	0.5 M phosphate buffer (pH 7) illumination (100 mW/cm^2)	2.1 mA/cm^2	[184]

Therefore, they are susceptible to photo corrosion and unstable in PEC-WS process [73]. This susceptibility elucidates the reason for unstable low-bandgap materials, while wide-bandgap semiconductors, such as SnO_2, ZrO_2, and Al_2O_3 are relatively stable [74,119,185,186]. As a result, material selection based on the capability of light absorption and bandgap is crucial for photoanode stability. Secondly, the photo corrosion property also depends on the electrolytes used during the test. It plays an essential role in the chemical stability of photoanode. For example, most semiconductors are unstable in acid electrolytes. Therefore, choosing electrolytes is a vital step toward achieving photoanode stability. Various kinds of electrolytes are used in the PEC test, such as potassium phosphate, KOH, HCl, Na_2SO_4, borate buffer, and so on, to achieve reaction stability. Thirdly, the relative bandgap position of the photoanode would also determine the potential of photo corrosion in a semiconductor material. It is related to the photoanode self-oxidation potential and the alignment of water oxidation potential to the valence band maximum (VBM) [77]. Consequently, selecting the photoanodes with appropriate energy band positions can promote a stable performance. Fourthly, during the PEC process, the generated holes are transferred to photoanode surfaces for an oxidation reaction. However, if the photogenerated holes accumulate at this moment and are too late to transfer for water oxidation reaction, it will cause deactivation to photoanode [78]. Regardless of metal oxide or sulfide photoanodes, photo corrosion may happen in several causes, as mentioned above. For

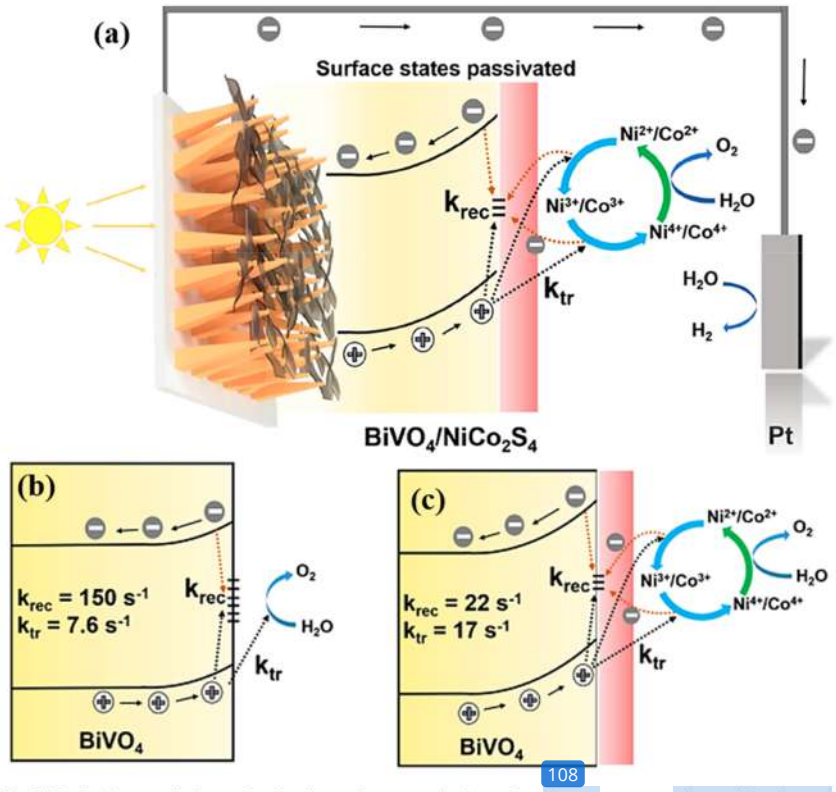

Fig. 9. (a) Pyramidal $BiVO_4/NiCo_2S_4$ photoanode for passivating the surface states by decreasing the rate constant of recombination and increasing that of charge transfer based on the comparison between (b) pure pyramidal $BiVO_4$ and (c) $NiCo_2S_4$-deposited $BiVO_4$ photoanodes. Copyright 2020 American Chemical Society. Reprinted with permission from [187].

example, the instability of $BiVO_4$ is also caused by the V dissolution during PEC process [79].

In the other case, the surface state of $BiVO_4$ can be passivated with Co/Ni sulfide [187]. It was found that the presence of $NiCo_2S_4$ did not significantly change the rate constant of charge transfer (K_{tr}) on the $BiVO_4$ photoanode compared to that of pristine $BiVO_4$ photoanode. It implies that the $NiCo_2S_4$ cocatalyst does not affect the charge transfer across the $BiVO_4$ and electrolyte interface [188]. As shown in Fig. 9b and c, the suppressed K_{rec} with a minor change of K_{tr} suggests the enhancement of water oxidation kinetics is influenced by the $NiCo_2S_4$ cocatalyst in the passivating surface state on the $BiVO_4$ surfaces [188]. The passivation of $NiCo_2S_4$ cocatalyst also enhances charge lifetimes at $BiVO_4/NiCo_2S_4$ photoanode interfaces based on the intensity-modulated photovoltage spectroscopy (IMVS). As indicated in Fig. 9a, the high activity of photogenerated holes in $BiVO_4$ contributed by the dual-metal Ni^{2+}/Co^{2+} ions that immediately capture the hole to be oxidized to Ni^{3+}/Co^{3+} ions and unstable Ni^{4+}/Co^{4+} ions. The unstable Ni^{4+}/Co^{4+} ions will oxidize water and subsequently, they will be reduced to initial Ni^{2+}/Co^{2+} ions. The $NiCo_2S_4$ catalyst with negligible K_{tr} acts as a hole reservoir that provides electrons to passivate the surface states and suppress surface recombination.

An intermediate layer is required to be added at the interfaces between semiconductor layers as their CB and VB band positions are pretty different to favorably transfer the generated electron and hole with a graded transition. Cao et al. improved the charge separation efficiency between ZnO, CdS, and $ZnFe_2O_4$ band structures [33]. Pan et al. confirmed a better charge separation with a double type-II heterojunction by adding a TiO_2 layer between SnO_2 and $BiVO_4$ [189]. Besides optimizing interface contact and reducing recombination, the band mismatching also can be solved with the use of an intermediate layer, as shown in Fig. 10a. [190] Luo and co-workers fabricated an Al_2O_3 layer between Si/SiO_x and Ni/NiO_x by atomic layer deposition to passivate the interface defects and reduce the pinning effect of the Fermi level in Fig. 10b [191].

In the specific sites at photoanode/electrolyte interface, charge carriers accumulate on the surface to cause severe recombination and

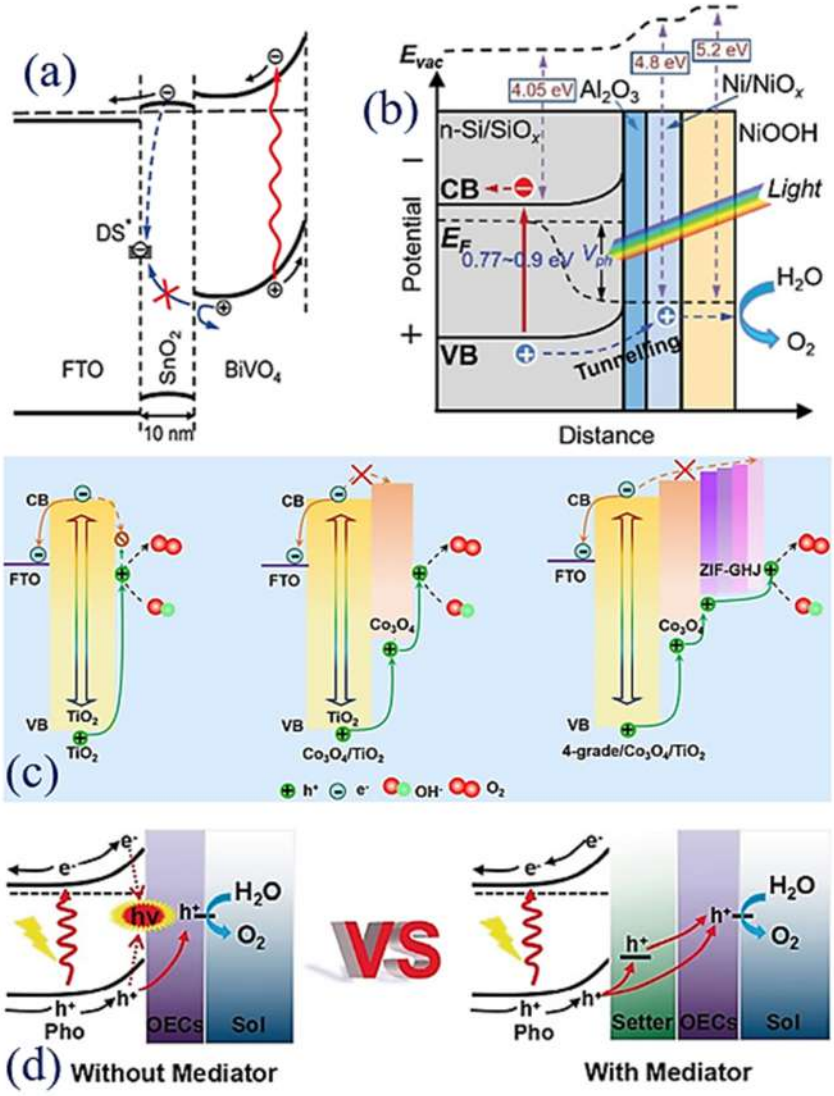

Fig. 10. (a) Band energy position with SnO_2 passivation layer. Reproduced with permission from [192] Copyright 2011, American Chemical Society, b)Band energy alignment of the $n\text{-}Si/SiO_x/Al_2O_3/Ni/NiO_x/NiOOH$ photoanode. Reproduced with permission from [191] Copyright 2019, Wiley-VCH, c) Schematic diagrams of the introduction of ZIF as a photogenerated hole extraction layer on the photoanode/electrolyte interface. Reproduced with permission from [193] Copyright 2021, Wiley-VCH, and (d) the photogenerated carrier transport process of composite photoanodes with and without mediator or setter. Reproduced with permission from [194] Copyright 2019, Wiley-VCH.

reduce the performance due to the electron transfer back and sluggish transfer dynamics [88,123,195,196]. To solve this issue, an intermediate layer can be used to promote charge transport for the WS process. Tang et al. confirmed that the TiO_2 layer induced electrons to the electrolyte interface, causing profound carrier loss [193]. With Co_3O_4/TiO_2 heterojunction in Fig. 10c, the electron transport from TiO_2 phase was suppressed. The type-II heterojunction also promoted the hole transfer to the electrolyte. Considering the ZIF-Co_xZn_{1-x} with a more negative VB than Co_3O_4, the hole extraction from TiO_2 layer was enhanced to the electrolyte interfaces by ZIF-$Co_xZn_{1-x}/Co_3O_4/TiO_2$ multi-graded heterojunction. The rapid transfer of holes will suppress the charge recombination. Ning et al. indicated that the significant potential difference between the water oxidation potential and VB of $BiVO_4$ decreased the cell performance [194]. 5,10,15,20-tetrakis(4-carboxyphenyl)porphyrin-Co(CoPy) was utilized as a transport channel similar to a volleyball setter to promote the transfer rate of holes to reach the photoanode surface. The IMPS with $\tau_d = (2\pi f_{max})^{-1}$ confirmed that the electron lifetime of $BiVO_4$/CoPy/$FeNi(OH)_x$ was longer than that of $BiVO_4$/$FeNi(OH)_x$. CoPy plays a crucial role in facilitating hole transfer from $BiVO_4$ to $FeNi(OH)_x$ and reducing carrier accumulation at photoanode/electrolysis interfaces. Therefore, introducing the intermediate layer with significant energy band differences can be used as a transition for effective transmission and separation of carriers and improving the performance of photoanode PEC-WS process. Table 4 briefly summarizes some useful functional intermediate layers to advance water oxidation on photoanodes.

3.4. Heterojunction formation

One of the essential strategies in improving light absorption, charge carrier separation, and redox capability with high energy conversion efficiency is using semiconductor heterojunction formation [33]. A heterojunction formation is the interfacial of two semiconductors inducing facile charge transfer between them. A PEC photoelectrode is expected to adsorb the sunlight efficiently with a strong redox potential; however, only a single semiconductor cannot satisfy these requirements. One of the essential solutions is utilizing a heterojunction photoelectrode composed of different semiconductors. [197–199] Therefore, a semiconductor with a wide bandgap can be combined with a smaller bandgap semiconductor to optimize the light absorption property and simultaneously maintain a strong redox potential [200,201]. By combining two or three semidonductors to form heterojunctions, the essential requirements of photoelectrode can be overcome smoothly. The exploration of heterojunctions in the PEC-WS field has been extensively studied [202]. As the energy band structure of each semiconductor is different, the heterojunction formation can be classified into straddling-gap junctions (type-I), staggered-gap junctions (type-II), and broken-gap junctions (type-III) [203,204]. Recently, another Z-scheme junction with a unique charge transfer pathway of a Z-shape is also extensively explored [205,206]. In addition, the heterojunction formation also can be defined as p-p, n-n, and p–n junctions [207]. The schematic drawing of heterojunction formation is depicted in Fig. 11. All the heterojunction formation indicates an efficient charge transfer except type-I heterojunction that tends to have a higher recombination rate.

In general, the heterojunction formation needs to have similar thermal expansion coefficients, lattice spacings, and crystal structures. The use of heterojunctions to improve PEC-WS performances has been widely developed to enhance carrier separation and charge transport. Furthermore, the surface area of active photoanodes may also be improved by constructing the heterojunction. In addition, the specific surface area of photoanodes may also increase by constructing heterojunctions. As a result, the contact region of electrode/electrolyte and the light-harvesting can be enhanced by utilizing a low bandgap semiconductor [208]. Nevertheless, heterojunction formation does not always show a good solution for the PEC process. In some conditions, unavoidable issues, such as slower carrier transfer and separation, will affect the PEC performances [209]. The lattice mismatch in the heterojunction formation causes the bonding at the interface not to be sufficiently strong and generates defects which is unfavorable for charge transfer and separation [210]. Simultaneously, the energy band positions of semiconductors should be carefully considered when constructing the heterojunctions. With the energy band structures of semiconductors match each other, the charge carriers can be accelerated to induce high photocurrent and good water oxidation performance. However, a poorly matched band structure will form an interface barrier, which hampers the charge transfer during redox reaction. Based on the knowledge of semiconductor band structure positions or the type of heterojunction formation, relevant strategies to solve the carrier transmission issue can be smoothly done. The promising staggered-gap and Z-scheme heterojunctions are discussed further.

3.4.1. Staggered-gap heterojunction

The band alignment of two semiconductors provides different heterojunctions, which are classified into type-I, type-II, type-III heterojunctions, p-n type, and Z-scheme formation [211]. The holes and electrons in a type-I heterojunction are transferred from semiconductor A to semiconductor B during the photoreaction. The accumulation of holes and electrons in VB and CB of the semiconductor will experience severe charge recombination due to the lower bandgap of semiconductor B. It is suggested that the type-I heterojunction is not appropriate as a strategy to enhance photoreaction performances. In a type-II heterojunction, the generated electrons in CB of semiconductor B will be drifted to CB of semiconductor A, while the generated holes in VB of semiconductor A will be transferred to VB of semiconductor B, implying a spatial separation of electron–hole pairs. Furthermore, there is no directional charge transfer between semiconductors in a type-III heterojunction. A low bandgap semiconductor combined with a wide bandgap semiconductor will induce light absorption and facilitate the extraction of generated carriers. Therefore, it is observed that constructing a heterojunction with an efficient photoexcited electron-hole pairs separation will be an effective way to improve carrier dynamics. Recently, type-II heterojunction has been widely explored to improve the PEC-WS process, such as ZnO/ZnS, [212] $WO_3/CdIn_2S_4$, [213] $WO_3/BiVO_4$, [214] etc [169,215,216].

Although type-II heterojunction is very effective for charge separation and light absorption, powerful Z-scheme heterojunctions have considerably attracted researchers' interest due to some advantages [211,217,218]. Selecting semiconductors with suitable energy bands is not an easy task to control and regulate an efficient charge transfer and

Table 4
Some proper functional intermediate layers to advance water oxidation on photoanodes.

Sample	Intermediate layer	J (1.23 V_{RHE})	IPCE	Measuring condition	Ref.
R-$BiVO_4$/CoPy/$FeNi(OH)_x$	Passivation layer Hole extraction layer	4.75 mA cm^{-2}	-	0.2 M Na_2SO_4	[194]
n-Si/SiO_x/Al_2O_3/Ni/NiO_x/NiOOH	Passivation layer	28 mA cm^{-2}	70% at 420–800 nm 1.23 V_{RHE}	1 M Na_2SO_4/0.1 M KPi	[191]
FTO/SnO_2/$BiVO_4$	Seed layer	-	46% at 450 nm, 1.63 V_{RHE}	0.15 M K_2SO_4	[192]
$ZnFe_2O_4$/CdS/ZnO	Protection layer	3.88 mA cm^{-2} (0 $V_{Ag/AgCl}$)	-	0.5 M Na_2S	[28]
ZIF-$Co_xZn_{1-x}/Co_3O_4/TiO_2$	Hole extraction layer	2.91 mA cm^{-2}	-	1 M NaOH	[193]

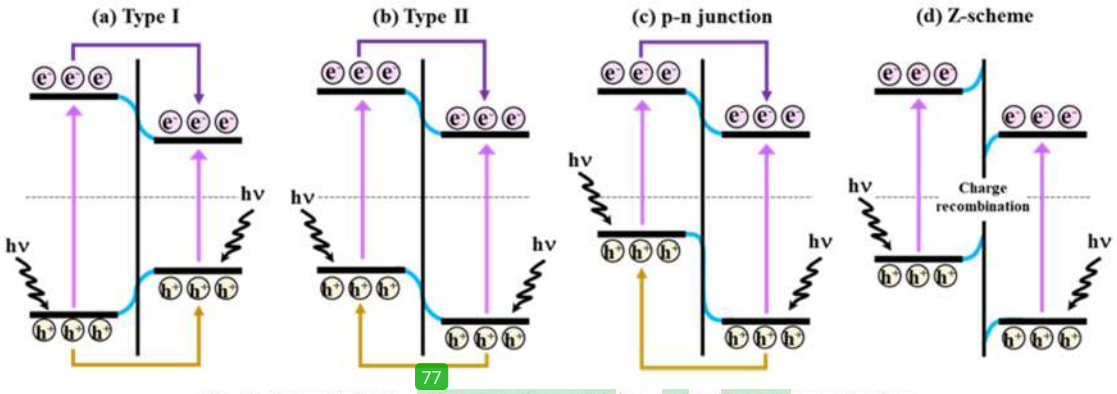

Fig. 11. Schematic drawing of (a) type-I, (b) type-II, (c) p-n, and (e) Z-scheme heterojunctions.

separation. However, doping can be one of the ways to adjust the energy band with donor and acceptor states. Doping also can form stepwise or gradient (continuous) energy bands, which are adequate to solve the charge transfer issues. Most heterojunctions are formed with step-by-step preparation since most semiconductors cannot be formed simultaneously. A semiconductor is first synthesized on a substrate, followed by another in a stepwise preparation [169,219–221]. Some recent works are shown as examples. Gao et al. fabricated TiO_2 nanorods on fluorine-doped tin oxide (FTO) with a hydrothermal method. The obtained TiO_2 layer is treated with a secondary hydrothermal to grow TiO_2 ultrathin nanosheets in situ on the first TiO_2 nanorods [222]. The nanorods and nanosheets with different facets promoted the charge separation efficiency, lengthened the carrier lifetime, and improved the hydrogen evolution rate. Zeng et al. successfully synthesized a B-C_3N_4/Mo-$BiVO_4$ photoanode to increase the charge separation by several steps of process [223]. However, in some cases, the stepwise preparation takes time and damages the first obtained layer while synthesizing the second layer semiconductor. To overcome this issue, some scientists developed a one-step preparation process to fabricate the heterojunctions. [224,225] As examples, Cao et al. synthesized a 3D pyramidal In_2O_3/ In_2S_3 array with an ion exchange method to obtain the best performance at 1.23 V_{RHE} with a good stability [226]. Hou et al. prepared a porous 2D lateral heterostructure of In_2O_{3-x}/In_2S_3 and the performance indicated a 21-fold enhancement compared to the single In_2S_3 atomic layers [227]. Dong et al. modulated ammonia thermal parameters with a one-step thermal route during the synthesis of Ta_3N_5/$BaTaO_2N$ heterostructures with a better PEC performance [228]. In addition, Meng et al. constructed a $CdIn_2S_4/In_2S_3$ heterojunction using Ni-phthalocyanine solution and achieved a charge separation efficiency up to 90% at 1.23 V_{RHE} [229]. Briefly, the type-II heterostructure promotes light absorption, charge carrier transfer, and separation due to the matched energy band with a built-in electric field. Moreover, the availability of electrostatic interaction will cause photo-excited electron-hole pairs to be hampered for the interface charge transfer. As a result, there are still many works to explore the heterojunctions to solve the reversed effect for the PEC process.

3.4.2. Z-scheme heterojunction

As the type-II heterojunction sacrifices the potential to separate photogenerated electrons and holes, it will be a drawback for its application. An existing strategy with Z-scheme heterojunction has become a new choice to enhance the PEC water-splitting performance. The Z-scheme heterojunction is referred to the pathway of charge transfer in a Z-shape during light illumination. There are three Z-scheme heterojunctions: ionic, [230] all-solid-state [231], and direct Z-scheme heterojunctions [232]. The depicted Z-scheme heterojunctions are shown in Fig. 12.

The ionic Z-scheme heterojunction, as shown in Fig. 12a was first introduced in 1979. In this type of Z-scheme heterojunction, a redox electron mediator is required to faster the charge transport, increasing the recombination rate between holes and electrons in VB of one semiconductor and CB of another semiconductor. Therefore, the electron in

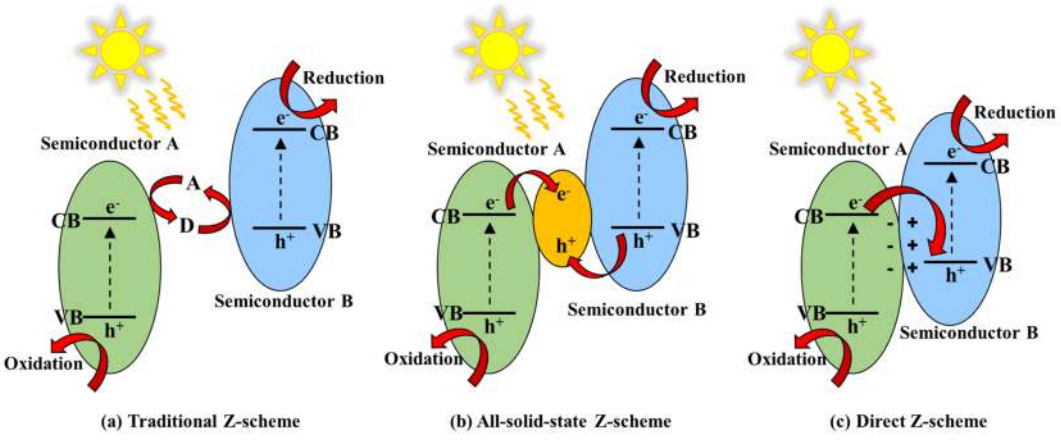

Fig. 12. (a) Ionic-, (b) all-solid-state-, (c) direct-type Z-scheme heterojunctions.

one's CB and hole in another's VB can actively induce oxidation and reduction reactions, respectively. There are some common redox electron mediators, such as IO^{3-}/I^-, NO^{3-}/NO^{2-}, Fe^{3+}/Fe^{2+}, $[Co(phen)_3]^{3+/2+}$, and $[Co(bpy)_3]^{3+/2+}$. However, the application of ionic state Z-scheme heterojunction is limited due to environmental concerns. A further improved Z-scheme type of all-solid-state has replaced its application. The so-called all-solid-state Z-scheme composes of a metal nanoparticle and two semiconductors with a matched energy band, as shown in Fig. 12b. The metal nanoparticles such as Pt, Ag, Au, Cd, W, and rGO play important roles in transferring the charge carrier with an ohmic contact. As a result, this action will promote the recombination between photoexcited electrons and hole from semiconductors A and B, respectively. Some interesting works by Chen et al. and Fu et al. indicated the effectiveness of all-solid-state Z-scheme heterojunction [233, 234]. Chen et al. constructed a g-C_3N_4/rGO/perylene diimide polymer (C_3N_4/rGO/PDIP) with a simple method. The heterojunction scheme achieved a high charge transfer ability for photocatalytic WS. The phenomenon was also supported by a transient absorption spectrum that indicated the lifetime of electrons was shortened and the lifetime of holes trapped by PDIP was enhanced. The charge transition happened in a timely and spa[51] manner to form a Z-scheme mechanism in g-C_3N_4/rGO/PDIP, as shown in Fig. 13a. In addition, Fu et al. fabricated an α-Fe_2O_3/Au/TiO_2 photoanode by coating Au particles on Fe_2O_3 surface, which further covered by TiO_2. The design can efficiently extract the photogenerated h[32] that are further accelerated with amorphous TiO_2 on the surface for the water oxidation reaction. However, the mediator of Au also induces a reverse reaction, shields the light and reduces the electron-hole pairs. Therefore, it is a challenge for Z-scheme heterojunctions, which require long-term stability.

To overcome the stability issue, a direct Z-scheme heterojunction that mimics photosynthesis is developed, as shown in Fig. 12c. in this type of Z-scheme, when tw[37] miconductors with different energy levels are connected, the excited electrons in CB of semiconductor A will drift to CB of semiconductor B till the system reaches an equilibrium Fermi level. As the positive charges continuously accumulate in VB of sem[62] conductor A and negative charges in CB of semiconductor B will form a built-in electric field and recombine. In the meantime, band edge bending occurs at the int[7]face between semiconductor A and semiconductor B. During light illumination, th[67]ilt-in electric field at the semiconductor interfaces will accelerate the recombination between electrons in CB of semiconductor A a[11]oles in the VB of semiconductor B. The Z-scheme heterojunction will drive the water oxidation on the VB of semiconductor A and the reduction reaction on the CB of semiconductor B. This mechanism obviously induces charge separation with an efficient pathway. The advantageous no-mediator Z-scheme heterojunction can transfer the charges directly through the interfaces, thus shortening its diffusion distance, improving the charge recombination, and enhancing the photovoltage of a PEC cell. As a result, the direct Z-scheme heterojunction can overcome the reverse reactions and light shielding phenomena. Furthermore, the density of effective photocarriers and resistance of photocorrosion are also improved. Specific work with the direct Z-scheme heterojunction of black phosphorus/monolayer Bi_2WO_6 photoanode is successfully prepared by Hu and coworkers . The as-designed photoanode indicated a potent photocatalytic activity on H_2 generation and NO removal. Another work by Liu et al. [236] also indicated a black phosphorus/red phosphorus (BP/RP) heterophase, as shown in Fig. 13b. The staggered alignment might help to separate and transfer charges, which proved with transient absorption spectrum (TAS) via a direct Z-scheme pathway. Zhou et al. utilized transient photovoltage (TPV) decay to analyze the charge carrier transfer in photoanode [237]. The carrier lifetime of ZnO/TiO_2 heterojunction was found to be longer than that of single TiO_2, implying that the heterojunction construction induced electron transport at the interface. Moreover, Xu et al. used time-resolved photoluminescence (TRPL) to prove $ZnIn_2S_4$/CdS/ZnO had a longer carrier lifetime than $ZnIn_2S_4$/CdS and $ZnIn_2S_4$ [235]. The construction of $ZnIn_2S_4$/CdS/ZnO ternary heterojunction promoted carrier separation and the ZnO layer prevented surface recombination and improved water oxidation reactions.

There are two severe problems of mediators and weak van der Waals interlayer inte[37]ion. Firstly, the problems caused the low recombination between generated electrons in the CB of semiconductor A and holes in the VB of semiconductor B. For in[124]e, Wang et al. synthesized ultrathin polymers with aza-conjugated microporous polymers (CMP) and C_2N nanosheets to construct a v[94]der Waals Z-scheme heterostructure [238]. The recombination through the van der Waals interactions increases at the interfaces between the two polymers in the Z-scheme heterojunction. Interestingly, the solar energy conversion efficiency to hydrogen (STH) could achieve 0.23%. The STH value was further enhanced to 0.4% when rGO was introduced as a solid electronic mediator into the Z-scheme heterostructure. Secondly, finding the cocatalyst and sacrificial agents to improve the surface catalytic activity is still a challenge, mainly for the slow four-electron involved OER. Wang et al. also utilized Pt and $Ca(OH)_2$ cocatalysts on their Z-scheme heterojun[7]ion to evolve H_2 and O_2. However, the characterization to identify th[35]ect Z-scheme heterojunction is still a challenge. Low et al. identified the formation of a dir[56]-scheme TiO_2/CdS heterojunction with hydroxyl radical test, in-situ X-ray photoelectron spectroscopy, and density functional theory (DFT) simulation [239]. The hydroxyl test confirmed the formation of ·OH radical was on TiO_2 phase, not on CdS via a Z-scheme charge transfer, indicating the generated photo electron in CB of TiO_2 recombined with VB of CdS. Therefore, the available holes

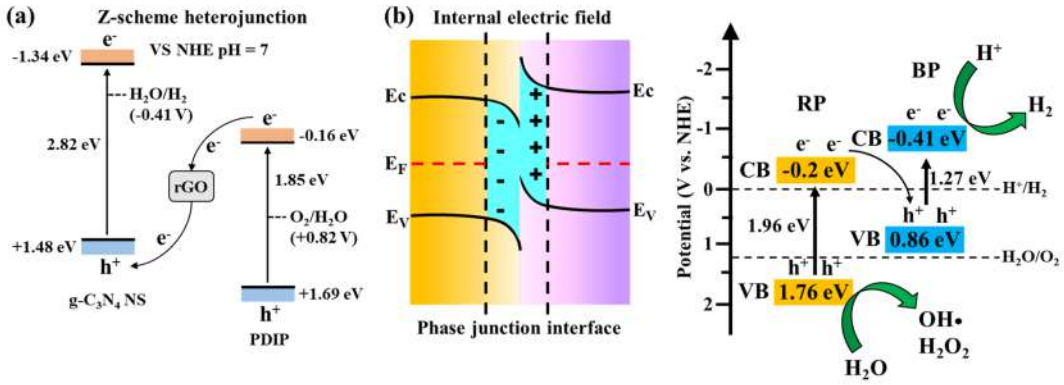

Fig. 13. (a) Z-scheme heterojunction with rGO as the mediator for recombination site [235] and (b) the Z-scheme energy band offsets diagram and heterojunction interface charge property [236].

in VB of TiO_2 would oxidize water to hydroxyl radical. In addition, the in-situ XPS also indicated a negative shift of Cd peak and a positive shift of Ti peak, indicating the electrons transferred from TiO_2 to CdS via a Z-scheme formation. The other significant characterization for identifying a Z-scheme heterojunction was also done by Wang et al. [240]. They used electron spin resonance (ESR) and surface photovoltaic spectroscopy (SPV) to study the carrier transfer in Sv-$ZnIn_2S_4$/$MoSe_2$ for photocatalytic hydrogen production. SPV analysis indicated the signal of Sv-$ZnIn_2S_4$ is higher than that of Sv-$ZnIn_2S_4$/$MoSe_2$, implying that the holes on the surface of Sv-$ZnIn_2S_4$/$MoSe_2$ were decreased. The natural CB position of $MoSe_2$ did not fit to reduce O_2 to $\cdot O_2^-$, however, the $\cdot O_2^-$ signal was detected in Sv-$ZnIn_2S_4$/$MoSe_2$ in ESR analysis, indicating that many electrons accumulated at CB of Sv-$ZnIn_2S_4$ with Z-scheme heterojunction formation. The advantage of Z-scheme heterojunction is the efficient separation of photocarrier while maintaining a strong redox potential although for charge separation in a bulk phase. The coexistence of high-efficiency bulk phase separation and strong redox capability contribute to a high efficient PEC water splitting. Nevertheless, the design and characterization for Z-scheme heterojunction are challenging.

3.5. Doping strategy

Doping is one of the efforts to improve specific activities in photoelectrodes with alien elements. By introducing a particular element to a matrix, some properties of materials can be improved, such as increasing conductivity, better charge separation, lower recombination rate, enhancing light absorption, and promoting directional charge transport. As the alien element is doped into a material, the conductivity will be influenced by amounts of carrier concentration and mobility with a relation: $\sigma = n_e\mu_e + n_h\mu_h$. The variable of σ, n, and μ represent the conductivity, carrier concentration, and charge mobility, respectively. Doping alien elements will increase the carrier concentration and conductivity [241]. Therefore, the introduced elements also can change the electronic structure of materials with certain positions of CB and VB. Based on the doping position, doping can be divided into substitutional and interstitial doping. According to the doping positions, it can be divided into interstitial and substitutional doping. The substitutional one requires a similar radius and number of valence electrons. Based on the distribution of dopant amounts, the doping should be incorporated into a matrix uniformly and gradually. Uniform doping requires a certain amount of dopant to ensure a uniform phase. If the dopant is excessive, it will act as a recombination center, inducing a smaller depletion layer and affecting the carrier separation [242,243].

Contrastly, gradient doping will form a gradient energy band structure and expand the depletion layer with better charge separation in a photoanode. The types of dopants can be classified into inorganic and organic materials [244–246]. Meng et al. successfully used In and Zn/In dopants to dope SnS_2 nanosheet to form a gradient energy band that enhances the carrier separation and its concentration with higher efficiency [247]. Hufnagel et al. demonstrated uniform Sn doping on hematite surfaces within 5 nm depth. Further analysis with IMPS indicated that the top 5-nm hematite layer exhibited higher charge transfer efficiency than the other area with uniform Sn doping throughout the hematite layer [248]. In this regard, the top Sn doping induced a gradient band that enhanced the charge transport and separation. The increased efficiency can be generated by a new energy level in the forbidden band that expands the light response of materials.

For example, in Fig. 14 a,b,c, Xiao et al. indicated the gradient doping of Mg^{2+} to substitute Ta^{5+} in Ta_3N_5 to form defect states to suppress the charge recombination [249]. The improvement is proved with time-resolved photoluminescence (TRPL) spectroscopy to detect the extended lifetime of charge carriers compared with the system with homogenous doping. In addition, Zhang et al. also investigated

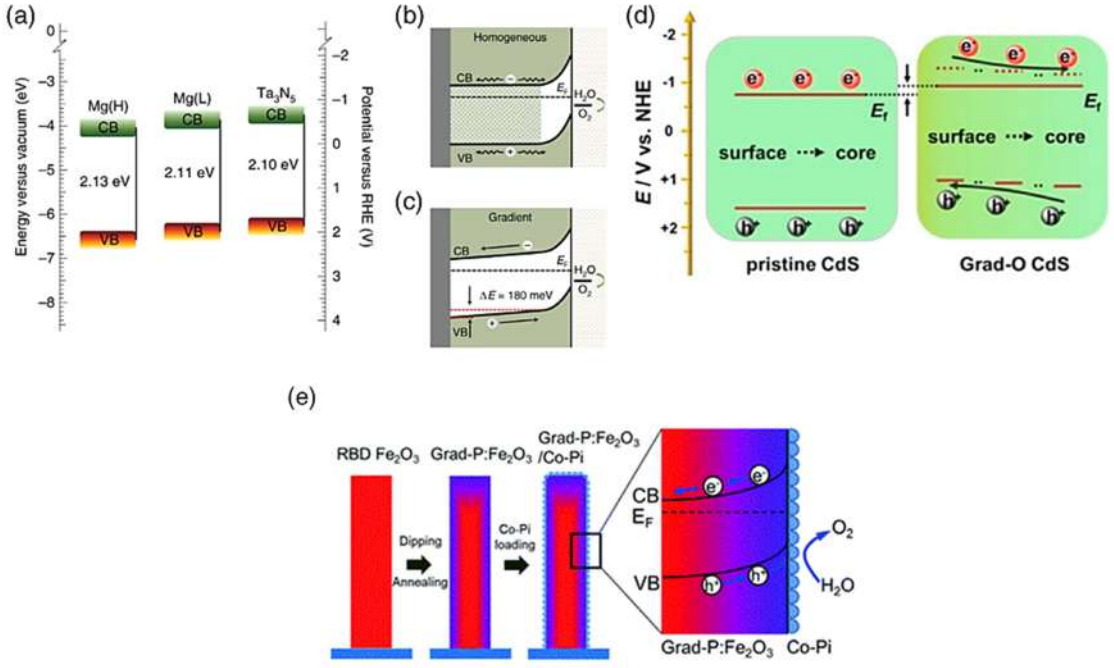

Fig. 14. a) Schematic energy band structures of Ta_3N_5, Mg(L):Ta_3N_5, and Mg(H):Ta_3N_5. with band bending for b) homogenous and c) gradient Ta_3N_5. Reproduced with permission [249]. Copyright 2022, Springer Nature. d) Band structure of pristine CdS and Grad-O CdS in charge transfer mechanisms. Reproduced with permission. [67] Copyright 2022, Elsevier. e) Diagrams of the preparation process and band bending of a grad-P: Fe_2O_3/Co-Pi photoanode. Reproduced with permission from Ref. [251] based on CC BY 3.0.

substitution Ta doping in hematite with linear electron energy loss spectroscopy (EELS) scanning [66]. The EELS analysis confirmed that a gradient doping of the core-shell hematite homojunction nanorods enhanced photocurrent density and improved the turn-on potential. In another group, the oxygen gradient doping could induce S vacancies in In_2S_3 with PVP treatment, which enhanced charge carrier, reactive sites, charge separation and transfer [250]. Moreover, Yu et al. doped oxygen to dendritic CdS nanorods with a radial doping gradient which induced a continuous band-bending structure to promote directional photocarrier transport from the surface to the core and Ti substrate, as seen in Fig. 14d [67]. Luo et al. also successfully created gradient P doping to cause upward bending in the energy band with a broader area, which increases the conductivity of Fe_2O_3. The P dopant also promoted a charge separation with a radial direction, as shown in Fig. 14e [251].

Introducing vacancies in lattices with a similar concept of doping produces lattice distortion and terminates the periodic arrangement of crystals that makes defects. The generated defect states in the bandgap expand the light response and promote charge carrier separation [252–254]. For example, Zheng et al. deposited a crystalline TiO_2 on a silicon-based photoanode with gradient oxygen vacancy [255]. The constructed gradient oxygen defects created channels for the charges to pass through the TiO_2 layer, which improved the distribution and number of transport channels, as evidenced by conductive atomic force microscopy (C-AFM). It was found that the gradient oxygen doping promoted PEC performances by increasing the conductivity and carrier concentration and also avoiding severe recombination in uniform oxygen doping. Therefore, the gradient energy band widened the depletion layer to promote effective directional charge transfer and separation.

Some works with suitable element doping will be discussed to show critical progress in hematite photoanode for PEC water splitting. The strategy is considered effective in alleviating carrier recombination as the experimental data indicates doping can enhance charge carrier mobility and concentration. Recent reports show various dopants of Nb (V) [256], Ti(IV) [257,258], Si(IV) [259], Zr(IV) [260], Sn(IV) [262], and Pt [261] incorporated in hematite demonstrated better charge separation and transfer. Among the n-type metal dopants, Ti (IV) in hematite exhibited higher photocurrent at 2.25 mA/m^2 at 1.23 V_{RHE} for water oxidation. There are no morphology and surface structure changes after Ti doping. However, the donor concentration was significantly increased with improved PEC water oxidation [257]. In the other work, the donor concentration of hematite was enhanced by 20 times after Ti-doping compared to the undoped hematite [258]. Moreover, Zr (IV) dopant in α-Fe_2O_3 increased one order magnitude of donor concentration, implying a higher conductivity of α-Fe_2O_3 [260]. In the case of non-transition metal dopants, Sn(IV) and Si(IV) exhibited a practical improvement in water oxidation activity [259,262]. Lukowski et al. confirmed that the Si-doped α-Fe_2O_3 nanowire has a donor concentration (4×10^{-3} Ωm), which is higher than the undoped one with donor density (4×10^{2} Ωm) [259]. The conductivity on charge transfer and injection in hematite was revealed by Ling et al. by preparing Sn-doped α-Fe_2O_3 through thermally-induced diffusion [262]. Further analysis by Tamirat et al. indicated that the Sn diffusion led to a gradient doping, creating steeper voltage and improving the carrier separation. These two factors significantly enhanced the PEC performance of hematite photoanode [263]. Although the gradient doping improved the PEC performance, some issues, such as radius mismatch with the matrix lattice, will limit the doping concentration [264]. Some scientists debated that mono doping will create recombination centers to lower the charge mobility and concentration [265]. Another study demonstrated that hematite with co-doping exhibited higher catalytic activities than single doping. The reason is that two-ion doping can reduce the recombination center and efficiently improve the charge transport [266]. For example, the result in Tamirat's group indicated that single gradient doping of Sn-hematite only achieved photocurrent at 0.86 mA/m^2 with 1.23 V_{RHE}. However, when it was co-doped with Zr, the photocurrent was further increased to 1.34 mA/m^2. The progress can be attributed to the synergistic effect of Sn and Zr dopants that alter the conductivity three times higher than the one with only Sn doping [263]. In addition, the other report on Si and Ti co-doped hematite also confirmed a higher PEC efficiency for water oxidation. The co-doping strategy successfully overcomes the mismatch of ion radius between Fe, Ti, and Si with improved carrier concentration, evidenced by Mott-Schottky analysis [70]. Therefore, the IPCE of Si, Ti codoped hematite film achieved to 34% at 365 nm and 0.6 $V_{Ag/AgCl}$ for the onset potential. The other improvement with codoping of Sn and Mg to hematite system also have been done by Xie et al. to reach a maximal 1.1 mA/cm^2 at 1.23 V_{RHE}, which increases about 3 times than that of pristine hematite [267]. The improvement is attributed to structural directing agents of Mg and Sn that lead a proper lattice arrangement. The realiving lattice distortion improves the charge injection and transfer efficiencies without changing the carrier concentration, which was evidenced with EIS analysis. As we can see from the above examples, the attempts of doping is to improve the limited conduction property of hematite, regardless of single or codoping strategy [268]. Nevertheless, some contraditive concepts are found in recent work on Ti^{4+} doped into hematite to generate electron-hole recombination centers on Ti surface sites. On the other hand, it is also reported that Ti^{4+} doped into hematite might capture and store the generated holes for water oxidation [269]. Further works on the special effect of surface defect on the charge transfer property of hematite are required. Some interesting works using gradient doping strategy are summarized in Table 6.

3.6. Ternary oxide-based photoanodes

Ternary oxides consist of two different metal ions in an oxide matrix. Significant progress has been made in investigating ternary oxide-based photoanodes for PEC-WS processes. The advantages of using ternary oxides are providing more opportunities to tune the atomic and electronic structures of photoelectrodes and their compositions that can directly influence their photoelectrochemical properties. The recent ternary oxide-based semiconductors crucial for PEC-WS can be classified as ternary iron oxide, tungsten oxide, and vanadate.

3.6.1. Ternary iron oxides

A relatively good photoanode activity was observed in the ternary spinel structures, such as $ZnFe_2O_4$, $MgFe_2O_4$, and $CuFe_2O_4$. The spinel $ZnFe_2O_4$, with many advantageous features of Fe_2O_3, has been widely studied as a photoanode. These advantages include low cost and environmentally benign nature, a visible-light active bandgap (1.9–2.1 eV), and excellent stability in base solution [270–273]. Despite this advantage, the performances of $ZnFe_2O_4$ photoanodes are inferior to those of Fe_2O_3. The most remarkable performances of $ZnFe_2O_4$ for PEC solar water oxidation are summarized in Table 7 [274–279].

In 1985, Blasse et al. investigated the $ZnFe_2O_4$ photoanode prepared as a pellet using solid-state methods, annealing at 700 °C in a nitrogen ambient to improve its n-type character. However, the generated photocurrent in NaOH electrolyte under 300 nm light illumination was low (0.01 mA/cm^2 at 1.23 V_{RHE}). Further improvement, Wijayantha et al. synthesized $ZnFe_2O_4$ photoanodes with aerogel-assisted chemical vapor deposition (CVD), in which the particle size and porosity of the sample could be controlled by changing the solvent during the preparation process [280]. They observed that a decrease in particle size and an increase in the surface area improved the photocurrent density of water oxidation from 0.08 to 0.16 mA/cm^2 at 1.23 V_{RHE} in NaOH electrolyte. The result implies that bulk charge carrier recombination is one of the main limitations of $ZnFe_2O_4$, which is also the primary challenge in Fe_2O_3.

In the other group, Lee et al. prepared $ZnFe_2O_4$/FeOOH nanorod arrays (diameter = 40 nm, thickness = 400 nm) on fluorine-doped tin oxide (FTO) glass using chemical bath deposition [274]. The $ZnFe_2O_4$ was drop-casted with aqueous $Zn(NO_3)_2$ solution on FeOOH electrodes and annealed to form $ZnFe_2O_4$. After removing the excess ZnO layer in

Table 5
Summary of PEC performances using heterojunction formations.

Sample	V_{onset}	J (1.23 V_{RHE})	Electrolyte	H_2 evolution rate	Ref.
$CdIn_2S_4/In_2S_3$	0.02 V_{RHE}	2.98 mA/cm^2	0.5 M Na_2SO_4	-	[229]
g-C_3N_4/rGO/PDIP	-	-	-	15.80 μmol h^{-1}	[233]
$ZnIn_2S_4$/CdS/ZnO	- 0.03 V_{RHE}	3.48 mA/cm^2	0.5 M Na_2SO_4	/	[235]
aza-CMP/C_2N	-	-	-	5.0 μmol g^{-1}	[238]
α-Fe_2O_3/Au/TiO_2	-	1.05 mA/cm^2	1 M NaOH	18.67 μmol cm^{-2}h^{-1}	[234]
BP/RP	-	-	-	0.33 mmol g^{-1}h^{-1}	[236]
BN ZnO/TiO_2	-	2.75 mA/cm^2	0.2 M Na_2SO_4	45.6 μmol cm^{-2}h^{-1}	[237]
aza-CMP/RGO/C_2N	-	-	-	10.0 μmol g^{-1}	[238]
TiO_2/CdS	-	-	-	11.9 mmol h^{-1}m^{-2} for CH_4	[239]
NiCoFe-B_i/Mg:Ta_3N_5/Nb	0.40 V_{RHE}	8.5 mA/cm^2	1.0 M KOH	-	[249]
NiFe(OH)$_x$/Ta:Fe_2O_3 @Fe_2O_3	0.55 V_{RHE}	3.22 mA/cm^2	1.0 M KOH	-	[66]
S_v-$ZnIn_2S_4$/$MoSe_2$	-	-	-	63.21 mmol g^{-1} h^{-1}	[240]
Zn/In:SnS_2	0.3 V_{RHE}	0.23 mA/cm^2	0.5 M Na_2SO_4	-	[247]
WO_3/In_2S_3-P	0.02 V_{RHE}	1.61 mA/cm^2	0.1 M Na_2SO_4	-	[250]
Grad-O CdS/Ti	-	6.0 0.1 mA/cm^2	1.0 M Na_2SO_4/1.0 M N_2H_4·H_2O	-	[67]
grad-P:Fe_2O_3/Co-Pi	-	2.0 mA/cm^2	1 M KOH	-	[251]
Pd/b2-TiO_2/b-Si	0.32 V_{RHE}	8.3 mA cm^{-2} (0 V_{RHE})	1.0 M NaOH	-	[255]
In_2O_{3-x}/In_2S_3	0.75 V_{RHE}	1.28 mA/cm^2	1.0 M KOH	-	[227]
FH-TiO_2	-	2.24 mA/cm^2	6 M KOH/10% v/v methanol	1.441 mmol g^{-1}h^{-1} 0.566 mmol g^{-1}h^{-1}	[222]
$NiFeO_x$/B-C_3N_4/Mo-$BiVO_4$	0.34 V_{RHE}	5.93 mA/cm^2	PPB (pH= 7)	77.5 μM h^{-1}	[220]
Ta_3N_5/$BaTaO_2N$	-	-	-	27.3 μmol h^{-1}	[228]

Table 6
Summary of PEC performances using gradient doping strategy.

Sample	J (1.23 V_{RHE})	V_{onset} (V_{RHE})	Electrolyte	Ref.
Grad-O CdS/Ti	6.0 0.1 mA/cm^2	-	1.0 M Na_2SO_4/1.0 M N_2H_4·H_2O	[67]
Pd/black-TiO_2/black-Si	8.3 mA cm^{-2} (0 V_{RHE})	0.32	1.0 M NaOH	[255]
grad-P:Fe_2O_3/Co-Pi	2.0 mA/cm^2	-	1 M KOH	[251]
WO_3/In_2S_3-P	1.61 mA/cm^2	0.02	0.1 M Na2SO4	[250]
Zn/In:SnS_2	0.23 mA/cm^2	0.30	0.5 M Na_2SO_4	[247]
NiFe(OH)$_x$/Ta:Fe_2O_3 @Fe_2O_3	3.22 mA/cm^2	0.55	1.0 M KOH	[66]
NiCoFe-B_i/Mg:Ta_3N_5/Nb	8.5 mA/cm^2	0.40	1.0 M KOH	[249]
Ti:Fe_2O_3	2.25 mA/cm^2	0.90	1.0 M NaOH	[257]
Sn:Fe_2O_3	1.86 mA/cm^2	0.85	1.0 M NaOH	[262]

NaOH solution, pure $ZnFe_2O_4$ films could be obtained. The obtained photocurrent density of as-prepared $ZnFe_2O_4$ photoanodes was 0.24 mA/cm^2 at 1.23 V_{RHE} after a microwave heat treatment [282,283]. The authors demonstrated that the microwave treatment could increase the charge separation from 4% to 8% at 1.23 V_{RHE} by improving the $ZnFe_2O_4$ crystallinity. The crystallinity was confirmed by a decrease in the full width at half-maximum (FWHM) of X-ray diffraction (XRD) peaks. In addition, they also showed that the microwave treatment increased oxidation efficiency from 10% to 80% at 1.23 V_{RHE} by decreasing surface defect sites, which formed during a removal process of the excess ZnO layer. Finally, the stability of $ZnFe_2O_4$ at 1.23 V_{RHE} could achieve 0.24 mA/cm^2 for 3 h.

In a further study, Lee et al. synthesized $ZnFe_2O_4$ using a combination treatment of microwave and H_2. [278] They introduced a thin TiO_2 layer between the FTO and $ZnFe_2O_4$ layer to hinder the electron transfer from FTO to the electrolyte. The TiO_2 layer was synthesized with spin coating using Ti(IV) diisopropoxide bis(acetylacetonate) solution on FTO, followed by annealing at 250 °C. The thickness of TiO_2 layer was ~2 – 7 nm. FeOOH nanorods were grown on the FTO/TiO_2 substrate using a reported method [274]. Subsequently, aqueous $Zn(NO_3)_2$ solution was drop-casted onto FeOOH nanorods with a 2-min microwave process to form $ZnFe_2O_4$ without annealing. The excess ZnO was soaked in NaOH solution. The microwave treatment produced $ZnFe_2O_4$ nanorods with a diameter of 60 – 80 nm, which is better than that prepared with annealing in a furnace to maintain the conductivity of FTO substrate [24]. As a result, the FTO/TiO_2/$ZnFe_2O_4$ photoanode could generate a photocurrent density of ~ 0.22 mA/cm^2 at 1.23 V_{RHE} in NaOH electrolyte. Further treatment with H_2 at 200 °C for 2 h, the photocurrent density increased from 0.22 to 0.79 mA/cm^2 at 1.23 V_{RHE} due to the increased oxygen vacancy sites. Further analysis showed that the H_2 treatment increased charge separation from 10% to 24% and oxidation efficiency from 51% to 77%. To further improve the performances of FTO/TiO_2/$ZnFe_2O_4$ photoanode, an amorphous $NiFeO_x$ as a co-catalyst layer was deposited on H_2-treated FTO/TiO_2/$ZnFe_2O_4$ with a photolysis method using 1-sun illumination for 10 min, followed by a heat treatment at 100 °C. The resulting FTO/TiO_2/$ZnFe_2O_4$/$NiFeO_x$ electrode generated a photocurrent density of ~ 0.92 mA/cm^2 at 1.23 V_{RHE} in NaOH electrolyte.

The primary carrier density of a material can be increased with atomic doping, which is another possible method to enhance charge separation efficiency. Li et al. fabricated Ti-doped $ZnFe_2O_4$ using spray pyrolysis and annealing steps to replace Fe^{3+} with Ti^{4+} [281]. The

Table 7
Solar water oxidation performances of ternary oxide photoanodes used a single photon absorber in KOH solution.

Sample	Synthesis method	Onset potential	J (1.23 V_{RHE})	IPCE (1.23 V_{RHE}) at 400 nm	References
$ZnFe_2O_4$	Drop casting	0.64	0.24	7%	[274]
$ZnFe_2O_4$	Chemical vapor deposition	0.88	0.35	10%	[280]
$MgFe_2O_4$/$NiFeO_x$	Drop casting	0.64	0.04	3.5% at 1.1 V_{RHE}	[276]
$CuFe_2O_4$/ $NiFeO_x$	Drop casting	0.80	0.15	4% at 1.1 V_{RHE}	[276]
$ZnFe_2O_4$	Atomic layer deposition	0.90	0.26	2%	[279]
$ZnFe_2O_4$	Spray pyrolysis	0.95	0.35	3%	[281]
$ZnFe_2O_4$/$NiFeO_x$	Drop casting	0.53	0.35	8% at 1.1 V_{RHE}	[276]
TiO_2/ $ZnFe_2O_4$/$NiFeO_x$	Drop casting	0.62	0.92	8%	[277]

incorporation of Ti into the $ZnFe_2O_4$ lattice was proved with a slight shift of the (220) peak in XRD pattern to a higher angle of two theta values. The authors confirmed that only 6% Ti in the site of Fe in $ZnFe_2O_4$ lattice with XPS analysis. It was observed that the J-V plot indicated photocurrent density was improved from 0.05 to 0.35 mA/cm^2 at 1.23 V_{RHE} in NaOH solution with the same onset potential. In addition, Mott-Schottky analysis showed that the carrier density of $ZnFe_2O_4$ increased without a change of flat-band potential. However, there is no basic explanation of Ti doping in improving the photocurrent. More investigation is needed to explore the doping effect on photoanode performance.

Furthermore, n-type $MgFe_2O_4$ also possesses a spinel structure with a bandgap of 2.0 – 2.2 eV [284]. However, only a few studies discussing $MgFe_2O_4$ as a photoanode have been reported recently [285–288]. Those works used $MgFe_2O_4$ as an overlayer on Fe_2O_3 [287] and as an n-type layer on p-type $CaFe_2O_4$ to form a heterojunction [288]. There is limited information available discussing $MgFe_2O_4$ properties used as an active light absorber. The CB position of $MgFe_2O_4$ was confirmed to be more negative than 0 V_{RHE} with Mott-Schottky measurements and detection of H_2 production on $MgFe_2O_4$ when it was used as a photocatalyst [289]. Another n-type $CuFe_2O_4$ has a bandgap reported to be 1.3–1.5 eV [284]. It has a disordered spinel structure, in which Cu^{2+} and Fe^{3+} ions can occupy Td and Oh sites [290,291]. The occupation degree of both ions on Td and Oh sites vary depending on the synthesis method. In addition, the $CuFe_2O_4$ CB position was also located above 0 V_{RHE} by H_2 generation detection on $CuFe_2O_4$ when used as a photocatalyst [292].

Sivula et al. compared the PEC performances of $MgFe_2O_4$ and $CuFe_2O_4$ with those of $ZnFe_2O_4$ [276]. $MgFe_2O_4$ and $CuFe_2O_4$ have a direct bandgap at 1.0 and 1.3 eV, respectively. $MgFe_2O_4$ and $CuFe_2O_4$ could generate photocurrent densities of ~ 0.1 and 0.30 mA/cm^2, respectively, at 1.23 V_{RHE} in NaOH electrolyte with H_2O_2 as a hole scavenger. Based on those results, the charge-carrier separation efficiency of $MgFe_2O_4$ and $CuFe_2O_4$ is determined to be 2% and 3%, respectively. The efficiency is much lower than that of $ZnFe_2O_4$ (12%) reported in the same paper. The authors claimed the flat-band potentials of $MgFe_2O_4$ and $CuFe_2O_4$ to be ~0.65 and ~0.8 V_{RHE} using the onset photocurrent measured for H_2O_2. However, it cannot explain if the positive flat-band potentials are insufficient doping level or fast surface recombination. In many papers, the limitation of $MgFe_2O_4$ and $CuFe_2O_4$ is similar to those of Fe_2O_3 and $ZnFe_2O_4$. The improvement of PEC properties of those spinel structures depends on their preparation methods.

3.6.2. Ternary tungsten oxides

One of the most studied materials with a bandgap of 2.2 – 2.3 eV is $CuWO_4$ [293]. $CuWO_4$ has several advantages compared to WO_3 in terms of a smaller bandgap, allowing greater utilization of visible light. The reduced bandgap energy is due to the upward shift of VB as hybridized Cu 3d and O 2p orbitals; however, the CB remains similar to that of WO_3 [294]. In addition, $CuWO_4$ is claimed to be stable in pH 7 – 9, in which WO_3 is unstable. [295–297] The samples of $CuWO_4$ and WO_3 photoanodes were synthesized with electrodeposition. $CuWO_4$ exhibited a very stable photocurrent for 12 h, while WO_3 experienced a continuous photocurrent decay [28,294]. The data proved that $CuWO_4$ is more durable than WO_3 during water oxidation without any additional oxygen-evolved catalyst. The works suggest that $CuWO_4$ is thermodynamically stable against photocorrosion at a slower rate than water oxidation.

Although $CuWO_4$ exhibits a relatively stable performance, it appears to have poor charge carrier separation. Smith et al. investigated photocurrent generation using $CuWO_4$ thin film in phosphate buffer solution using H_2O_2 as a hole scavenger. They reported that the charge carrier separation of porous $CuWO_4$ film prepared with spray pyrolysis was 3% at 1.23 V_{RHE} [298]. The utilization of H_2O_2 will give a current doubling effect that delivers a biased value of charge separation efficiency. The actual value may be lower than the reported one [299]. Furthermore, Hamann et al. confirmed the current doubling effect of H_2O_2 by investigating the oxidation of sulfite and H_2O_2 in borate buffer at pH= 9. By comparing photocurrents generated with oxidation of H_2O_2, H_2O, and sulfite in borate buffer. The photocurrent obtained from H_2O_2 oxidation is higher than that for sulfite oxidation. [300] The sulfite oxidation induced an onset potential shift from 0.85 to 0.6 V_{RHE} compared to water oxidation. The result reveals that the main challenge of using $CuWO_4$ photoanodes is poor charge separation, and water oxidation is not a limiting factor. Additional co-catalyst of oxygen evolution cannot significantly enhance the water oxidation due to its intrinsic high recombination rate, except manganese phosphate as the co-catalyst in a $CuWO_4/WO_3$ composite photoanode [28,301].

As discussed in the previous section, doping is a good strategy for designing photoanode. The improvement in charge separation, carrier density, and charge transport properties in ternary oxide also can be done with atomic doping. Smith et al. incorporated Fe^{3+} into a $CuWO_4$ lattice, substituting the octahedrally coordinated Cu^{2+} with spray pyrolysis [298]. It is noticed that the doped $CuWO_4$ exhibited an increase in photocurrent for water and H_2O_2 oxidation at 1.23 V_{RHE} in neutral phosphate buffer. Although the photocurrent is improved, the role of the dopant was not clearly determined, and no direct evidence was observed in the charge carrier density. In addition, Co^{2+}, Fe^{3+}, and Zn^{2+} as dopants to substitute Cu^{2+} were also demonstrated to advance the PEC performances [28,302]. Besides the doping, H_2-treatments were also employed to increase the carrier density and charge carrier separation of $CuWO_4$ [303,304]. It is demonstrated by Diao et al. by annealing CuWO4 film in a 5% H_2-dissolved Ar at 250 °C. The photocurrent density enhanced from 0.30 to 0.45 mA/cm^2 at 1.23 V_{RHE} in a neutral phosphate buffer [304]. Moreover, the carrier density was improved by 2.7 times, confirmed by Mott-Schottky analysis. The importance of H_2 treatment is to increase W^{5+} concentration to balance the positive charge oxygen vacancy.

The other crucial improvement of $CuWO_4$ is decreasing the bulk resistance of a material. For instance, the additional multi-walled carbon nanotubes (MWCNTs) to $CuWO_4$ induced an alternative charge-carrier pathway [305]. In the study, spray-pyrolyzed $CuWO_4$ films were added with MWCNTs with a MWCNT:$CuWO_4$ precursor weight ratio of 1:10,000. However, the increase of photocurrent of water oxidation in the carbonate buffer solution was not obvious, as the current change was from 0.20 to 0.225 mA/cm^2 at 1.23 V_{RHE}. Therefore, the nanostructured films with a particle size smaller than the charge carrier diffusion length, which has been discussed, is an important strategy to improve the charge carrier separation. It was determined that the hole diffusion length of $CuWO_4$ was ~ 30 nm with time-resolved microwave conductivity (TRMC) measurements [306]. The relatively small diffusion length of $CuWO_4$ is a challenge to nanostructuring materials that can enhance bulk charge separation. Recently, several attempts were done to nanostructure $CuWO_4$ electrodes with high surface area, including the nanostructured WO_3 [296,304,307]. Li et al. prepared a $CuWO_4$ photoanode with vertically oriented $CuWO_4$ nanoflakes and showed the best photocurrent only reached ~0.4 mA/cm^2 at 1.23 V_{RHE} due to surface states [304]. The presence of surface states in $CuWO_4$ photoelectrodes was investigated and the results showed a possible cause for this low photocurrent. Barlett et al. fabricated a dense polycrystalline $CuWO_4$ film by spin-coating a sol-gel precursor and studied the presence of surface states with electrochemical impedance spectroscopy (EIS) [308]. Mott-Schottky analysis was used to reveal the Fermi level pinning of $CuWO_4$, which was found in the potential region of 0.81 – 1.01 V_{RHE} as low frequencies were used. At a higher frequency, the Fermi level pinning is disappeared. It was observed that the Fermi level pinning was at the same potential region in the dark and light-illuminated conditions. The data revealed that the Fermi level was pinned at the permanent surface states in their $CuWO_4$. However, the particular position of the Fermi level could not be determined. In addition, they also discussed that the surface states limit water oxidation rate and serve as

recombination centers that cause a late photocurrent onset. The Fermi level pinning was also investigated by Hamann et al. that the atomic layer deposited $CuWO_4$ films did not show Fermi level pinning in Mott-Schottky analysis in dark and illuminated conditions [309]. They proved that the surface states were available with Bode plots, cyclic voltammetry (CV), and EIS analysis. The surface states are formed only during electrochemical or photoelectrochemical water oxidation. Based upon the results, those surface states in $CuWO_4$ electrodes are not intrinsic states, suggesting they are formed due to water oxidation intermediates. They also concluded that the intermediates recombined with electron in CB were responsible for the photocurrent difference for sulfite and water oxidation.

Besides the challenges of bulk recombination and existing surface states, $CuWO_4$ possesses relatively wide bandgap energy. Therefore, an effort to decrease its bandgap was conducted to improve the light absorption capability. Choi et al. synthesized solid solutions by combining $CuWO_4$ and $CuMoO_4$ to form $CuW_{1-x}Mo_xO_4$ films with electrodeposition and annealing treatment at 500 °C in air [309]. The as-prepared $CuW_{0.35}Mo_{0.65}O_4$ photoanode decreased its bandgap from 2.3 to 2.0 eV. Subsequently, the photocurrent generation of $CuW_{0.35}Mo_{0.65}O_4$ photoanode enhanced for water oxidation from 0.06 to 0.15 mA at 1.23 V_{RHE} in a neutral phosphate buffer. On the other hand, density functional theory (DFT) calculations revealed that Mo doping decreases due to the lowered CBM without raising the VBM, thus thermodynamically unfavorable for HER. Most studies suggest common strategies to improve $CuWO_4$; there is no new improvement in the approach to separate the charge carrier. Further attempts to improve the PEC properties of $CuWO_4$ as a single light absorber are challenging. Especially compared with ternary metal ferrites, the CB and VB $CuWO_4$ are less favorable, suggesting $CuWO_4$ is less promising for a photoanode application.

As the ternary oxide metal ferrites are more promising than $CuWO_4$, Fe_2WO_6 with a bandgap of 1.5 – 1.7 eV may be favorable for development. Nevertheless, only a few studies reported the PEC performances of Fe_2WO_6 [310,311]. Fe_2WO_6 has several limitations when used as a photoanode for a PEC-WS process. Abdi et al. fabricated Fe_2WO_6 thin films with spray pyrolysis and found their flat-band potential at 0.6 – 0.65 V_{RHE} using Mott-Schottky analysis [311]. Furthermore, the VB position is determined with ultraviolet photoelectron spectroscopy (UPS) measurements and the result shows it is at 1.7 eV below the Fermi level. As a result, the CB position is very close to the Fermi level and limits the photovoltage gain for water oxidation. Another major limitation of Fe_2WO_6 is its relatively low absorbance coefficient with long α^{-1} of 1000 nm at $\lambda = 450$ nm, which reveals that Fe_2WO_6 is not a good light absorber [311]. The charge carrier separation and hole diffusion length of Fe_2WO_6 film were only 5% and 10 nm, respectively [311]. After some studies of this material, the unfavorable band edges, poor light absorption, and severe charge recombination make Fe_2WO_6 not a promising photoanode for the PEC-WS process. As a result, More work is required to improve the iron tungsten-oxide-based photoanodes to overcome all the limitations.

3.6.3. Ternary vanadate oxides

One of the promising and common ternary vanadate oxides for photoanode material is n-type $BiVO_4$ with a bandgap of ~2.4 – 2.5 eV [270]. $BiVO_4$ is reported to have a flat-band potential lower than hydrogen reduction potential at ~0.1 V_{RHE} [312–319]. Most photocurrent onset appeared at ~0.25 V_{RHE} has been demonstrated for water oxidation as $BiVO_4$ was composited with co-catalysts [312–317]. As the photocurrent onset could achieve at 0.25 V_{RHE}, the photovoltage of $BiVO_4$ is equivalent to ~1 V for water oxidation, which is very rare in many photoanode materials. This feature makes $BiVO_4$ an exciting material for photoanode development. Consequently, $BiVO_4$ is potentially used for a no-external-biased WS process when coupling with a photocathode (e.g. p-Si, p-Cu_2O) which photovoltages for water reduction are limited [312]. Another advantage feature of BiVO4 is the excellent charge carrier separation that reaches ≥ 90% at 1.23 V_{RHE}. As a comparison, typical oxide-based photoanodes only exhibit charge carrier separation efficiency of < 10% at 1.23 V_{RHE} [312,313]. Although at low bias potential, $BiVO_4$ still indicates 70% charge carrier separation, approximately at 0.6 V_{RHE} [313]. In addition, the charge recombination rate of $BiVO_4$ is not as high as many other oxide-based materials. For instance, the surface hole can ultimately be used for sulfite oxidation, in which the sulfite oxidation can reach 100%. In other words, the photocurrent onset for sulfite oxidation is very close to the flat-band potential of $BiVO_4$. Therefore, when $BiVO_4$ is composited with another oxygen-evolved catalyst, the water oxidation rate can be enhanced, equivalent to that of sulfite, indicating that the photocurrent onset for water oxidation is very close to its flat-band potential. Another advantage of $BiVO_4$ is stability against photocorrosion, in which the photocorrosion rate is relatively low. The phenomenon indicates that the holes are easily consumed during the interfacial charge transfer reactions. As a result, the PEC cell with $BiVO_4$ commonly performed an unbiased WS process for at least 1-h stability in composited cells, as shown in Tables 8 and 9 [272,312,316,320,321].

Besides bismuth vanadate, copper vanadates also received growing attention as photoanode candidates for the PEC WS process. The first investigation on copper vanadates (γ-$Cu_3V_2O_8$) was done by Neale et al. [327] The copper vanadates were prepared with dip coating FTO substrate into $Cu_3V_2O_7(OH)_2 \bullet 2\ H_2O$ solution followed by annealing to form γ-$Cu_3V_2O_8$. The interconnected 20-nm nanoparticles of γ-$Cu_3V_2O_8$ with a hole diffusion length of ~20 – 40 nm could deliver a photocurrent of 10 μA/cm^2 at 1.23 V_{RHE} during water oxidation reaction at pH= 9.2 in borate buffer. [328] The CuO-V_2O_5 phases were reported as copper vanadate phases with bandgaps of ~2 eV [328,329]. Different β-$Cu_2V_2O_7$, γ-$Cu_3V_2O_8$, α-CuV_2O_6, $Cu_{11}V_6O_{26}$, and $Cu_5V_2O_{10}$ have been studied as photoanodes for solar-water splitting [327,328,330, 331–335]. The bandgap values of all these copper vanadates exhibit a bandgap of 1.8 – 2.0 eV, which is favorable for a visible-light absorbance. Nevertheless, the obtained photocurrent for water oxidation was still below 100 μA/cm^2 at 1.23 V_{RHE}, regardless of the preparation conditions and phases. To improve the photocurrent, one of the strategies is doping Mo and W into V sites. The Mo^{6+} and W^{6+} replace V^{5+} ions in ternary vanadate oxides, such as $BiVO_4$, can effectively increase the carrier densities of materials [336,337]. For instance, Neale et al. showed that Mo doping of γ-$Cu_3V_2O_8$ successfully enhanced the photocurrent density from 10 to 25 μA/cm^2 at 1.23 V_{RHE} at pH= 9.2 in borate buffer [327]. It was confirmed that the increased photocurrent was due to the enhanced carrier density, as observed by Mott-Schottky analysis. The onset potential was not shifted in water and sulfide oxidation reactions. Choi et al. prepared Mo- and W-codoped $Cu_{11}V_6O_{26}$ by preparing CuO nanofiber films and annealing with a $VO(acac)_2$ solution containing Mo or W precursors [334,338]. The incorporation of Mo and W was confirmed with peak shifts to lower two-theta in XRD analysis. Mott-Schottky plots indicated a decrease in the slope and a negative shift in the flat-band potential, suggesting an increase in the carrier concentration. The highest photocurrent density was achieved with W-doped $Cu_{11}V_6O_{26}$ film and reached a value of 70 μA/cm^2 for water oxidation at 1.23 V_{RHE} in borate buffer. Moreover, the onset potential was shifted from 0.99 to 0.87 V_{RHE} for water oxidation.

Another triclinic $FeVO_4$ is promising for photoanode since it can form under ambient conditions. The potential of triclinic $FeVO_4$ as a photoanode was introduced by Sayama et al. [339]. The bandgap of $FeVO_4$ is ~2.0 eV, smaller than that of $BiVO_4$ [11,340–344]. The flat-band potential of $FeVO_4$ is about 0.7 V below the water reduction potential that limits the photovoltage to ~ 0.5 V. [345] The reported performance of $FeVO_4$ remains relatively low and the improvement of photocurrent generation with substitutional doping into the V-site is one of the possibilities. Baeg et al. doped 5% W to $FeVO_4$ photoanode by spin-coating on FTO substrates followed by annealing [342]. The doping of W was proved with a peak shift in XRD analysis due to the larger ionic radius of W^{6+} compared to V^{5+}. The pristine $FeVO_4$ film exhibited an

Table 8
$BiVO_4$-based photoanodes with solar cells to support the external bias of cells.

$BiVO_4$-based photoanodes	Power Systems	Electrolytes	$J_{operational}$ (mA/cm^2)	STH (%)	References
W:$BiVO_4$/CoPi	Si-solar cells (Si SCs)	Carbonate (pH= 7)	3 – 4.2	3.6–5.2	[311,321]
Mo:$BiVO_4$/CoCi	$CH_3NH_3PbI_3$	Carbonate (pH= 9)	3.5	4.3	[48]
Mo:$BiVO_4$/FeOOH/NiOOH and Ti:Fe_2O_3/TiO_2/NiFeOx	Si-SCs	Carbonate (pH= 9)	4.5 3.2	5.6 3.9	[312]
Mo:$BiVO_4$/FeOOH/NiOOH	Perovskite SCs ($FA_{0.83}Cs_{0.17}PbI_2Br$)	Phosphate (pH= 7)	5.7	7.0	[322]
Mo:$BiVO_4$/FeOOH/NiOOH	$CH_3NH_3PbI_3$	Phosphate (pH= 7)	5.0	6.2	[320]
Mo:$BiVO_4$/FeOOH/NiOOH	Cu_2O/Ga_2O_3/TiO_2	Borate (pH= 9)	2.5	3.0	[272]

Table 9
Single-photon-absorber $BiVO_4$-based photoanodes for water oxidation with external bias.

Electrodes	Electrolytes	Onset (V_{RHE})	J at 1.23 V (mA/cm^2)	References
W:$BiVO_4$/CoPi	Phosphate (pH= 7)	0.30	4.0	[321]
$BiVO_4$/$NiFeO_x$-B	Borate (pH= 9)	0.22	4.9	[323]
$BiVO_4$/NiFeOOH	Borate (pH= 9)	0.25	3.8	[324]
$BiVO_4$/FeOOH/NiOOH	Phosphate (pH= 7)	0.2	4.5	[314]
$BiVO_4$/FeOOH/NiOOH	Borate (pH= 9)	0.32	5.9	[325]
$BiVO_4$/FeOOH/NiOOH (N_2 treatment)	Borate (pH= 9)	0.24	4.7	[326]
Mo:$BiVO_4$/FeOOH/NiOOH (H_2 treatment)	Carbonate (pH= 9)	0.24	5.0	[312]
Mo:$BiVO_4$/FeOOH/NiOOH (nanocone substrate)	Phosphate (pH= 7)	0.21	5.8	[320]
Mo:$BiVO_4$/FeOOH/NiOOH (inverse nanocone substrate)	Phosphate (pH= 7)	0.22	6.0	[322]

increased photocurrent generation by 50% at 1.23 V_{RHE} in phosphate buffer with an onset potential of ~0.7 V_{RHE}. IPCE of the W-doped $FeVO_4$ photoanode could reach a maximum value of 6.5% at 400 nm with an external bias of 1.7 V_{RHE}. Besides the doping method, nanoporous morphology is a crucial strategy to shorten the charge extraction path length of $FeVO_4$ [343]. One of the methods to prepare a nanoporous $FeVO_4$ film is using a drop-casting method with citric acid to provide pore formation. The pore size and diameter were observed with SEM images, showing interconnected nanoparticles with diameter and pore sizes of ~50 – 100 nm and ~50 – 200 nm, respectively. The photocurrent of nanoporous $FeVO_4$ film for water oxidation is 100 $\mu A/cm^2$ at 1.23 V_{RHE}. The generated photocurrent with pristine $FeVO_4$ photoanodes remains low. In the other group, Abdi et al. performed thorough studies on pristine and Mo-doped $FeVO_4$ photoanodes to investigate the origin of this low photocurrent generation [345]. After annealing, the spray-pyrolyzed $FeVO_4$ and Mo-doped $FeVO_4$ films on FTO exhibited densely packed particles with a diameter of ~500 nm and thickness varied from 25 to 800 nm. However, the sample with 200 – 400 nm thickness could generate the highest photocurrent. The incorporation of Mo into the lattice was also confirmed with a slight shift in XRD peaks to lower two-theta values. The 2% Mo-doped film exhibited the highest photocurrent generation, supported by a decrease in the Mott-Schottky slope to indicate an increase in the carrier concentration. Flat-band potentials of both pristine and 2% Mo-doped $FeVO_4$ were the same at 0.7 V_{RHE}. The increased photocarrier separation is observed, changing from 2% to 2.5% at 1.6 V_{RHE}. After Mo doping, the water oxidation efficiency was enhanced by 20% at 1.6 V_{RHE}. Those results reveal that the Mo doping effects were negligible, indicating severe bulk recombination is one of the significant limitations of $FeVO_4$. In addition, IPCE values of pristine and Mo-doped $FeVO_4$ photoanodes for water oxidation at 375 nm were 2% and 8%, respectively, in neutral phosphate buffer at 1.6 V_{RHE}. Time-resolved microwave conductivity (TRMC) analysis indicated the hole mobilities of $FeVO_4$ and 2% Mo-doped $FeVO_4$ were 4.6×10^{-5} and 1.3×10^{-4} $cm^2 V^{-1} s^{-1}$, respectively. The hole diffusion length was also enhanced from ~2 nm to ~7 nm after Mo doping. As the diffusion length is concise, improving the bulk separation by nanostructuring may be difficult.

Besides the most investigation on triclinic $FeVO_4$, some studies on other iron vanadates, such as Fe_2VO_4, FeV_2O_4, $Fe_2V_4O_{13}$ have been done [346,347]. The iron and vanadium species (Fe^{2+}, V^{3+}, and V^{4+}) in iron vanadates may not be stable during PEC water oxidation. As a result, the photostability of those compounds needs to be investigated carefully. Bhattacharya et al. performed a photostability analysis for water oxidation in a neutral phosphate buffer at 1.6 V_{RHE}. The results indicated that FeV_2O_4, Fe_2VO_4, and $FeVO_4$ exhibited a significant photocurrent decay after 30 min [346] The studies suggested iron vanadates suffered from short hole diffusion lengths and severe bulk recombination. Successful atomic doping with considerable charge separation has not been demonstrated. Therefore, nanostructuring can be one of the strategies to overcome the extremely short hole diffusion lengths. Another limitation of iron vanadates is the flat-band position is very positive ($\geq$ 0.5 V_{RHE}) even with doping [345,347]. The investigation suggests that the iron vanadates have the same issues as copper vanadates when used as photoanodes in a PEC-WS process.

4. Conclusion and outlooks

In summary, PEC water splitting is a promising technology for generating hydrogen fuel using sunlight. However, the PEC-WS process efficiency is still in the early commercialization step. The progress in developing photoanode materials in the last ten years hints at the charge separation and transfer in modified photoanode materials. The basic required parameters in designing photoanodes and some crucial performance metrics have been briefly discussed. An improved photoanode must indicate cathodically shifted onset photocurrent with a plateau curve to show a good fill factor and high stability performance. Some essential strategies to improve photoanode performances include nanostructuring, co-catalyst, surface passivation, heterojunction (type-II and Z-scheme junctions), gradient doping, and application of ternary oxide-based photoanodes are reviewed.

Some crucial outlooks related to the design of semiconductor nanomaterials for PEC photoanodes are emphasized as follows:

1. Nanostructuring allows a higher aspect ratio to make a shorter hole diffusion length and the charge separation effective with improved light absorption properties. Therefore, 2D materials with a unique morphology offer a promising alternative for photoanode design. Integrating 2D materials with metal oxides (MOs) is an exciting solution to overcome their drawbacks of narrow light absorption, short

charge lifetime, high charge recombination rate, and poor structural stability. Additional strategies with suitable co-catalysts are required to further improve the redox activities on the electrode, reduce the reaction energy barrier, and accelerate the charge transfer for boosting surface chemical reactions. However, the uncontrollable photo corrosion due to excess holes on photoanode surfaces during the PEC-WS process causes material instability. An intermediate inert thin layer is beneficial to add at the interfaces between semiconductor layers with pretty different CB and VB band positions to favorably transfer the generated electron and hole. The fast-moving carriers without delay on the electrode surface help to decrease photo corrosion and improve cell stability. Therefore, introducing the intermediate layer with significant energy band differences can be used as a transition for effective transmission and separation of carriers, thus improving the performance of photoanode PEC-WS process. In addition, a selected suitable electrolyte with an appropriate pH value also plays a vital role in photoanode stab

2. Designing photoanodes with heterojunction formation is a great strategy to improve light absorption, charge carrier separation redox capability with high energy conversion efficiency. A semiconductor with a wide bandgap can be combined with another with a smaller bandgap to optimize the light absorption property and simultaneously maintain a strong redox potential. Nevertheless, it is indicated that the type-II heterojunction sacrifices the generated photovoltages as the charg migration between two CBs and VBs in semiconductor materials. As a result, Z-scheme charge transfer in heterojunc n is intensely explored to overcome a lower photovoltage in type-II heterojunction. The Z-scheme heterojunction will drive the water oxidation on the lowest VB of one semiconductor and the reduction reaction on the highest CB of another semiconductor. This mechanism obviously induces charge separation with an efficient pathway. The advantage of Z-scheme heterojunction is the efficient separation of photocarrier while maintaining a strong redox potential. The coexistence of high-efficiency k phase separation and strong redox capability contributes to a highly efficient PEC water splitting. Nevertheless, the design and characterization of Z-scheme heterojunctions are challenging and need more effective methods for the identification of Z-scheme heterojunctions.
3. The attempt with gradient doping to promote directional charge transport is crucial to improve PEC-WS efficiency. Gradient doping will form a gradient energy band structure and expand the depletion layer with better charge separation in a photoanode. Doping alien elements will increase carrier concentration and conductivity. However, if the dopant is excessive, it will act as a recombination center, inducing a smaller depletion layer and affecting carrier separation. An appropriate dopant with a specific dose will increase the light response of materials by creating a new energy level in the forbidden band. In a particular case, it was found that the gradient oxygen doping in TiO_2 promoted PEC performances by increasing the conductivity and carrier concentration and avoiding severe recombination in uniform oxygen doping. Therefore, the gradient energy band widened the depletion layer to promote effective directional charge transfer and separation.
4. The strategies with nanostructuring, co-catalyst, surface passivation, heterojunction, and doping on photoanodes have been demonstrated to overcome the sluggish water oxidation steps. All the attempts of photoanode do not use only a single semiconductor. Recently, the utilization of multiple semiconductors has been a significant interest in constructing photoelectrode. An effective heterojunction of multiple semiconductors still has issues with unclear charge transfer and separation, which must be addressed carefully to differentiate type II or Z-scheme heterojunctions.
5. Some factors with physical and chemical properties, such as lattice constants, thermal expansion, and band position, should be considered in the heterojunction formation. Although exploring new systems of nanomaterials is crucial for current heterojunction engineering, the mechanism for improving the heterojunction interfaces is still the primary direction of future research instead of selecting materials for trial and stacking.
6. In addition, the recent studies on ternary oxide-based photoanodes, such as ternary iron oxides, tungsten oxides, and vanadates, give some hints at improving the PEC properties. Although the ternary oxide photoanodes are promising, they still need some modifications with doping, nanostructuring, co-catalyst, nitrogen or hydrogen treatments to enhance the water oxidation property. An essential study in the ternary oxide is that the incorporation of different metal doping can vary the energy band position in the oxide, thus varying the PEC properties. The most important ternary oxide photoanode is $BiVO_4$, with many favorable PEC properties, such as the appropriate band position and photostability. Therefore, Modifying $BIVO_4$ by cocatalyst, doping, heterojunction, and coupling with solar cells is interesting to obtain external-bias free PEC water-splitting cells.

Declaration of Competing Interest

The authors declare that they have no known competing financial interests or personal relationships that could have appeared to influence the work reported in this paper.

Data availability

The authors do not have permission to share data.

Acknowledgment

This work is supported by the National Science and Technology Council (NSTC) of Taiwan with a grant number of MOST: 110–2221-E-011–070-MY3.

References

[1] A.R. Fareza, F.A.A. Nugroho, F.F. Abdi, V. Fauzia, Nanoscale metal oxides–2D materials heterostructures for photoelectrochemical water splitting—a review, J. Mater. Chem. A 10 (16) (2022) 8656–8686.
[2] A.M.M.I. Qureshy, M. Ahmed, I. Dincer, Performance assessment study of photo-electro-chemical water-splitting reactor designs for hydrogen production, Int. J. Hydrog. Energy 44 (18) (2019) 9237–9247.
[3] Z. Li, M. Hu, P. Wang, J. Liu, J. Yao, C. Li, Heterojunction catalyst in electrocatalytic water splitting, Coord. Chem. Rev. 439 (2021), 213953.
[4] M.T. Bender, X. Yuan, K.-S. Choi, Alcohol oxidation as alternative anode reactions paired with (photo)electrochemical fuel production reactions, Nat. Commun. 11 (1) (2020) 4594.
[5] D. Liu, J.-C. Liu, W. Cai, J. Ma, H.B. Yang, H. Xiao, J. Li, Y. Xiong, Y. Huang, B. Liu, Selective photoelectrochemical oxidation of glycerol to high value-added dihydroxyacetone, Nat. Commun. 10 (1) (2019) 1779.
[6] H.G. Cha, K.-S. Choi, Combined biomass valorization and hydrogen production in a photoelectrochemical cell, Nat. Chem. 7 (4) (2015) 328–333.
[7] Y. Liu, M. Wang, B. Zhang, D. Yan, X. Xiang, Mediating the oxidizing capability of surface-bound hydroxyl radicals produced by photoelectrochemical water oxidation to convert glycerol into dihydroxyacetone, ACS Catal. 12 (12) (2022) 6946–6957.
[8] L. Luo, Z.-j Wang, X. Xiang, D. Yan, J. Ye, Selective activation of benzyl alcohol coupled with photoelectrochemical water oxidation via a radical relay strategy, ACS Catal. 10 (9) (2020) 4906–4913.
[9] T.H. Jeon, H. Kim, H.-I. Kim, W. Choi, Highly durable photoelectrochemical H2O2 production via dual photoanode and cathode processes under solar simulating and external bias-free conditions, Energy Environ. Sci. 13 (6) (2020) 1730–1742.
[10] S. Bhattacharjee, V. Andrei, C. Pornrungroj, M. Rahaman, C.M. Pichler, E. Reisner, Reforming of Soluble Biomass and Plastic Derived Waste Using a Bias-Free Cu30Pd70|Perovskite|Pt Photoelectrochemical Device, *Adv. Funct. Mater.* 32 (7) (2022) 2109313.
[11] S.W. Hwang, G.S. Han, J.Y. Cho, D.U. Lee, H.S. Han, I.S. Cho, Sharp-edged nanoflakes array of CuO with enhanced optical and charge transport properties for Bias-Free tandem solar Water-splitting, Appl. Surf. Sci. 585 (2022), 152632.
[12] W. He, R. Wang, L. Zhang, J. Zhu, X. Xiang, F. Li, Enhanced photoelectrochemical water oxidation on a BiVO4 photoanode modified with multi-functional layered double hydroxide nanowalls, J. Mater. Chem. A 3 (35) (2015) 17977–17982.
[13] W. He, Y. Yang, L. Wang, J. Yang, X. Xiang, D. Yan, F. Li, Photoelectrochemical Water Oxidation Efficiency of a Core/Shell Array Photoanode Enhanced by a Dual Suppression Strategy, ChemSusChem 8 (9) (2015) 1568–1576.

[14] Y. Li, L. Zhang, X. Xiang, D. Yan, F. Li, Engineering of ZnCo-layered double hydroxide nanowalls toward high-efficiency electrochemical water oxidation, J. Mater. Chem. A 2 (33) (2014) 13250–13258.

[15] S. Shiva Kumar, V. Himabindu, Hydrogen production by PEM water electrolysis – A review, Mater. Sci. Energy Technol. 2 (3) (2019) 442–454.

[16] A. Fujishima, K. Honda, Electrochemical photolysis of water at a semiconductor electrode, Nature 238 (5358) (1972) 37–38.

[17] T.T.A. Lucas, M.A. Melo, A.L.M. Freitas, F.L. Souza, R.V. Gonçalves, Enhancing the solar water splitting activity of TiO2 nanotube-array photoanode by surface coating with La-doped SrTiO3, Sol. Energy Mater. Sol. Cells 208 (2020), 110428.

[18] Y. Chen, X. Feng, Y. Liu, X. Guan, C. Burda, L. Guo, Metal oxide-based tandem cells for self-biased photoelectrochemical water splitting, ACS Energy Lett. 5 (3) (2020) 844–866.

[19] A. Landman, R. Halabi, P. Dias, H. Dotan, A. Mehlmann, G.E. Shter, M. Halabi, O. Naseraldeen, A. Mendes, G.S. Grader, A. Rothschild, Decoupled photoelectrochemical water splitting system for centralized hydrogen production, Joule 4 (2) (2020) 448–471.

[20] C. Ding, J. Shi, Z. Wang, C. Li, Photoelectrocatalytic water splitting: significance of cocatalysts, electrolyte, and interfaces, ACS Catal. 7 (1) (2017) 675–688.

[21] N. Karjule, J. Barrio, L. Xing, M. Volokh, M. Shalom, Highly efficient polymeric carbon nitride photoanode with excellent electron diffusion length and hole extraction properties, Nano Lett. 20 (6) (2020) 4618–4624.

[22] H. Zhu, M. Zhao, J. Zhou, W. Li, H. Wang, Z. Xu, L. Lu, L. Pei, Z. Shi, S. Yan, Z. Li, Z. Zou, Surface states as electron transfer pathway enhanced charge separation in TiO2 nanotube water splitting photoanodes, Appl. Catal. B: Environ. 234 (2018) 100–108.

[23] X.-L. Zheng, J.-P. Song, T. Ling, Z.P. Hu, P.-F. Yin, K. Davey, X.-W. Du, S.-Z. Qiao, Strongly Coupled Nafion Molecules and Ordered Porous CdS Networks for Enhanced Visible-Light Photoelectrochemical Hydrogen Evolution, Adv. Mater. 28 (24) (2016) 4935–4942.

[24] H. Zhu, Y. Zhang, J. Zhu, Y. Li, S. Jiang, N. Wu, Y. Wei, J. Zhou, Y. Song, Crack-free hematite inverse opal photo-anodes for enhancing photo-electrochemical water splitting, J. Mater. Chem. A 8 (43) (2020) 22929–22937.

[25] M. Zhou, Z. Liu, Q. Song, X. Li, B. Chen, Z. Liu, Hybrid 0D/2D edamame shaped ZnIn2S4 photoanode modified by Co-Pi and Pt for charge management towards efficient photoelectrochemical water splitting, Appl. Catal. B: Environ. 244 (2019) 188–196.

[26] G. Liu, Z. Li, T. Hasan, X. Chen, W. Zheng, W. Feng, D. Jia, Y. Zhou, P. Hu, Vertically aligned two-dimensional SnS2 nanosheets with a strong photon capturing capability for efficient photoelectrochemical water splitting, J. Mater. Chem. A 5 (5) (2017) 1989–1995.

[27] F. Ning, M. Shao, S. Xu, Y. Fu, R. Zhang, M. Wei, D.G. Evans, X. Duan, TiO2/graphene/NiFe-layered double hydroxide nanorod array photoanodes for efficient photoelectrochemical water splitting, Energy Environ. Sci. 9 (8) (2016) 2633–2643.

[28] R. Wang, X. Li, L. Wang, X. Zhao, G. Yang, A. Li, C. Wu, Q. Shen, Y. Zhou, Z. Zou, Construction of Al-ZnO/CdS photoanodes modified with distinctive alumina passivation layer for improvement of photoelectrochemical efficiency and stability, Nanoscale 10 (41) (2018) 19621–19627.

[29] S. Chu, S. Vanka, Y. Wang, J. Gim, Y. Wang, Y.-H. Ra, R. Hovden, H. Guo, I. Shih, Z. Mi, Solar Water Oxidation by an InGaN Nanowire Photoanode with a Bandgap of 1.7 eV, ACS Energy Lett. 3 (2) (2018) 307–314.

[30] S. Bai, X. Yang, C. Liu, X. Xiang, R. Luo, J. He, A. Chen, An Integrating Photoanode of WO3/Fe2O3 Heterojunction Decorated with NiFe-LDH to Improve PEC Water Splitting Efficiency, ACS Sustain. Chem. Eng. 6 (10) (2018) 12906–12913.

[31] H. Zhang, W. Zhou, Y. Yang, C. Cheng, 3D WO3/BiVO4/Cobalt Phosphate Composites Inverse Opal Photoanode for Efficient Photoelectrochemical Water Splitting, Small 13 (16) (2017) 1603840.

[32] Z. Zhang, C. Gao, Z. Wu, W. Han, Y. Wang, W. Fu, X. Li, E. Xie, Toward efficient photoelectrochemical water-splitting by using screw-like SnO2 nanostructures as photoanode after being decorated with CdS quantum dots, Nano Energy 19 (2016) 318–327.

[33] S. Cao, X. Yan, Z. Kang, Q. Liang, X. Liao, Y. Zhang, Band alignment engineering for improved performance and stability of ZnFe2O4 modified CdS/ZnO nanostructured photoanode for PEC water splitting, Nano Energy 24 (2016) 25–31.

[34] B. Lamm, L. Zhou, P. Rao, M. Stefik, Atomic Layer Deposition of Space-Efficient SnO2 Underlayers for BiVO4 Host–Guest Architectures for Photoassisted Water Splitting, ChemSusChem 12 (9) (2019) 1916–1924.

[35] Z. Wang, X. Li, H. Ling, C.K. Tan, L.P. Yeo, A.C. Grimsdale, A.I.Y. Tok, 3D FTO/FTO-Nanocrystal/TiO2 Composite Inverse Opal Photoanode for Efficient Photoelectrochemical Water Splitting, Small 14 (20) (2018) 1800395.

[36] C.Y. Toe, S. Zhou, M. Gunawan, X. Lu, Y.H. Ng, R. Amal, Recent advances and the design criteria of metal sulfide photocathodes and photoanodes for photoelectrocatalysis, J. Mater. Chem. A 9 (36) (2021) 20277–20319.

[37] Z. Wang, H. Zhu, W. Tu, X. Zhu, Y. Yao, Y. Zhou, Z. Zou, Host/Guest nanostructured photoanodes integrated with targeted enhancement strategies for photoelectrochemical water splitting, Adv. Sci. 9 (2) (2022) 2103744.

[38] S. Li, W. Xu, L. Meng, W. Tian, L. Li, Recent progress on semiconductor heterojunction-based photoanodes for photoelectrochemical water splitting, Small. Sci. 2 (5) (2022) 2100112.

[39] H. Shuwanto, H. Abdullah, D.-H. Kuo, Nanostructuring Bi-Doped α-Fe2O3 Thin-Layer Photoanode to Advance the Water Oxidation Performance, ACS Appl. Energy Mater. 5 (8) (2022) 9902–9913.

[40] L. Meng, L. Li, Recent research progress on operational stability of metal oxide/sulfide photoanodes in photoelectrochemical cells, Nano Res. Energy 1 (2022), e9120020.

[41] J. Liu, J. Li, M. Shao, M. Wei, Directed synthesis of SnO2@BiVO4/Co-Pi photoanode for highly efficient photoelectrochemical water splitting and urea oxidation, J. Mater. Chem. A 7 (11) (2019) 6327–6336.

[42] L. Zhang, X. Chen, Z. Hao, X. Chen, Y. Li, Y. Cui, C. Yuan, H. Ge, TiO2/Au Nanoring/p-Si Nanohole Photocathode for Hydrogen Generation, ACS Appl. Nano Mater. 2 (6) (2019) 3654–3661.

[43] S. Fu, W. Feng, Y. Jia, T. Deng, W. Wang, G. Zhang, J. Fu, Enhanced photo-electrochemical activity of ZnO/Cu2S nanotube arrays photocathodes, Int. J. Hydrog. Energy 46 (21) (2021) 11544–11555.

[44] S. Yang, H. Guan, Y. Zhong, J. Quan, N. Luo, Q. Gao, Y. Xu, F. Peng, S. Zhang, Y. Fang, CdS@Ni3S2 for efficient and stable photo-assisted electrochemical (P-EC) overall water splitting, Chem. Eng. J. 405 (2021), 126231.

[45] G.G. Bessegato, T.T. Guaraldo, J.F. de Brito, M.F. Brugnera, M.V.B. Zanoni, Achievements and Trends in Photoelectrocatalysis: from Environmental to Energy Applications, Electrocatalysis 6 (5) (2015) 415–441.

[46] B. Safizade, S.M. Masoudpanah, M. Hasheminiasari, A. Ghasemi, Photocatalytic activity of BiFeO3/ZnFe2O4 nanocomposites under visible light irradiation, RSC Adv. 8 (13) (2018) 6988–6995.

[47] D.K. Lee, D. Lee, M.A. Lumley, K.-S. Choi, Progress on ternary oxide-based photoanodes for use in photoelectrochemical cells for solar water splitting, Chem. Soc. Rev. 48 (7) (2019) 2126–2157.

[48] J. Jia, X. Du, Q. Zhang, E. Liu, J. Fan, Z-scheme MgFe2O4/Bi2MoO6 heterojunction photocatalyst with enhanced visible light photocatalytic activity for malachite green removal, Appl. Surf. Sci. 492 (2019) 527–539.

[49] M. Tarek, K.M. Rezaul Karim, S.M. Sarkar, A. Deb, H.R. Ong, H. Abdullah, C. K. Cheng, M.M. Rahman Khan, Hetero-structure CdS–CuFe2O4 as an efficient visible light active photocatalyst for photoelectrochemical reduction of CO_2 to methanol, Int. J. Hydrog. Energy 44 (48) (2019) 26271–26284.

[50] S.B. Rawal, D.P. Ojha, S.D. Sung, W.I. Lee, Fe2WO6/TiO2, an efficient visible-light photocatalyst driven by hole-transport mechanism, Catal. Commun. 56 (2014) 55–59.

[51] Q. Wang, K. Domen, Particulate photocatalysts for light-driven water splitting: mechanisms, challenges, and design strategies, Chem. Rev. 120 (2) (2020) 919–985.

[52] Y. He, T. Hamann, D. Wang, Thin film photoelectrodes for solar water splitting, Chem. Soc. Rev. 48 (7) (2019) 2182–2215.

[53] S.M. Thalluri, L. Bai, C. Lv, Z. Huang, X. Hu, L. Liu, Strategies for Semiconductor/Electrocatalyst Coupling toward Solar-Driven Water Splitting, Adv. Sci. 7 (6) (2020) 1902102.

[54] X. Zhang, H. Guo, G. Dong, Y. Zhang, G. Lu, Y. Bi, Homostructural Ta3N5 nanotube/nanoparticle photoanodes for highly efficient solar-driven water splitting, Appl. Catal. B: Environ. 277 (2020), 119217.

[55] M. Kim, B. Lee, H. Ju, J.Y. Kim, J. Kim, S.W. Lee, Oxygen-Vacancy-Introduced $BaSnO_{3-\delta}$ Photoanodes with Tunable Band Structures for Efficient Solar-Driven Water Splitting, Adv. Mater. 31 (33) (2019) 1903316.

[56] H. Zhao, X. Li, M. Cai, C. Liu, Y. You, R. Wang, A.I. Channa, F. Lin, D. Huo, G. Xu, X. Tong, Z.M. Wang, Role of Copper Doping in Heavy Metal-Free InP/ZnSe Core/Shell Quantum Dots for Highly Efficient and Stable Photoelectrochemical Cell, Adv. Energy Mater. 11 (31) (2021) 2101230.

[57] B. Zhang, H. Zhang, Z. Wang, X. Zhang, X. Qin, Y. Dai, Y. Liu, P. Wang, Y. Li, B. Huang, Doping strategy to promote the charge separation in BiVO4 photoanodes, Appl. Catal. B: Environ. 211 (2017) 258–265.

[58] M. Sun, R.-T. Gao, J. He, X. Liu, T. Nakajima, X. Zhang, L. Wang, Photo-driven oxygen vacancies extends charge carrier lifetime for efficient solar water splitting, Angew. Chem. Int. Ed. 60 (32) (2021) 17601–17607.

[59] Z. Wu, Y. Zhao, W. Jin, B. Jia, J. Wang, T. Ma, Recent progress of vacancy engineering for electrochemical energy conversion related applications, Adv. Funct. Mater. 31 (9) (2021) 2009070.

[60] L. Ran, S. Qiu, P. Zhai, Z. Li, J. Gao, X. Zhang, B. Zhang, C. Wang, L. Sun, J. Hou, Conformal Macroporous Inverse Opal Oxynitride-Based Photoanode for Robust Photoelectrochemical Water Splitting, J. Am. Chem. Soc. 143 (19) (2021) 7402–7413.

[61] Y. Pihosh, V. Nandal, T. Minegishi, M. Katayama, T. Yamada, K. Seki, M. Sugiyama, K. Domen, Development of a Core-Shell Heterojunction Ta3N5-Nanorods/BaTaO2N Photoanode for Solar Water Splitting, ACS Energy Lett. 5 (8) (2020) 2492–2497.

[62] Y. Wu, X. Liu, H. Zhang, J. Li, M. Zhou, L. Li, Y. Wang, Atomic Sandwiched p-n Homojunctions, Angew. Chem. Int. Ed. 60 (7) (2021) 3487–3492.

[63] S. Liu, R.-T. Gao, M. Sun, Y. Wang, T. Nakajima, X. Liu, W. Zhang, L. Wang, In situ construction of hybrid Co(OH)2 nanowires for promoting long-term water splitting, Appl. Catal. B: Environ. 292 (2021), 120063.

[64] B. Zhang, X. Huang, Y. Zhang, G. Lu, L. Chou, Y. Bi, Unveiling the Activity and Stability Origin of BiVO4 Photoanodes with FeNi Oxyhydroxides for Oxygen Evolution, Angew. Chem. Int. Ed. 59 (43) (2020) 18990–18995.

[65] F. Li, H. Yang, Q. Zhuo, D. Zhou, X. Wu, P. Zhang, Z. Yao, L. Sun, A Cobalt@Cucurbit[5]uril Complex as a Highly Efficient Supramolecular Catalyst for Electrochemical and Photoelectrochemical Water Splitting, Angew. Chem. Int. Ed. 60 (4) (2021) 1976–1985.

[66] H. Zhang, D. Li, W.J. Byun, X. Wang, T.J. Shin, H.Y. Jeong, H. Han, C. Li, J.S. Lee, Gradient tantalum-doped hematite homojunction photoanode improves both photocurrents and turn-on voltage for solar water splitting, Nat. Commun. 11 (1) (2020) 4622.

[67] Y. Yu, Y. Huang, Y. Yu, Y. Shi, B. Zhang, Design of continuous built-in band bending in self-supported CdS nanorod-based hierarchical architecture for efficient photoelectrochemical hydrogen production, Nano Energy 43 (2018) 236–243.

[68] J.M. Yu, J. Lee, Y.S. Kim, J. Song, J. Oh, S.M. Lee, M. Jeong, Y. Kim, J.H. Kwak, S. Cho, C. Yang, J.-W. Jang, High-performance and stable photoelectrochemical water splitting cell with organic-photoactive-layer-based photoanode, Nat. Commun. 11 (1) (2020) 5509.

[69] L. Steier, S. Holliday, A bright outlook on organic photoelectrochemical cells for water splitting, J. Mater. Chem. A 6 (44) (2018) 21809–21826.

[70] M. Zhang, W. Luo, Z. Li, T. Yu, Z. Zou, Improved photoelectrochemical responses of Si and Ti codoped α-Fe2O3 photoanode films, Appl. Phys. Lett. 97 (4) (2010), 042105.

[71] Y. Yang, S. Niu, D. Han, T. Liu, G. Wang, Y. Li, Progress in Developing Metal Oxide Nanomaterials for Photoelectrochemical Water Splitting, Adv. Energy Mater. 7 (19) (2017) 1700555.

[72] W.P. Utomo, M.K.H. Leung, Z. Yin, H. Wu, Y.H. Ng, Advancement of Bismuth-Based Materials for Electrocatalytic and Photo(electro)catalytic Ammonia Synthesis, Adv. Funct. Mater. 32 (4) (2022) 2106713.

[73] X. Chen, X. Shen, S. Shen, M.O. Reese, S. Hu, Stable CdTe Photoanodes with Energetics Matching Those of a Coating Intermediate Band, ACS Energy Lett. 5 (6) (2020) 1865–1871.

[74] M. Zhong, T. Hisatomi, Y. Sasaki, S. Suzuki, K. Teshima, M. Nakabayashi, N. Shibata, H. Nishiyama, M. Katayama, T. Yamada, K. Domen, Highly Active GaN-Stabilized Ta3N5 Thin-Film Photoanode for Solar Water Oxidation, Angew. Chem. Int. Ed. 56 (17) (2017) 4739–4743.

[75] G. Wang, Y. Yang, Y. Ling, H. Wang, X. Lu, Y.-C. Pu, J.Z. Zhang, Y. Tong, Y. Li, An electrochemical method to enhance the performance of metal oxides for photoelectrochemical water oxidation, J. Mater. Chem. A 4 (8) (2016) 2849–2855.

[76] L. Yang, D.K. Nandakumar, L. Suresh, S. Zhang, Y. Zhang, L. Zhang, J. Wang, J. W. Ager, S.C. Tan, Solar-driven gas-phase moisture to hydrogen with zero bias, ACS Nano 15 (12) (2021) 19119–19127.

[77] S. Chen, D. Huang, P. Xu, W. Xue, L. Lei, M. Cheng, R. Wang, X. Liu, R. Deng, Semiconductor-based photocatalysts for photocatalytic and photoelectrochemical water splitting: will we stop with photocorrosion? J. Mater. Chem. A 8 (5) (2020) 2286–2322.

[78] J. Fu, Z. Fan, M. Nakabayashi, H. Ju, N. Pastukhova, Y. Xiao, C. Feng, N. Shibata, K. Domen, Y. Li, Interface engineering of Ta3N5 thin film photoanode for highly efficient photoelectrochemical water splitting, Nat. Commun. 13 (1) (2022) 729.

[79] B. He, S. Jia, M. Zhao, Y. Wang, T. Chen, S. Zhao, Z. Li, Z. Lin, Y. Zhao, X. Liu, General and Robust Photothermal-Heating-Enabled High-Efficiency Photoelectrochemical Water Splitting, Adv. Mater. 33 (16) (2021) 2004406.

[80] C. Kranz, M. Wächtler, Characterizing photocatalysts for water splitting: from atoms to bulk and from slow to ultrafast processes, Chem. Soc. Rev. 50 (2) (2021) 1407–1437.

[81] B. Klahr, S. Gimenez, F. Fabregat-Santiago, T. Hamann, J. Bisquert, Water oxidation at hematite photoelectrodes: the role of surface states, J. Am. Chem. Soc. 134 (9) (2012) 4294–4302.

[82] W. Xu, L. Meng, W. Tian, S. Li, F. Cao, L. Li, Polypyrrole serving as multifunctional surface modifier for photoanode enables efficient photoelectrochemical water oxidation, Small 18 (1) (2022) 2105240.

[83] J. Hou, C. Yang, H. Cheng, S. Jiao, O. Takeda, H. Zhu, High-performance p-Cu2O/n-TaON heterojunction nanorod photoanodes passivated with an ultrathin carbon sheath for photoelectrochemical water splitting, Energy Environ. Sci. 7 (11) (2014) 3758–3768.

[84] R. Tang, S. Zhou, Z. Yuan, L. Yin, Metal–Organic Framework Derived Co3O4/TiO2/Si Heterostructured Nanorod Array Photoanodes for Efficient Photoelectrochemical Water Oxidation, Adv. Funct. Mater. 27 (37) (2017) 1701102.

[85] L. Meng, J. He, W. Tian, M. Wang, R. Long, L. Li, Ni/Fe Codoped In2S3 Nanosheet Arrays Boost Photo-Electrochemical Performance of Planar Si Photocathodes, Adv. Energy Mater. 9 (38) (2019) 1902135.

[86] J. Han, Z. Liu, K. Guo, B. Wang, X. Zhang, T. Hong, High-efficiency photoelectrochemical electrodes based on ZnIn2S4 sensitized ZnO nanotube arrays, Appl. Catal. B: Environ. 163 (2015) 179–188.

[87] M. Linxing, L. Liang, Recent research progress on operational stability of metal oxide/sulfide photoanodes in photoelectrochemical cells, Nano Res. Energy 1 (2022), e9120020.

[88] M. Zhong, T. Hisatomi, Y. Kuang, J. Zhao, M. Liu, A. Iwase, Q. Jia, H. Nishiyama, T. Minegishi, M. Nakabayashi, N. Shibata, R. Niishiro, C. Katayama, H. Shibano, M. Katayama, A. Kudo, T. Yamada, K. Domen, Surface Modification of CoOx Loaded BiVO4 Photoanodes with Ultrathin p-Type NiO Layers for Improved Solar Water Oxidation, J. Am. Chem. Soc. 137 (15) (2015) 5053–5060.

[89] Y. Zhao, E.A. Hernandez-Pagan, N.M. Vargas-Barbosa, J.L. Dysart, T.E. Mallouk, A. High, Yield synthesis of ligand-free iridium oxide nanoparticles with high electrocatalytic activity, J. Phys. Chem. Lett. 2 (5) (2011) 402–406.

[90] Y. Dong, K. He, L. Yin, A. Zhang, A facile route to controlled synthesis of Co3O4nanoparticles and their environmental catalytic properties, Nanotechnology 18 (43) (2007), 435602.

[91] L. Trotochaud, S.L. Young, J.K. Ranney, S.W. Boettcher, Nickel–Iron Oxyhydroxide Oxygen-Evolution Electrocatalysts: The Role of Intentional and Incidental Iron Incorporation, J. Am. Chem. Soc. 136 (18) (2014) 6744–6753.

[92] G.P. Gardner, Y.B. Go, D.M. Robinson, P.F. Smith, J. Hadermann, A. Abakumov, M. Greenblatt, G.C. Dismukes, Structural Requirements in Lithium Cobalt Oxides for the Catalytic Oxidation of Water, Angew. Chem. Int. Ed. 51 (7) (2012) 1616–1619.

[93] M. Barroso, A.J. Cowan, S.R. Pendlebury, M. Grätzel, D.R. Klug, J.R. Durrant, The Role of Cobalt Phosphate in Enhancing the Photocatalytic Activity of α-Fe2O3 toward Water Oxidation, J. Am. Chem. Soc. 133 (38) (2011) 14868–14871.

[94] J.S. Kim, B. Kim, H. Kim, K. Kang, Recent progress on multimetal oxide catalysts for the oxygen evolution reaction, Adv. Energy Mater. 8 (11) (2018) 1702774.

[95] E. Thimsen, A.B.F. Martinson, J.W. Elam, M.J. Pellin, Energy Levels, Electronic Properties, and Rectification in Ultrathin p-NiO Films Synthesized by Atomic Layer Deposition, J. Phys. Chem. C. 116 (32) (2012) 16830–16840.

[96] A. Liao, H. He, Y. Zhou, Z. Zou, Typical strategies to facilitate charge transfer for enhanced oxygen evolution reaction: Case studies on hematite, J. Semicond. 41 (9) (2020), 091709.

[97] X. Wang, Q. Li, C. Zhou, Z. Cao, R. Zhang, ZnO rod/reduced graphene oxide sensitized by α-Fe2O3 nanoparticles for effective visible-light photoreduction of CO_2, J. Colloid Interface Sci. 554 (2019) 335–343.

[98] R. Zhang, L. Yang, X. Huang, T. Chen, F. Qu, Z. Liu, G. Du, A.M. Asiri, X. Sun, Se doping: an effective strategy toward Fe2O3 nanorod arrays for greatly enhanced solar water oxidation, J. Mater. Chem. A 5 (24) (2017) 12086–12090.

[99] P. Senthilkumar, D.A. Jency, T. Kavinkumar, D. Dhayanithi, S. Dhanuskodi, M. Umadevi, S. Manivannan, N.V. Giridharan, V. Thiagarajan, M. Sriramkumar, K. Jothivenkatachalam, Built-in Electric Field Assisted Photocatalytic Dye Degradation and Photoelectrochemical Water Splitting of Ferroelectric Ce Doped BaTiO3 Nanoassemblies, ACS Sustain. Chem. Eng. 7 (14) (2019) 12032–12043.

[100] X.-L. Li, W.-P. Han, J.-B. Wu, X.-F. Qiao, J. Zhang, P.-H. Tan, Layer-Number Dependent Optical Properties of 2D Materials and Their Application for Thickness Determination, Adv. Funct. Mater. 27 (19) (2017) 1604468.

[101] A.G. Chaves, J. Azadani, H. Alsalman, D.R. da Costa, R. Frisenda, A. Chaves, S. Song, Y.D. Kim, D. He, J. Zhou, A. Castellanos-Gómez, F.M. Peeters, Z. Liu, C. L. Hinkle, S.H. Oh, P.D. Ye, S.J. Koester, Y.H. Lee, P. Avouris, X. Wang, T. Low, Bandgap engineering of two-dimensional semiconductor materials, npj 2D Mater. Appl. 4 (2020) 1–21.

[102] X. Cai, Y. Luo, B. Liu, H.-M. Cheng, Preparation of 2D material dispersions and their applications, Chem. Soc. Rev. 47 (16) (2018) 6224–6266.

[103] L. Banszerus, M. Schmitz, S. Engels, J. Dauber, M. Oellers, F. Haupt, K. Watanabe, T. Taniguchi, B. Beschoten, C. Stampfer, Ultrahigh-mobility graphene devices from chemical vapor deposition on reusable copper, in: *Science Advances*, 1, 2015, e1500222.

[104] N. Gillgren, D. Wickramaratne, Y. Shi, T. Espiritu, J. Yang, J. Hu, J. Wei, X. Liu, Z. Mao, K. Watanabe, T. Taniguchi, M. Bockrath, Y. Barlas, R.K. Lake, C. Ning Lau, Gate tunable quantum oscillations in air-stable and high mobility few-layer phosphorene heterostructures, 2D Mater. 2 (1) (2014), 011001.

[105] J.W. Yang, S.H. Ahn, H.W. Jang, Crucial role of heterostructures in highly advanced water splitting photoelectrodes, Curr. Opin. Green. Sustain. Chemistry 29 (2021), 100454.

[106] K. Karmakar, D. Maity, D. Pal, K. Mandal, G.G. Khan, Photo-Induced Exciton Dynamics and Broadband Light Harvesting in ZnO Nanorod-Templated Multilayered Two-Dimensional MoS2/MoO3 Photoanodes for Solar Fuel Generation, ACS Appl. Nano Mater. 3 (2) (2020) 1223–1231.

[107] H. Li, C. Yang, X. Wang, J. Zhang, J. Xi, G. Du, Z. Ji, Mixed 3D/2D dimensional TiO2 nanoflowers/MoSe2 nanosheets for enhanced photoelectrochemical hydrogen generation, J. Am. Ceram. Soc. 103 (2) (2020) 1187–1196.

[108] N.A. Arzaee, M.F. Mohamad Noh, N.S.H. Mohd Ita, N.A. Mohamed, S.N.F. Mohd Nasir, I.N. Nawas Mumthas, A.F. Ismail, M.A. Mat Teridi, Nanostructure-assisted charge transfer in α-Fe2O3/g-C3N4 heterojunctions for efficient and highly stable photoelectrochemical water splitting, Dalton Trans. 49 (32) (2020) 11317–11328.

[109] S. Alam, T.K. Sahu, D. Gogoi, N.R. Peela, M. Qureshi, Bio-template assisted hierarchical ZnO superstructures coupled with graphene quantum dots for enhanced water oxidation kinetics, Sol. Energy 199 (2020) 39–46.

[110] M. Tayebi, A. Tayyebi, Z. Masoumi, B.-K. Lee, Photocorrosion suppression and photoelectrochemical (PEC) enhancement of ZnO via hybridization with graphene nanosheets, Appl. Surf. Sci. 502 (2020), 144189.

[111] M.K. Mohanta, T.K. Sahu, D. Gogoi, N.R. Peela, M. Qureshi, Hexagonal Boron Nitride Quantum Dots as a Superior Hole Extractor for Efficient Charge Separation in WO3-Based Photoelectrochemical Water Oxidation, ACS Appl. Energy Mater. 2 (10) (2019) 7457–7466.

[112] S. Bai, J. Han, Y. Zhao, H. Chu, S. Wei, J. Sun, L. Sun, R. Luo, D. Li, A. Chen, rGO decorated BiVO4/Cu2O n-n heterojunction photoanode for photoelectrochemical water splitting, Renew. Energy 148 (2020) 380–387.

[113] W. Li, K. Wang, X. Yang, F. Zhan, Y. Wang, M. Liu, X. Qiu, J. Li, J. Zhan, Q. Li, Y. Liu, Surfactant-assisted controlled synthesis of a metal-organic framework on Fe2O3 nanorod for boosted photoelectrochemical water oxidation, Chem. Eng. J. 379 (2020), 122256.

[114] W. Cui, J. Shang, H. Bai, J. Hu, D. Xu, J. Ding, W. Fan, W. Shi, In-situ implantation of plasmonic Ag into metal-organic frameworks for constructing efficient Ag/NH2-MIL-125/TiO2 photoanode, Chem. Eng. J. 388 (2020), 124206.

[115] W. Cui, H. Bai, J. Shang, F. Wang, D. Xu, J. Ding, W. Fan, W. Shi, Organic-inorganic hybrid-photoanode built from NiFe-MOF and TiO2 for efficient PEC water splitting, Electrochim. Acta 349 (2020), 136383.

[116] S. Zhou, K. Chen, J. Huang, L. Wang, M. Zhang, B. Bai, H. Liu, Q. Wang, Preparation of heterometallic CoNi-MOFs-modified BiVO4: a steady photoanode for improved performance in photoelectrochemical water splitting, Appl. Catal. B: Environ. 266 (2020), 118513.

[117] D. Yan, X. Fu, Z. Shang, J. Liu, H. a Luo, A BiVO4 film photoanode with re-annealing treatment and 2D thin Ti3C2TX flakes decoration for enhanced photoelectrochemical water oxidation, Chem. Eng. J. 361 (2019) 853–861.
[118] J. Park, T.H. Lee, C. Kim, S.A. Lee, M.-J. Choi, H. Kim, J.W. Yang, J. Lim, H. W. Jang, Hydrothermally obtained type-II heterojunction nanostructures of In2S3 / TiO2 for remarkably enhanced photoelectrochemical water splitting, Appl. Catal. B: Environ. 295 (2021), 120276.
[119] B.R. Lee, S. Choi, W.S. Cheon, J.W. Yang, M.G. Lee, S.H. Park, H.W. Jang, Interfacial Engineering of In2O3/In2S3 Heterojunction Photoanodes for Photoelectrochemical Water Oxidation, Electron. Mater. Lett. 18 (4) (2022) 391–399.
[120] M.-J. Choi, T.L. Kim, K.S. Choi, W. Sohn, T.H. Lee, S.A. Lee, H. Park, S.Y. Jeong, J. W. Yang, S. Lee, H.W. Jang, Controlled band offsets in ultrathin hematite for enhancing the photoelectrochemical water splitting performance of heterostructured photoanodes, ACS Appl. Mater. Interfaces 14 (6) (2022) 7788–7795.
[121] M.G. Lee, J.W. Yang, H. Park, C.W. Moon, D.M. Andoshe, J. Park, C.-K. Moon, T. H. Lee, K.S. Choi, W.S. Cheon, J.-J. Kim, H.W. Jang, Crystal Facet Engineering of TiO2 Nanostructures for Enhancing Photoelectrochemical Water Splitting with BiVO4 Nanodots, Nano-Micro Lett. 14 (1) (2022) 48.
[122] P. Chaudhary, P.P. Ingole, In-Situ solid-state synthesis of 2D/2D interface between Ni/NiO hexagonal nanosheets supported on g-C3N4 for enhanced photo-electrochemical water splitting, Int. J. Hydrog. Energy 45 (32) (2020) 16060–16070.
[123] K. Zhang, B. Jin, C. Park, Y. Cho, X. Song, X. Shi, S. Zhang, W. Kim, H. Zeng, J. H. Park, Black phosphorene as a hole extraction layer boosting solar water splitting of oxygen evolution catalysts, Nat. Commun. 10 (1) (2019) 2001.
[124] M. Zhou, Z. Guo, Q. Song, X. Li, Z. Liu, Improved photoelectrochemical response of CuWO4/BiOI p-n heterojunction embedded with plasmonic Ag nanoparticles, Chem. Eng. J. 370 (2019) 218–227.
[125] L. Yao, W. Wang, T. Zhu, Y. Wang, Y. Liang, J. Fu, J. Wang, Y. Cheng, S. Liu, A rational design of CdS/ZnFe2O4/Cu2O core-shell nanorod array photoanode with stair-like type-II band alignment for highly efficient bias-free visible-light-driven H2 generation, Appl. Catal. B: Environ. 268 (2020), 118460.
[126] X. Liu, F. Zhan, D. Li, M. Xue, α-Fe2O3 nanoarrays photoanodes decorated with Ni-MOFs for enhancing photoelectrochemical water oxidation, Int. J. Hydrog. Energy 45 (53) (2020) 28836–28846.
[127] Z. Peng, S.C. Abbas, J. Lv, R. Yang, M. Wu, Y. Wang, Mixed-metal organic framework-coated ZnO nanowires array for efficient photoelectrochemical water oxidation, Int. J. Hydrog. Energy 44 (5) (2019) 2446–2453.
[128] T.K. Sahu, M.K. Mohanta, M. Qureshi, Modulating water oxidation kinetics utilizing h-BN quantum dots as an efficient hole extractor on fluorine doped hematite photoanode, J. Power Sources 445 (2020), 227341.
[129] H. Abdullah, D.-H. Kuo, X. Chen, High efficient noble metal free Zn(O,S) nanoparticles for hydrogen evolution, Int. J. Hydrog. Energy 42 (9) (2017) 5638–5648.
[130] G. Sisay, H. Abdullah, D.-H. Kuo, W. Lakew, H. Shuwanto, S. Fentie, Zn-Ce-Ga trimetal oxysulfide as a dual-functional catalyst: Hydrogen evolution and hydrogenation reactions in a mild condition, Appl. Surf. Sci. 563 (2021), 150383.
[131] D. Jariwala, T.J. Marks, M.C. Hersam, Mixed-dimensional van der Waals heterostructures, Nat. Mater. 16 (2) (2017) 170–181.
[132] Y. Liu, N.O. Weiss, X. Duan, H.-C. Cheng, Y. Huang, X. Duan, Van der Waals heterostructures and devices, Nat. Rev. Mater. 1 (9) (2016) 16042.
[133] K.S. Novoselov, A. Mishchenko, A. Carvalho, A.H. Castro Neto, 2D materials and van der Waals heterostructures, Science 353 (6298) (2016) aac9439.
[134] J. Su, J. He, J. Zhang, Z. Lin, J. Chang, J. Zhang, Y. Hao, Unusual properties and potential applications of strain BN-MS2 (M = Mo, W) heterostructures, Sci. Rep. 9 (1) (2019) 3518.
[135] J. Ye, J. Liu, Y. An, Electric field and strain effects on the electronic and optical properties of g-C3N4/WSe2 van der Waals heterostructure, Appl. Surf. Sci. 501 (2020), 144262.
[136] D. Bae, B. Seger, P.C.K. Vesborg, O. Hansen, I. Chorkendorff, Strategies for stable water splitting via protected photoelectrodes, Chem. Soc. Rev. 46 (7) (2017) 1933–1954.
[137] S.S.M. Bhat, S.A. Pawar, D. Potphode, C.-K. Moon, J.M. Suh, C. Kim, S. Choi, D. S. Patil, J.-J. Kim, J.C. Shin, H.W. Jang, Substantially enhanced photoelectrochemical performance of TiO2 nanorods/CdS nanocrystals heterojunction photoanode decorated with MoS2 nanosheets, Appl. Catal. B: Environ. 259 (2019), 118102.
[138] G. Zhang, Z.-A. Lan, X. Wang, Surface engineering of graphitic carbon nitride polymers with cocatalysts for photocatalytic overall water splitting, Chem. Sci. 8 (8) (2017) 5261–5274.
[139] Z. He, J. Fu, B. Cheng, J. Yu, S. Cao, Cu2(OH)2CO3 clusters: Novel noble-metal-free cocatalysts for efficient photocatalytic hydrogen production from water splitting, Appl. Catal. B: Environ. 205 (2017) 104–111.
[140] R. Asai, H. Nemoto, Q. Jia, K. Saito, A. Iwase, A. Kudo, A visible light responsive rhodium and antimony-codoped SrTiO3 powdered photocatalyst loaded with an IrO2 cocatalyst for solar water splitting, Chem. Commun. 50 (19) (2014) 2543–2546.
[141] D. Cao, W. Luo, J. Feng, X. Zhao, Z. Li, Z. Zou, Cathodic shift of onset potential for water oxidation on a Ti4+ doped Fe2O3 photoanode by suppressing the back reaction, Energy Environ. Sci. 7 (2) (2014) 752–759.
[142] J.Y. Kim, D.H. Youn, K. Kang, J.S. Lee, Highly Conformal Deposition of an Ultrathin FeOOH Layer on a Hematite Nanostructure for Efficient Solar Water Splitting, Angew. Chem. Int. Ed. 55 (36) (2016) 10854–10858.
[143] H. Zhang, J.H. Kim, J.H. Kim, J.S. Lee, Engineering highly ordered iron titanate nanotube array photoanodes for enhanced solar water splitting activity, Adv. Funct. Mater. 27 (35) (2017) 1702428.
[144] J.-W. Jang, C. Du, Y. Ye, Y. Lin, X. Yao, J. Thorne, E. Liu, G. McMahon, J. Zhu, A. Javey, J. Guo, D. Wang, Enabling unassisted solar water splitting by iron oxide and silicon, Nat. Commun. 6 (1) (2015) 7447.
[145] W. Li, S.W. Sheehan, D. He, Y. He, X. Yao, R.L. Grimm, G.W. Brudvig, D. Wang, Hematite-based solar water splitting in acidic solutions: functionalization by mono- and multilayers of iridium oxygen-evolution catalysts, Angew. Chem. Int. Ed. 54 (39) (2015) 11428–11432.
[146] H. Cao, T. Wang, J. Li, J. Wu, P. Du, A molecular cobaloxime cocatalyst and ultrathin FeOOH nanolayers co-modified BiVO4 photoanode for efficient photoelectrochemical water oxidation, J. Energy Chem. 69 (2022) 497–505.
[147] M. Karimi-Nazarabad, E.K. Goharshadi, Decoration of graphene oxide as a cocatalyst on Bi doped g-C3N4 photoanode for efficient solar water splitting, J. Electroanal. Chem. 904 (2022), 115933.
[148] S. Hu, Solid-Solid Interfaces in Photoelectrochemistry: Co-catalysts, Surface Passivation, and Corrosion Protection, in: D. Bahnemann, A.O.T. Patrocinio (Eds.), Springer Handbook of Inorganic Photochemistry, Springer International Publishing, Cham, 2022, pp. 879–921.
[149] J. Deng, Y. Li, Y. Xiao, K. Feng, C. Lu, K. Nie, X. Lv, H. Xu, J. Zhong, Improved Water Oxidation of Fe2O3/Fe2TiO5 Photoanode by Functionalizing with a Hydrophilic Organic Hole Storage Overlayer, ACS Catal. 12 (13) (2022) 7833–7842.
[150] P. Arunachalam, H.A. AlOraij, M.S. Amer, M. Hezam, M.N. Shaddad, J. Madhavan, Activation effect of nickel phosphate co-catalysts on the photoelectrochemical water oxidation performance of TiO2 nanotubes, J. Saudi Chem. Soc. 26 (4) (2022), 101484.
[151] V. Burungale, C. Seong, H. Bae, P. Mane, S.-W. Ryu, S.-H. Kang, J.-S. Ha, Surface modification of p/n heterojunction based TiO2-Cu2O photoanode with a cobalt-phosphate (CoPi) co-catalyst for effective oxygen evolution reaction, Appl. Surf. Sci. 573 (2022), 151445.
[152] Y. Lin, W. Fang, R. Xv, L. Fu, TiO2 nanoparticles modified with ZnIn2S4 nanosheets and Co-Pi groups: Type II heterojunction and cocatalysts coexisted photoanode for efficient photoelectrochemical water splitting, Int. J. Hydrog. Energy (2022).
[153] J. Ran, J. Zhang, J. Yu, M. Jaroniec, S.Z. Qiao, Earth-abundant cocatalysts for semiconductor-based photocatalytic water splitting, Chem. Soc. Rev. 43 (22) (2014) 7787–7812.
[154] Q. Yu, X. Meng, T. Wang, P. Li, J. Ye, Hematite Films Decorated with Nanostructured Ferric Oxyhydroxide as Photoanodes for Efficient and Stable Photoelectrochemical Water Splitting, Adv. Funct. Mater. 25 (18) (2015) 2686–2692.
[155] J. Wang, J. Yang, Z. Zheng, T. Lu, W. Gao, The role of thin NiPi film for enhancing solar water splitting performance of Ti doped hematite, Appl. Catal. B: Environ. 218 (2017) 277–286.
[156] G. Liu, X. Lu, L. Yang, G. Chen, L. Cheng, B. Mao, Z. Zhao, Q. Yang, 5-Aminolevulinic acid photodynamic therapy: an effective treatment modality for female precancerous lesions: experience of a single center, Vol. 11070, SPIE,, 2019.
[157] D. Li, J. Shi, C. Li, Transition-Metal-Based Electrocatalysts as Cocatalysts for Photoelectrochemical Water Splitting: A Mini Review, Small 14 (23) (2018) 1704179.
[158] S. Cao, C.-J. Wang, W.-F. Fu, Y. Chen, Metal Phosphides as Co-Catalysts for Photocatalytic and Photoelectrocatalytic Water Splitting, ChemSusChem 10 (22) (2017) 4306–4323.
[159] G. Ai, R. Mo, H. Li, J. Zhong, Cobalt phosphate modified TiO2 nanowire arrays as co-catalysts for solar water splitting, Nanoscale 7 (15) (2015) 6722–6728.
[160] H. Li, M. Yin, X. Li, R. Mo, Enhanced Photoelectrochemical Water Oxidation Performance in Bilayer TiO2/α-Fe2O3 Nanorod Arrays Photoanode with Cu: NiOx as Hole Transport Layer and Co−Pi as Cocatalyst, ChemSusChem 14 (11) (2021) 2331–2340.
[161] Q. Liu, R. Mo, X. Li, S. Yang, J. Zhong, H. Li, Cobalt phosphate modified 3D TiO2/BiVO4 composite inverse opals photoanode for enhanced photoelectrochemical water splitting, Appl. Surf. Sci. 464 (2019) 544–551.
[162] P. Wen, F. Su, H. Li, Y. Sun, Z. Liang, W. Liang, J. Zhang, W. Qin, S.M. Geyer, Y. Qiu, L. Jiang, A Ni2P nanocrystal cocatalyst enhanced TiO2 photoanode towards highly efficient photoelectrochemical water splitting, Chem. Eng. J. 385 (2020), 123878.
[163] X. Li, A.M. Elshahawy, C. Guan, J. Wang, Metal Phosphides and Phosphates-based Electrodes for Electrochemical Supercapacitors, Small 13 (39) (2017) 1701530.
[164] J. Zhang, Y. Yang, Z. Zhang, X. Xu, X. Wang, Rapid synthesis of mesoporous NixCo3−x(PO4)2 hollow shells showing enhanced electrocatalytic and supercapacitor performance, J. Mater. Chem. A 2 (47) (2014) 20182–20188.
[165] Y. Zhao, Z. Chen, D.-B. Xiong, Y. Qiao, Y. Tang, F. Gao, Hybridized Phosphate with Ultrathin Nanoslices and Single Crystal Microplatelets for High Performance Supercapacitors, Sci. Rep. 6 (1) (2016) 17613.
[166] G. Liu, N. Li, Y. Zhao, R. Yao, M. Wang, D. He, J. Li, Fabrication of Fe-doped Co2P nanoparticles as efficient electrocatalyst for electrochemical and photoelectrochemical water oxidation, Electrochim. Acta 283 (2018) 1490–1497.
[167] Q. Bu, S. Li, S. Cao, Q. Zhao, Y. Chen, D. Wang, T. Xie, A Ni2P modified Ti4+ doped Fe2O3 photoanode for efficient solar water oxidation by promoting hole injection, Dalton Trans. 46 (32) (2017) 10549–10552.
[168] R. Chong, B. Wang, D. Li, Z. Chang, L. Zhang, Enhanced photoelectrochemical activity of Nickel-phosphate decorated phosphate-Fe2O3 photoanode for glycerol-based fuel cell, Sol. Energy Mater. Sol. Cells 160 (2017) 287–293.

[169] D.E. Schipper, Z. Zhao, A.P. Leitner, L. Xie, F. Qin, M.K. Alam, S. Chen, D. Wang, Z. Ren, Z. Wang, J. Bao, K.H. Whitmire, A TiO2/FeMnP core/shell nanorod array photoanode for efficient photoelectrochemical oxygen evolution, ACS Nano 11 (4) (2017) 4051–4059.

[170] X. Cao, P. Wen, R. Ma, Y. Liu, S. Sun, Q. Ma, P. Zhang, Y. Qiu, Ni2P nanocrystals modification on Ta:α-Fe2O3 photoanode for efficient photoelectrochemical water splitting: In situ formation and synergistic catalysis of Ni2P@NiOOH cocatalyst, Chem. Eng. J. 449 (2022), 137792.

[171] J.W. Yang, I.J. Park, S.A. Lee, M.G. Lee, T.H. Lee, H. Park, C. Kim, J. Park, J. Moon, J.Y. Kim, H.W. Jang, Near-complete charge separation in tailored BiVO4-based heterostructure photoanodes toward artificial leaf, Appl. Catal. B: Environ. 293 (2021), 120217.

[172] P. Yue, H. She, L. Zhang, B. Niu, R. Lian, J. Huang, L. Wang, Q. Wang, Super-hydrophilic CoAl-LDH on BiVO4 for enhanced photoelectrochemical water oxidation activity, Appl. Catal. B: Environ. 286 (2021), 119875.

[173] X. Hu, Q. Wang, Y. Li, Y. Meng, L. Wang, H. She, J. Huang, The hydrophilic treatment of a novel co-catalyst for greatly improving the solar water splitting performance over Mo-doped bismuth vanadate, J. Colloid Interface Sci. 607 (2022) 219–228.

[174] Y. Tang, R. Wang, Y. Yang, D. Yan, X. Xiang, Highly Enhanced Photoelectrochemical Water Oxidation Efficiency Based on Triadic Quantum Dot/Layered Double Hydroxide/BiVO4 Photoanodes, ACS Appl. Mater. Interfaces 8 (30) (2016) 19446–19455.

[175] J.A. Seabold, K.-S. Choi, Efficient and stable photo-oxidation of water by a bismuth vanadate photoanode coupled with an iron oxyhydroxide oxygen evolution catalyst, J. Am. Chem. Soc. 134 (4) (2012) 2186–2192.

[176] B. Zhang, X. Huang, H. Hu, L. Chou, Y. Bi, Defect-rich and ultrathin CoOOH nanolayers as highly efficient oxygen evolution catalysts for photoelectrochemical water splitting, J. Mater. Chem. A 7 (9) (2019) 4415–4419.

[177] B. Gao, T. Wang, X. Fan, H. Gong, P. Li, Y. Feng, X. Huang, J. He, J. Ye, Enhanced water oxidation reaction kinetics on a BiVO4 photoanode by surface modification with Ni4O4 cubane, J. Mater. Chem. A 7 (1) (2019) 278–288.

[178] C. Zachäus, F.F. Abdi, L.M. Peter, R. van de Krol, Photocurrent of BiVO4 is limited by surface recombination, not surface catalysis, Chem. Sci. 8 (5) (2017) 3712–3719.

[179] Q. Sun, T. Cheng, Z. Liu, L. Qi, A cobalt silicate modified BiVO4 photoanode for efficient solar water oxidation, Appl. Catal. B: Environ. 277 (2020), 119189.

[180] H. Sun, W. Hua, Y. Li, J.-G. Wang, Conformal coating of superhydrophilic metal-organic complex toward substantially improved photoelectrochemical water oxidation, Chem. Eng. J. 427 (2022), 131004.

[181] Z. Tian, P. Zhang, P. Qin, D. Sun, S. Zhang, X. Guo, W. Zhao, D. Zhao, F. Huang, Novel Black BiVO4/TiO2−x Photoanode with Enhanced Photon Absorption and Charge Separation for Efficient and Stable Solar Water Splitting, Adv. Energy Mater. 9 (27) (2019) 1901287.

[182] K. Dang, X. Chang, T. Wang, J. Gong, Enhancement of photoelectrochemical oxidation by an amorphous nickel boride catalyst on porous BiVO4, Nanoscale 9 (42) (2017) 16133–16137.

[183] B. Zhang, L. Wang, Y. Zhang, Y. Ding, Y. Bi, Ultrathin FeOOH Nanolayers with Abundant Oxygen Vacancies on BiVO4 Photoanodes for Efficient Water Oxidation, Angew. Chem. Int. Ed. 57 (8) (2018) 2248–2252.

[184] S. Bae, H. Kim, D. Jeon, J. Ryu, Catalytic multilayers for efficient solar water oxidation through catalyst loading and surface-state passivation of BiVO4 photoanodes, ACS Appl. Mater. Interfaces 11 (8) (2019) 7990–7999.

[185] X. Wan, Y. Xu, X. Wang, X. Guan, Y. Fu, C. Hu, H. Hu, N. Rong, Atomic layer deposition assisted surface passivation on bismuth vanadate photoanodes for enhanced solar water oxidation, Appl. Surf. Sci. 573 (2022), 151492.

[186] F. Wu, Y. Chang, W. Zhai, J. Wang, Ultrasonic passivated hematite photoanode with efficient hole transfer pathway for enhanced photoelectrochemical water oxidation, J. Mater. Sci. 57 (31) (2022) 14936–14947.

[187] Y. Lu, J. Su, J. Shi, D. Zhou, Surface Recombination Passivation of the BiVO4 Photoanode by the Synergistic Effect of the Cobalt/Nickel Sulfide Cocatalyst, ACS Appl. Energy Mater. 3 (9) (2020) 9089–9097.

[188] J.E. Thorne, J.-W. Jang, E.Y. Liu, D. Wang, Understanding the origin of photoelectrode performance enhancement by probing surface kinetics, Chem. Sci. 7 (5) (2016) 3347–3354.

[189] Q. Pan, A. Li, Y. Zhang, Y. Yang, C. Cheng, Rational Design of 3D Hierarchical Ternary SnO2/TiO2/BiVO4 Arrays Photoanode toward Efficient Photoelectrochemical Performance, Adv. Sci. 7 (3) (2020) 1902235.

[190] P. Wang, F. Li, X. Long, T. Wang, H. Chai, H. Yang, S. Li, J. Ma, J. Jin, Bifunctional citrate-Ni0.9Co0.1(OH)x layer coated fluorine-doped hematite for simultaneous hole extraction and injection towards efficient photoelectrochemical water oxidation, Nanoscale 13 (33) (2021) 14197–14206.

[191] Z. Luo, B. Liu, H. Li, X. Chang, W. Zhu, T. Wang, J. Gong, Multifunctional Nickel Film Protected n-Type Silicon Photoanode with High Photovoltage for Efficient and Stable Oxygen Evolution Reaction, Small *Methods* 3 (10) (2019) 1900212.

[192] Y. Liang, T. Tsubota, L.P.A. Mooij, R. van de Krol, Highly Improved Quantum Efficiencies for Thin Film BiVO4 Photoanodes, J. Phys. Chem. C. 115 (35) (2011) 17594–17598.

[193] R. Tang, L. Wang, M. Ying, W. Yang, A. Kheradmand, Y. Jiang, Z. Li, Y. Cui, R. Zheng, J. Huang, Multigraded Heterojunction Hole Extraction Layer of ZIF-CoxZn1−x on Co3O4/TiO2 Skeleton for a New Photoanode Architecture in Water Oxidation, Small *Science* 1 (4) (2021) 2000033.

[194] X. Ning, B. Lu, Z. Zhang, P. Du, H. Ren, D. Shan, J. Chen, Y. Gao, X. Lu, An Efficient Strategy for Boosting Photogenerated Charge Separation by Using Porphyrins as Interfacial Charge Mediators, Angew. Chem. Int. Ed. 58 (47) (2019) 16800–16805.

[195] H. Chai, P. Wang, T. Wang, L. Gao, F. Li, J. Jin, Surface reconstruction of cobalt species on amorphous cobalt silicate-coated fluorine-doped hematite for efficient photoelectrochemical water oxidation, ACS Appl. Mater. Interfaces 13 (40) (2021) 47572–47580.

[196] T. Wang, X. Long, S. Wei, P. Wang, C. Wang, J. Jin, G. Hu, Boosting Hole Transfer in the Fluorine-Doped Hematite Photoanode by Depositing Ultrathin Amorphous FeOOH/CoOOH Cocatalysts, ACS Appl. Mater. Interfaces 12 (44) (2020) 49705–49712.

[197] J. Su, T. Hisatomi, T. Minegishi, K. Domen, Enhanced Photoelectrochemical Water Oxidation from CdTe Photoanodes Annealed with CdCl2, Angew. Chem. Int. Ed. 59 (33) (2020) 13800–13806.

[198] G.V. Govindaraju, G.P. Wheeler, D. Lee, K.-S. Choi, Methods for electrochemical synthesis and photoelectrochemical characterization for photoelectrodes, Chem. Mater. 29 (1) (2017) 355–370.

[199] H. Zhu, Q. Yang, D. Liu, D. Liu, W. Zhang, Z. Chu, X. Wang, S. Yan, Z. Li, Z. Zou, Polaron states as a massive electron-transfer pathway at heterojunction interface, J. Phys. Chem. Lett. 11 (21) (2020) 9184–9194.

[200] D. Chen, Z. Liu, S. Zhang, Enhanced PEC performance of hematite photoanode coupled with bimetallic oxyhydroxide NiFeOOH through a simple electroless method, Appl. Catal. B: Environ. 265 (2020), 118580.

[201] Y. Fu, Y.-R. Lu, F. Ren, Z. Xing, J. Chen, P. Guo, W.-F. Pong, C.-L. Dong, L. Zhao, S. Shen, Surface electronic structure reconfiguration of hematite nanorods for efficient photoanodic water oxidation, Sol. RRL 4 (1) (2020) 1900349.

[202] Y. Gu, A. Wu, Y. Jiao, H. Zheng, X. Wang, Y. Xie, L. Wang, C. Tian, H. Fu, Two-Dimensional Porous Molybdenum Phosphide/Nitride Heterojunction Nanosheets for pH-Universal Hydrogen Evolution Reaction, Angew. Chem. Int. Ed. 60 (12) (2021) 6673–6681.

[203] J. Low, J. Yu, M. Jaroniec, S. Wageh, A.A. Al-Ghamdi, Heterojunction Photocatalysts, Adv. Mater. 29 (20) (2017) 1601694.

[204] M. Xiao, B. Luo, Z. Wang, S. Wang, L. Wang, Recent Advances of Metal-Oxide Photoanodes: Engineering of Charge Separation and Transportation toward Efficient Solar Water Splitting, Sol. RRL 4 (8) (2020) 1900509.

[205] Q. Xu, L. Zhang, B. Cheng, J. Fan, J. Yu, S-Scheme Heterojunction Photocatalyst, Chem 6 (7) (2020) 1543–1559.

[206] Z. Wang, C. Li, K. Domen, Recent developments in heterogeneous photocatalysts for solar-driven overall water splitting, Chem. Soc. Rev. 48 (7) (2019) 2109–2125.

[207] Y. Tang, P. Zhou, K. Wang, F. Lin, J. Lai, Y. Chao, H. Li, S. Guo, BiOCl/ultrathin polyaniline core/shell nanosheets with a sensitization mechanism for efficient visible-light-driven photocatalysis, Sci. China *Materials* 62 (1) (2019) 95–102.

[208] S.-S. Yi, Z.-Y. Wang, H.-M. Li, Z. Zafar, Z.-T. Zhang, L.-Y. Zhang, D.-L. Chen, Z.-Y. Liu, X.-Z. Yue, Coupling effects of indium oxide layer on hematite enabling efficient photoelectrochemical water splitting, Appl. Catal. B: Environ. 283 (2021), 119649.

[209] S. Lee, J. Song, Y.-R. Jo, K.S. Choi, J. Lee, S. Seo, T.L. Kim, H.W. Jang, C. Jeon, B.-J. Kim, B. Kim, S. Lee, In Situ Growth of Nanostructured BiVO4–Bi2O3 Mixed-Phase via Nonequilibrium Deposition Involving Metal Exsolution for Enhanced Photoelectrochemical Water Splitting, ACS Appl. Mater. Interfaces 11 (47) (2019) 44069–44076.

[210] Z. Yan, H. Sun, X. Chen, H. Liu, Y. Zhao, H. Li, W. Xie, F. Cheng, J. Chen, Anion insertion enhanced electrodeposition of robust metal hydroxide/oxide electrodes for oxygen evolution, Nat. Commun. 9 (1) (2018) 2373.

[211] D. Zhao, Y. Wang, C.-L. Dong, Y.-C. Huang, J. Chen, F. Xue, S. Shen, L. Guo, Boron-doped nitrogen-deficient carbon nitride-based Z-scheme heterostructures for photocatalytic overall water splitting, Nat. Energy 6 (4) (2021) 388–397.

[212] X. Zhao, J. Feng, J. Liu, W. Shi, G. Yang, G.-C. Wang, P. Cheng, An Efficient, Visible-Light-Driven, Hydrogen Evolution Catalyst NiS/ZnxCd1−xS Nanocrystal Derived from a Metal–Organic Framework, Angew. Chem. Int. Ed. 57 (31) (2018) 9790–9794.

[213] C.-Y. Pei, Y.-G. Chen, L. Wang, W. Chen, G.-B. Huang, Step-scheme WO3/CdIn2S4 hybrid system with high visible light activity for tetracycline hydrochloride photodegradation, Appl. Surf. Sci. 535 (2021), 147682.

[214] I. Grigioni, L. Ganzer, V.A. Camargo, F. Bozzini, B. Cerullo, G. Selli, E., In Operando Photoelectrochemical Femtosecond Transient Absorption Spectroscopy of WO3/BiVO4 Heterojunctions, ACS Energy Lett. 4 (9) (2019) 2213–2219.

[215] J. Deng, X. Lv, K. Nie, X. Lv, X. Sun, J. Zhong, Lowering the Onset Potential of Fe2TiO5/Fe2O3 Photoanodes by Interface Structures: F- and Rh-Based Treatments, ACS Catal. 7 (6) (2017) 4062–4069.

[216] F.M. Pesci, M.S. Sokolikova, C. Grotta, P.C. Sherrell, F. Reale, K. Sharda, N. Ni, P. Palczynski, C. Mattevi, MoS2/WS2 Heterojunction for Photoelectrochemical Water Oxidation, ACS Catal. 7 (8) (2017) 4990–4998.

[217] S. Vanka, B. Zhou, R.A. Awni, Z. Song, F.A. Chowdhury, X. Liu, H. Hajibabaei, W. Shi, Y. Xiao, I.A. Navid, A. Pandey, R. Chen, G.A. Botton, T.W. Hamann, D. Wang, Y. Yan, Z. Mi, InGaN/Si Double-Junction Photocathode for Unassisted Solar Water Splitting, ACS Energy Lett. 5 (12) (2020) 3741–3751.

[218] F.F. Abdi, L. Han, A.H.M. Smets, M. Zeman, B. Dam, R. van de Krol, Efficient solar water splitting by enhanced charge separation in a bismuth vanadate-silicon tandem photoelectrode, Nat. Commun. 4 (1) (2013) 2195.

[219] T.H. Jeon, G.-h Moon, H. Park, W. Choi, Ultra-efficient and durable photoelectrochemical water oxidation using elaborately designed hematite nanorod arrays, Nano Energy 39 (2017) 211–218.

[220] K.-H. Ye, H. Li, D. Huang, S. Xiao, W. Qiu, M. Li, Y. Hu, W. Mai, H. Ji, S. Yang, Enhancing photoelectrochemical water splitting by combining work function tuning and heterojunction engineering, Nat. Commun. 10 (1) (2019) 3687.

[221] H. Chai, L. Gao, P. Wang, F. Li, G. Hu, J. Jin, In2S3/F-Fe2O3 type-II heterojunction bonded by interfacial S-O for enhanced charge separation and

transport in photoelectrochemical water oxidation, Appl. Catal. B: Environ. 305 (2022), 121011.
[222] C. Gao, T. Wei, Y. Zhang, X. Song, Y. Huan, H. Liu, M. Zhao, J. Yu, X. Chen, A. Photoresponsive, Rutile TiO2 Heterojunction with Enhanced Electron–Hole Separation for High-Performance Hydrogen Evolution, Adv. Mater. 31 (8) (2019) 1806596.
[223] G. Zeng, X. Wang, X. Yu, J. Guo, Y. Zhu, Y. Zhang, Ultrathin g-C3N4/Mo:BiVO4 photoanode for enhanced photoelectrochemical water oxidation, in: *Journal of Power Sources*, 444, 2019, 227300.
[224] L. Meng, X. Zhou, S. Wang, Y. Zhou, W. Tian, P. Kidkhunthod, S. Tunmee, Y. Tang, R. Long, Y. Xin, L. Li, A Plasma-Triggered O–S Bond and P–N Junction Near the Surface of a SnS2 Nanosheet Array to Enable Efficient Solar Water Oxidation, Angew. Chem. Int. Ed. 58 (46) (2019) 16668–16675.
[225] L. Cai, J. Zhao, H. Li, J. Park, I.S. Cho, H.S. Han, X. Zheng, One-Step Hydrothermal Deposition of Ni:FeOOH onto Photoanodes for Enhanced Water Oxidation, ACS Energy Lett. 1 (3) (2016) 624–632.
[226] S. Cao, Y. Wu, J. Hou, B. Zhang, Z. Li, X. Nie, L. Sun, 3D porous pyramid heterostructure array realizing efficient photo-electrochemical performance, Adv. Energy Mater. 10 (5) (2020) 1902935.
[227] J. Hou, S. Cao, Y. Sun, Y. Wu, F. Liang, Z. Lin, L. Sun, Atomically Thin Mesoporous In2O3–x/In2S3 Lateral Heterostructures Enabling Robust Broadband-Light Photo-Electrochemical Water Splitting, Adv. Energy Mater. 8 (9) (2018) 1701114.
[228] B. Dong, J. Cui, Y. Gao, Y. Qi, F. Zhang, C. Li, Heterostructure of 1D Ta3N5 Nanorod/BaTaO2N Nanoparticle Fabricated by a One-Step Ammonia Thermal Route for Remarkably Promoted Solar Hydrogen Production, Adv. Mater. 31 (15) (2019) 1808185.
[229] L. Meng, M. Wang, H. Sun, W. Tian, C. Xiao, S. Wu, F. Cao, L. Li, Designing a Transparent CdIn2S4/In2S3 Bulk-Heterojunction Photoanode Integrated with a Perovskite Solar Cell for Unbiased Water Splitting, Adv. Mater. 32 (30) (2020) 2002893.
[230] A.J. Bard, Photoelectrochemistry and heterogeneous photo-catalysis at semiconductors, J. Photochem. 10 (1) (1979) 59–75.
[231] H. Tada, T. Mitsui, T. Kiyonaga, T. Akita, K. Tanaka, All-solid-state Z-scheme in CdS–Au–TiO2 three-component nanojunction system, Nat. Mater. 5 (10) (2006) 782–786.
[232] J. Yu, S. Wang, J. Low, W. Xiao, Enhanced photocatalytic performance of direct Z-scheme g-C3N4–TiO2 photocatalysts for the decomposition of formaldehyde in air, Phys. Chem. Chem. Phys. 15 (39) (2013) 16883–16890.
[233] X. Chen, J. Wang, Y. Chai, Z. Zhang, Y. Zhu, Efficient Photocatalytic Overall Water Splitting Induced by the Giant Internal Electric Field of a g-C3N4/rGO/PDIP Z-Scheme Heterojunction, Adv. Mater. 33 (7) (2021) 2007479.
[234] Y. Fu, C.-L. Dong, W. Zhou, Y.-R. Lu, Y.-C. Huang, Y. Liu, P. Guo, L. Zhao, W.-C. Chou, S. Shen, A ternary nanostructured α-Fe2O3/Au/TiO2 photoanode with reconstructed interfaces for efficient photoelectrocatalytic water splitting, Appl. Catal. B: Environ. 260 (2020), 118206.
[235] W. Xu, W. Tian, L. Meng, F. Cao, L. Li, Interfacial Chemical Bond-Modulated Z-Scheme Charge Transfer for Efficient Photoelectrochemical Water Splitting, Adv. Energy Mater. 11 (8) (2021) 2003500.
[236] F. Liu, R. Shi, Z. Wang, Y. Weng, C.-M. Che, Y. Chen, Direct Z-Scheme Hetero-phase Junction of Black/Red Phosphorus for Photocatalytic Water Splitting, Angew. Chem. Int. Ed. 58 (34) (2019) 11791–11795.
[237] T. Zhou, J. Wang, S. Chen, J. Bai, J. Li, Y. Zhang, L. Li, L. Xia, M. Rahim, Q. Xu, B. Zhou, Bird-nest structured ZnO/TiO2 as a direct Z-scheme photoanode with enhanced light harvesting and carriers kinetics for highly efficient and stable photoelectrochemical water splitting, Appl. Catal. B: Environ. 267 (2020), 118599.
[238] L. Wang, X. Zheng, L. Chen, Y. Xiong, H. Xu, Van der Waals heterostructures comprised of ultrathin polymer nanosheets for efficient Z-scheme overall water splitting, Angew. Chem. Int. Ed. 57 (13) (2018) 3454–3458.
[239] J. Low, B. Dai, T. Tong, C. Jiang, J. Yu, In Situ Irradiated X-Ray Photoelectron Spectroscopy Investigation on a Direct Z-Scheme TiO2/CdS Composite Film Photocatalyst, Adv. Mater. 31 (6) (2019) 1802981.
[240] X. Wang, X. Wang, J. Huang, S. Li, A. Meng, Z. Li, Interfacial chemical bond and internal electric field modulated Z-scheme Sv-ZnIn2S4/MoSe2 photocatalyst for efficient hydrogen evolution, Nat. Commun. 12 (1) (2021) 4112.
[241] S. Wei, C. Wang, X. Long, T. Wang, P. Wang, M. Zhang, S. Li, J. Ma, J. Jin, L. Wu, A oxygen vacancy-modulated homojunction structural CuBi2O4 photocathodes for efficient solar water reduction, Nanoscale 12 (28) (2020) 15193–15200.
[242] L. Meng, D. Rao, W. Tian, F. Cao, X. Yan, L. Li, Simultaneous Manipulation of O-Doping and Metal Vacancy in Atomically Thin Zn10In16S34 Nanosheet Arrays toward Improved Photoelectrochemical Performance, Angew. Chem. Int. Ed. 57 (51) (2018) 16882–16887.
[243] W. Qiu, S. Xiao, J. Ke, Z. Wang, S. Tang, K. Zhang, W. Qian, Y. Huang, D. Huang, Y. Tong, S. Yang, Freeing the Polarons to Facilitate Charge Transport in BiVO4 from Oxygen Vacancies with an Oxidative 2D Precursor, Angew. Chem. Int. Ed. 58 (52) (2019) 19087–19095.
[244] R. Shi, H.-F. Ye, F. Liang, Z. Wang, K. Li, Y. Weng, Z. Lin, W.-F. Fu, C.-M. Che, Y. Chen, Interstitial P-Doped CdS with Long-Lived Photogenerated Electrons for Photocatalytic Water Splitting without Sacrificial Agents, Adv. Mater. 30 (6) (2018) 1705941.
[245] J. Zheng, Y. Lyu, C. Xie, R. Wang, L. Tao, H. Wu, H. Zhou, S. Jiang, S. Wang, Defect-Enhanced Charge Separation and Transfer within Protection Layer/Semiconductor Structure of Photoanodes, Adv. Mater. 30 (31) (2018) 1801773.
[246] K. Zhang, G. Zhang, J. Qu, H. Liu, Disordering the Atomic Structure of Co(II) Oxide via B-Doping: An Efficient Oxygen Vacancy Introduction Approach for High Oxygen Evolution Reaction Electrocatalysts, Small 14 (41) (2018) 1802760.
[247] L. Meng, S. Wang, F. Cao, W. Tian, R. Long, L. Li, Doping-Induced Amorphization, Vacancy, and Gradient Energy Band in SnS2 Nanosheet Arrays for Improved Photoelectrochemical Water Splitting, Angew. Chem. Int. Ed. 58 (20) (2019) 6761–6765.
[248] A.G. Hufnagel, H. Hajiyani, S. Zhang, T. Li, O. Kasian, B. Gault, B. Breitbach, T. Bein, D. Fattakhova-Rohlfing, C. Scheu, R. Pentcheva, Why Tin-Doping Enhances the Efficiency of Hematite Photoanodes for Water Splitting—The Full Picture, Adv. Funct. Mater. 28 (52) (2018) 1804472.
[249] Y. Xiao, C. Feng, J. Fu, F. Wang, C. Li, V.F. Kunzelmann, C.-M. Jiang, M. Nakabayashi, N. Shibata, I.D. Sharp, K. Domen, Y. Li, Band structure engineering and defect control of Ta3N5 for efficient photoelectrochemical water oxidation, Nat. Catal. 3 (11) (2020) 932–940.
[250] W. Tian, C. Chen, L. Meng, W. Xu, F. Cao, L. Li, PVP Treatment Induced Gradient Oxygen Doping in In2S3 Nanosheet to Boost Solar Water Oxidation of WO3 Nanoarray Photoanode, Adv. Energy Mater. 10 (18) (2020) 1903951.
[251] Z. Luo, C. Li, S. Liu, T. Wang, J. Gong, Gradient doping of phosphorus in Fe2O3 nanoarray photoanodes for enhanced charge separation, Chem. Sci. 8 (1) (2017) 91–100.
[252] Z. Zhang, I. Karimata, H. Nagashima, S. Muto, K. Ohara, K. Sugimoto, T. Tachikawa, Interfacial oxygen vacancies yielding long-lived holes in hematite mesocrystal-based photoanodes, Nat. Commun. 10 (1) (2019) 4832.
[253] Y. Liu, C. Xiao, Z. Li, Y. Xie, Vacancy Engineering for Tuning Electron and Phonon Structures of Two-Dimensional Materials, Adv. Energy Mater. 6 (23) (2016) 1600436.
[254] Q. He, Y. Wan, H. Jiang, Z. Pan, C. Wu, M. Wang, X. Wu, B. Ye, P.M. Ajayan, L. Song, Nickel Vacancies Boost Reconstruction in Nickel Hydroxide Electrocatalyst, ACS Energy Lett. 3 (6) (2018) 1373–1380.
[255] J. Zheng, Y. Lyu, R. Wang, C. Xie, H. Zhou, S.P. Jiang, S. Wang, Crystalline TiO2 protective layer with graded oxygen defects for efficient and stable silicon-based photocathode, Nat. Commun. 9 (1) (2018) 3572.
[256] H.-W. Chang, Y. Fu, W.-Y. Lee, Y.-R. Lu, Y.-C. Huang, J.-L. Chen, C.-L. Chen, W. C. Chou, J.-M. Chen, J.-F. Lee, S. Shen, C.-L. Dong, Visible light-induced electronic structure modulation of Nb- and Ta-doped α-Fe2O3 nanorods for effective photoelectrochemical water splitting, Nanotechnology 29 (6) (2018), 064002.
[257] A. Pu, J. Deng, M. Li, J. Gao, H. Zhang, Y. Hao, J. Zhong, X. Sun, Coupling Ti-doping and oxygen vacancies in hematite nanostructures for solar water oxidation with high efficiency, J. Mater. Chem. A 2 (8) (2014) 2491–2497.
[258] D. Cao, W. Luo, M. Li, J. Feng, Z. Li, Z. Zou, A transparent Ti4+ doped hematite photoanode protectively grown by a facile hydrothermal method, CrystEngComm 15 (13) (2013) 2386–2391.
[259] M.A. Lukowski, S. Jin, Improved Synthesis and Electrical Properties of Si-Doped α-Fe2O3 Nanowires, J. Phys. Chem. C. 115 (25) (2011) 12388–12395.
[260] J.C. Launay, G. Horowitz, Crystal growth and photoelectrochemical study of Zr-doped α-Fe2O3 single crystal, J. Cryst. Growth 57 (1) (1982) 118–124.
[261] Y.-S. Hu, A. Kleiman-Shwarsctein, A.J. Forman, D. Hazen, J.-N. Park, E. W. McFarland, Pt-Doped α-Fe2O3 Thin Films Active for Photoelectrochemical Water Splitting, Chem. Mater. 20 (12) (2008) 3803–3805.
[262] Y. Ling, G. Wang, D.A. Wheeler, J.Z. Zhang, Y. Li, Sn-doped hematite nanostructures for photoelectrochemical water splitting, Nano Lett. 11 (5) (2011) 2119–2125.
[263] A.G. Tamirat, W.-N. Su, A.A. Dubale, H.-M. Chen, B.-J. Hwang, Photoelectrochemical water splitting at low applied potential using a NiOOH coated codoped (Sn, Zr) α-Fe2O3 photoanode, J. Mater. Chem. A 3 (11) (2015) 5949–5961.
[264] A. Annamalai, H.H. Lee, S.H. Choi, S.Y. Lee, E. Gracia-Espino, A. Subramanian, J. Park, K.-J. Kong, J.S. Jang, Sn/Be Sequentially co-doped Hematite Photoanodes for Enhanced Photoelectrochemical Water Oxidation: Effect of Be2+ as co-dopant, Sci. Rep. 6 (1) (2016) 23183.
[265] S. Shen, J. Chen, M. Wang, X. Sheng, X. Chen, X. Feng, S.S. Mao, Titanium dioxide nanostructures for photoelectrochemical applications, Prog. Mater. Sci. 98 (2018) 299–385.
[266] S. Li, J. Cai, Y. Liu, M. Gao, F. Cao, G. Qin, Tuning orientation of doped hematite photoanodes for enhanced photoelectrochemical water oxidation, Sol. Energy Mater. Sol. Cells 179 (2018) 328–333.
[267] J. Cai, H. Chen, C. Liu, S. Yin, H. Li, L. Xu, H. Liu, Q. Xie, Engineered Sn- and Mg-doped hematite photoanodes for efficient photoelectrochemical water oxidation, Dalton Trans. 49 (32) (2020) 11282–11289.
[268] K. Sivula, F. Le Formal, M. Grätzel, Solar Water Splitting: Progress Using Hematite (α-Fe2O3) Photoelectrodes, ChemSusChem 4 (4) (2011) 432–449.
[269] F. Amano, B. Ohtani, H. Yoshida, Role of doped titanium species in the enhanced photoelectrochemical properties of iron oxide films: Comparison between water oxidation and iodide ion oxidation, J. Electroanal. Chem. 766 (2016) 100–106.
[270] K. Sivula, R. van de Krol, Semiconducting materials for photoelectrochemical energy conversion, Nat. Rev. Mater. 1 (2) (2016) 15010.
[271] A. Paracchino, V. Laporte, K. Sivula, M. Grätzel, E. Thimsen, Highly active oxide photocathode for photoelectrochemical water reduction, Nat. Mater. 10 (6) (2011) 456–461.
[272] L. Pan, J.H. Kim, M.T. Mayer, M.-K. Son, A. Ummadisingu, J.S. Lee, A. Hagfeldt, J. Luo, M. Grätzel, Boosting the performance of Cu2O photocathodes for unassisted solar water splitting devices, Nat. Catal. 1 (6) (2018) 412–420.
[273] X. Xu, A.K. Azad, J.T.S. Irvine, Photocatalytic H2 generation from spinels ZnFe2O4, ZnFeGaO4 and ZnGa2O4, Catal. Today 199 (2013) 22–26.

[274] J.H. Kim, J.H. Kim, J.-W. Jang, J.Y. Kim, S.H. Choi, G. Magesh, J. Lee, J.S. Lee, Awakening Solar Water-Splitting Activity of ZnFe2O4 Nanorods by Hybrid Microwave Annealing, Adv. Energy Mater. 5 (6) (2015) 1401933.

[275] J.H. Kim, Y.J. Jang, J.H. Kim, J.-W. Jang, S.H. Choi, J.S. Lee, Defective ZnFe2O4 nanorods with oxygen vacancy for photoelectrochemical water splitting, Nanoscale 7 (45) (2015) 19144–19151.

[276] N. Guijarro, P. Bornoz, M. Prévot, X. Yu, X. Zhu, M. Johnson, X. Jeanbourquin, F. Le Formal, K. Sivula, Evaluating spinel ferrites MFe2O4 (M = Cu, Mg, Zn) as photoanodes for solar water oxidation: prospects and limitations, Sustain. Energy Fuels 2 (1) (2018) 103–117.

[277] J.H. Kim, Y.J. Jang, S.H. Choi, B.J. Lee, J.H. Kim, Y.B. Park, C.-M. Nam, H.G. Kim, J.S. Lee, A multitude of modifications strategy of ZnFe2O4 nanorod photoanodes for enhanced photoelectrochemical water splitting activity, J. Mater. Chem. A 6 (26) (2018) 12693–12700.

[278] X. Zhu, N. Guijarro, Y. Liu, P. Schouwink, R.A. Wells, F. Le Formal, S. Sun, C. Gao, K. Sivula, Spinel Structural Disorder Influences Solar-Water-Splitting Performance of ZnFe2O4 Nanorod Photoanodes, Adv. Mater. 30 (34) (2018) 1801612.

[279] A.G. Hufnagel, K. Peters, A. Müller, C. Scheu, D. Fattakhova-Rohlfing, T. Bein, Zinc Ferrite Photoanode Nanomorphologies with Favorable Kinetics for Water-Splitting, Adv. Funct. Mater. 26 (25) (2016) 4435–4443.

[280] A.A. Tahir, K.G.U. Wijayantha, Photoelectrochemical water splitting at nanostructured ZnFe2O4 electrodes, J. Photochem. Photobiol. A: Chem. 216 (2) (2010) 119–125.

[281] Y. Guo, N. Zhang, X. Wang, Q. Qian, S. Zhang, Z. Li, Z. Zou, A facile spray pyrolysis method to prepare Ti-doped ZnFe2O4 for boosting photoelectrochemical water splitting, J. Mater. Chem. A 5 (16) (2017) 7571–7577.

[282] H. Dotan, K. Sivula, M. Grätzel, A. Rothschild, S.C. Warren, Probing the photoelectrochemical properties of hematite (α-Fe2O3) electrodes using hydrogen peroxide as a hole scavenger, Energy Environ. Sci. 4 (3) (2011) 958–964.

[283] K. Itoh, J.O.M. Bockris, Thin Film Photoelectrochemistry: Iron Oxide, J. Electrochem. Soc. 131 (6) (1984) 1266.

[284] D. Taffa, R. Dillert, A. Ulpe, K.C. Bauerfeind, T. Bredow, D. Bahnemann, M. Wark, Photoelectrochemical and theoretical investigations of spinel type ferrites (MxFe3−xO4) for water splitting: a mini-review, J. Photonics Energy 7 (1) (2016), 012009.

[285] L.G.J. De Haart, G. Blasse, Photoelectrochemical properties of ferrites with the spinel structure, Solid State Ion. 16 (1985) 137–139.

[286] F.A. Benko, F.P. Koffyberg, The effect of defects on some photoelectrochemical properties of semiconducting MgFe2O4, Mater. Res. Bull. 21 (10) (1986) 1183–1188.

[287] Y. Hou, F. Zuo, A. Dagg, P. Feng, A. Three-Dimensional, Branched Cobalt-Doped α-Fe2O3 Nanorod/MgFe2O4 Heterojunction Array as a Flexible Photoanode for Efficient Photoelectrochemical Water Oxidation, Angew. Chem. Int. Ed. 52 (4) (2013) 1248–1252.

[288] H.G. Kim, P.H. Borse, J.S. Jang, E.D. Jeong, O.-S. Jung, Y.J. Suh, J.S. Lee, Fabrication of CaFe2O4/MgFe2O4 bulk heterojunction for enhanced visible light photocatalysis, Chem. Commun. 39 (2009) 5889–5891.

[289] R. Dom, P.H. Borse, K.-S. Hong, S. Choi, B.S. Lee, M.G. Ha, J.P. Kim, E.D. Jeong, H.G. Kim, Nanocrystalline magnesium ferrite prepared for photocatalytic applications by using the polymerized complex method, J. Korean Phys. Soc. 67 (9) (2015) 1639–1645.

[290] T. Tsoncheva, E. Manova, N. Velinov, D. Paneva, M. Popova, B. Kunev, K. Tenchev, I. Mitov, Thermally synthesized nanosized copper ferrites as catalysts for environment protection, Catal. Commun. 12 (2) (2010) 105–109.

[291] A.M. Balagurov, I.A. Bobrikov, M.S. Maschenko, D. Sangaa, V.G. Simkin, Structural phase transition in CuFe2O4 spinel, Crystallogr. Rep. 58 (5) (2013) 710–717.

[292] H. Yang, J. Yan, Z. Lu, X. Cheng, Y. Tang, Photocatalytic activity evaluation of tetragonal CuFe2O4 nanoparticles for the H2 evolution under visible light irradiation, J. Alloy. Compd. 476 (1) (2009) 715–719.

[293] Y. Gao, O. Zandi, T.W. Hamann, Atomic layer stack deposition-annealing synthesis of CuWO4, J. Mater. Chem. A 4 (8) (2016) 2826–2830.

[294] J.E. Yourey, B.M. Bartlett, Electrochemical deposition and photoelectrochemistry of CuWO4, a promising photoanode for water oxidation, J. Mater. Chem. 21 (21) (2011) 7651–7660.

[295] J.E. Yourey, K.J. Pyper, J.B. Kurtz, B.M. Bartlett, Chemical Stability of CuWO4 for Photoelectrochemical Water Oxidation, J. Phys. Chem. C. 117 (17) (2013) 8708–8718.

[296] J.C. Hill, K.-S. Choi, Synthesis and characterization of high surface area CuWO4 and Bi2WO6 electrodes for use as photoanodes for solar water oxidation, J. Mater. Chem. A 1 (16) (2013) 5006–5014.

[297] C.R. Lhermitte, B.M. Bartlett, Advancing the Chemistry of CuWO4 for Photoelectrochemical Water Oxidation, Acc. Chem. Res. 49 (6) (2016) 1121–1129.

[298] D. Bohra, W.A. Smith, Improved charge separation via Fe-doping of copper tungstate photoanodes, Phys. Chem. Chem. Phys. 17 (15) (2015) 9857–9866.

[299] A. Theuwis, I.E. Vermeir, W.P. Gomes, Chemical and electrochemical interaction of acidic H2O2 solutions with (100) InP, J. Electroanal. Chem. 410 (1) (1996) 31–42.

[300] Y. Gao, T.W. Hamann, Quantitative hole collection for photoelectrochemical water oxidation with CuWO4, Chem. Commun. 53 (7) (2017) 1285–1288.

[301] K.M. Nam, E.A. Cheon, W.J. Shin, A.J. Bard, Improved Photoelectrochemical Water Oxidation by the WO3/CuWO4 Composite with a Manganese Phosphate Electrocatalyst, Langmuir 31 (39) (2015) 10897–10903.

[302] J.E. Yourey, J.B. Kurtz, B.M. Bartlett, Structure, Optical Properties, and Magnetism of the Full Zn1−xCuxWO4 ($0 \leq x \leq 1$) Composition Range, Inorg. Chem. 51 (19) (2012) 10394–10401.

[303] Y. Tang, N. Rong, F. Liu, M. Chu, H. Dong, Y. Zhang, P. Xiao, Enhancement of the photoelectrochemical performance of CuWO4 films for water splitting by hydrogen treatment, Appl. Surf. Sci. 361 (2016) 133–140.

[304] D. Hu, P. Diao, D. Xu, M. Xia, Y. Gu, Q. Wu, C. Li, S. Yang, Copper(ii) tungstate nanoflake array films: sacrificial template synthesis, hydrogen treatment, and their application as photoanodes in solar water splitting, Nanoscale 8 (11) (2016) 5892–5901.

[305] N. Gaillard, Y. Chang, A. DeAngelis, S. Higgins, A. Braun, A nanocomposite photoelectrode made of 2.2 eV band gap copper tungstate (CuWO4) and multi-wall carbon nanotubes for solar-assisted water splitting, Int. J. Hydrog. Energy 38 (8) (2013) 3166–3176.

[306] D. Peeters, O. Mendoza Reyes, L. Mai, A. Sadlo, S. Cwik, D. Rogalla, H.W. Becker, H.M. Schütz, J. Hirst, S. Müller, D. Friedrich, D. Mitoraj, M. Nagli, M.C. Toroker, R. Eichberger, R. Beranek, A. Devi, CVD-grown copper tungstate thin films for solar water splitting, J. Mater. Chem. A 6 (22) (2018) 10206–10216.

[307] W. Ye, F. Chen, F. Zhao, N. Han, Y. Li, CuWO4 nanoflake array-based single-junction and heterojunction photoanodes for photoelectrochemical water oxidation, ACS Appl. Mater. Interfaces 8 (14) (2016) 9211–9217.

[308] K.J. Pyper, J.E. Yourey, B.M. Bartlett, Reactivity of CuWO4 in photoelectrochemical water oxidation is dictated by a midgap electronic state, J. Phys. Chem. C. 117 (47) (2013) 24726–24732.

[309] Y. Gao, T.W. Hamann, Elucidation of CuWO4 surface states during photoelectrochemical water oxidation, J. Phys. Chem. Lett. 8 (12) (2017) 2700–2704.

[310] M.M. Khader, M.M. Saleh, E.M. El-Naggar, Photoelectrochemical characteristics of ferric tungstate, J. Solid State Electrochem. 2 (3) (1998) 170–175.

[311] F.F. Abdi, A. Chemseddine, S.P. Berglund, R. van de Krol, Assessing the Suitability of Iron Tungstate (Fe2WO6) as a Photoelectrode Material for Water Oxidation, J. Phys. Chem. C. 121 (1) (2017) 153–160.

[312] J.H. Kim, J.-W. Jang, Y.H. Jo, F.F. Abdi, Y.H. Lee, R. van de Krol, J.S. Lee, Hetero-type dual photoanodes for unbiased solar water splitting with extended light harvesting, Nat. Commun. 7 (1) (2016) 13380.

[313] K.J. McDonald, K.-S. Choi, A new electrochemical synthesis route for a BiOI electrode and its conversion to a highly efficient porous BiVO4 photoanode for solar water oxidation, Energy Environ. Sci. 5 (9) (2012) 8553–8557.

[314] T.W. Kim, K.-S. Choi, Nanoporous BiVO4 Photoanodes with Dual-Layer Oxygen Evolution Catalysts for Solar Water Splitting, Science 343 (6174) (2014) 990–994.

[315] Y. Park, D. Kang, K.-S. Choi, Marked enhancement in electron–hole separation achieved in the low bias region using electrochemically prepared Mo-doped BiVO4 photoanodes, Phys. Chem. Chem. Phys. 16 (3) (2014) 1238–1246.

[316] T.W. Kim, Y. Ping, G.A. Galli, K.-S. Choi, Simultaneous enhancements in photon absorption and charge transport of bismuth vanadate photoanodes for solar water splitting, Nat. Commun. 6 (1) (2015) 8769.

[317] J.H. Kim, Y. Jo, J.H. Kim, J.W. Jang, H.J. Kang, Y.H. Lee, D.S. Kim, Y. Jun, J. S. Lee, Wireless Solar Water Splitting Device with Robust Cobalt-Catalyzed, Dual-Doped BiVO4 Photoanode and Perovskite Solar Cell in Tandem: A Dual Absorber Artificial Leaf, ACS Nano 9 (12) (2015) 11820–11829.

[318] C. Ding, J. Shi, D. Wang, Z. Wang, N. Wang, G. Liu, F. Xiong, C. Li, Visible light driven overall water splitting using cocatalyst/BiVO4 photoanode with minimized bias, Phys. Chem. Chem. Phys. 15 (13) (2013) 4589–4595.

[319] A.J.E. Rettie, H.C. Lee, L.G. Marshall, J.-F. Lin, C. Capan, J. Lindemuth, J. S. McCloy, J. Zhou, A.J. Bard, C.B. Mullins, Combined Charge Carrier Transport and Photoelectrochemical Characterization of BiVO4 Single Crystals: Intrinsic Behavior of a Complex Metal Oxide, J. Am. Chem. Soc. 135 (30) (2013) 11389–11396.

[320] Y. Qiu, W. Liu, W. Chen, W. Chen, G. Zhou, P.-C. Hsu, R. Zhang, Z. Liang, S. Fan, Y. Zhang, Y. Cui, Efficient solar-driven water splitting by nanocone BiVO4-perovskite tandem cells, Sci. Adv. 2 (6) (2016), e1501764.

[321] L. Han, F.F. Abdi, R. van de Krol, R. Liu, Z. Huang, H.-J. Lewerenz, B. Dam, M. Zeman, A.H.M. Smets, Efficient Water-Splitting Device Based on a Bismuth Vanadate Photoanode and Thin-Film Silicon Solar Cells, ChemSusChem 7 (10) (2014) 2832–2838.

[322] S. Xiao, C. Hu, H. Lin, X. Meng, Y. Bai, T. Zhang, Y. Yang, Y. Qu, K. Yan, J. Xu, Y. Qiu, S. Yang, Integration of inverse nanocone array based bismuth vanadate photoanodes and bandgap-tunable perovskite solar cells for efficient self-powered solar water splitting, J. Mater. Chem. A 5 (36) (2017) 19091–19097.

[323] Y. Kuang, Q. Jia, H. Nishiyama, T. Yamada, A. Kudo, K. Domen, A. Front-Illuminated, Nanostructured Transparent BiVO4 Photoanode for >2% Efficient Water Splitting, Adv. Energy Mater. 6 (2) (2016) 1501645.

[324] Y. Kuang, Q. Jia, G. Ma, T. Hisatomi, T. Minegishi, H. Nishiyama, M. Nakabayashi, N. Shibata, T. Yamada, A. Kudo, K. Domen, Ultrastable low-bias water splitting photoanodes via photocorrosion inhibition and in situ catalyst regeneration, Nat. Energy 2 (1) (2016) 16191.

[325] S. Wang, P. Chen, Y. Bai, J.-H. Yun, G. Liu, L. Wang, New BiVO4 Dual Photoanodes with Enriched Oxygen Vacancies for Efficient Solar-Driven Water Splitting, Adv. Mater. 30 (20) (2018) 1800486.

[326] D.K. Lee, K.-S. Choi, Enhancing long-term photostability of BiVO4 photoanodes for solar water splitting by tuning electrolyte composition, Nat. Energy 3 (1) (2018) 53–60.

[327] J.A. Seabold, N.R. Neale, All first row transition metal oxide photoanode for water splitting based on Cu3V2O8, Chem. Mater. 27 (3) (2015) 1005–1013.

[328] C.-M. Jiang, M. Farmand, C.H. Wu, Y.-S. Liu, J. Guo, W.S. Drisdell, J.K. Cooper, I. D. Sharp, Electronic Structure, Optoelectronic Properties, and Photoelectrochemical Characteristics of γ-Cu3V2O8 Thin Films, Chem. Mater. 29 (7) (2017) 3334–3345.
[329] P.F. Newhouse, D.A. Boyd, A. Shinde, D. Guevarra, L. Zhou, E. Soedarmadji, G. Li, J.B. Neaton, J.M. Gregoire, Solar fuel photoanodes prepared by inkjet printing of copper vanadates, J. Mater. Chem. A 4 (19) (2016) 7483–7494.
[330] W. Guo, W.D. Chemelewski, O. Mabayoje, P. Xiao, Y. Zhang, C.B. Mullins, Synthesis and Characterization of CuV2O6 and Cu2V2O7: Two Photoanode Candidates for Photoelectrochemical Water Oxidation, J. Phys. Chem. C. 119 (49) (2015) 27220–27227.
[331] M.-w Kim, B. Joshi, H. Yoon, T.Y. Ohm, K. Kim, S.S. Al-Deyab, S.S. Yoon, Electrosprayed copper hexaoxodivanadate (CuV2O6) and pyrovanadate (Cu2V2O7) photoanodes for efficient solar water splitting, J. Alloy. Compd. 708 (2017) 444–450.
[332] I. Khan, A. Qurashi, Shape controlled synthesis of copper vanadate platelet nanostructures, their optical band edges, and solar-driven water splitting properties, Sci. Rep. 7 (1) (2017) 14370.
[333] D. Cardenas-Morcoso, A. Peiro-Franch, I. Herraiz-Cardona, S. Gimenez, Chromium doped copper vanadate photoanodes for water splitting, Catal. Today 290 (2017) 65–72.
[334] M.A. Lumley, K.-S. Choi, Investigation of Pristine and (Mo, W)-Doped Cu11V6O26 for Use as Photoanodes for Solar Water Splitting, Chem. Mater. 29 (21) (2017) 9472–9479.
[335] C.-M. Jiang, G. Segev, L.H. Hess, G. Liu, G. Zaborski, F.M. Toma, J.K. Cooper, I. D. Sharp, Composition-Dependent Functionality of Copper Vanadate Photoanodes, ACS Appl. Mater. Interfaces 10 (13) (2018) 10627–10633.
[336] Y. Park, K.J. McDonald, K.-S. Choi, Progress in bismuth vanadate photoanodes for use in solar water oxidation, Chem. Soc. Rev. 42 (6) (2013) 2321–2337.
[337] H. Ye, H.S. Park, A.J. Bard, Screening of Electrocatalysts for Photoelectrochemical Water Oxidation on W-Doped BiVO4 Photocatalysts by Scanning Electrochemical Microscopy, J. Phys. Chem. C. 115 (25) (2011) 12464–12470.
[338] A.C. Cardiel, K.J. McDonald, K.-S. Choi, Electrochemical Growth of Copper Hydroxy Double Salt Films and Their Conversion to Nanostructured p-Type CuO Photocathodes, Langmuir 33 (37) (2017) 9262–9270.
[339] T. Arai, Y. Konishi, Y. Iwasaki, H. Sugihara, K. Sayama, High-Throughput Screening Using Porous Photoelectrode for the Development of Visible-Light-Responsive Semiconductors, J. Comb. Chem. 9 (4) (2007) 574–581.
[340] B. Robertson, E. Kostiner, Crystal structure and Mössbauer effect investigation of FeVO4, J. Solid State Chem. 4 (1) (1972) 29–37.
[341] C.D. Morton, I.J. Slipper, M.J.K. Thomas, B.D. Alexander, Synthesis and characterisation of Fe–V–O thin film photoanodes, J. Photochem. Photobiol. A: Chem. 216 (2) (2010) 209–214.
[342] S.K. Biswas, J.-O. Baeg, Enhanced photoactivity of visible light responsive W incorporated FeVO4 photoanode for solar water splitting, Int. J. Hydrog. Energy 38 (34) (2013) 14451–14457.
[343] W. Wang, Y. Zhang, L. Wang, Y. Bi, Facile synthesis of Fe3+/Fe2+ self-doped nanoporous FeVO4 photoanodes for efficient solar water splitting, J. Mater. Chem. A 5 (6) (2017) 2478–2482.
[344] M. Balamurugan, G. Yun, K.-S. Ahn, S.H. Kang, Revealing the Beneficial Effects of FeVO4 Nanoshell Layer on the BiVO4 Inverse Opal Core Layer for Photoelectrochemical Water Oxidation, J. Phys. Chem. C. 121 (14) (2017) 7625–7634.
[345] M. Zhang, Y. Ma, D. Friedrich, R. van de Krol, L.H. Wong, F.F. Abdi, Elucidation of the opto-electronic and photoelectrochemical properties of FeVO4 photoanodes for solar water oxidation, J. Mater. Chem. A 6 (2) (2018) 548–555.
[346] H. Mandal, S. Shyamal, P. Hajra, A. Bera, D. Sariket, S. Kundu, C. Bhattacharya, Development of ternary iron vanadium oxide semiconductors for applications in photoelectrochemical water oxidation, RSC Adv. 6 (6) (2016) 4992–4999.
[347] D. Tang, A.J.E. Rettie, O. Mabayoje, B.R. Wygant, Y. Lai, Y. Liu, C.B. Mullins, Facile growth of porous Fe2V4O13 films for photoelectrochemical water oxidation, J. Mater. Chem. A 4 (8) (2016) 3034–3042.

ORIGINALITY REPORT

16%	10%	12%	5%
SIMILARITY INDEX	INTERNET SOURCES	PUBLICATIONS	STUDENT PAPERS

PRIMARY SOURCES

1	pureadmin.qub.ac.uk Internet Source	1%
2	www.jos.ac.cn Internet Source	1%
3	Shan Wang, Dandan Cui, Weichang Hao, Yi Du. " Roles of Cocatalysts on BiVO Photoanodes for Photoelectrochemical Water Oxidation: A Minireview ", Energy & Fuels, 2022 Publication	1%
4	Yumeng Lu, Jinzhan Su, Jinwen Shi, Di Zhou. " Surface Recombination Passivation of the BiVO Photoanode by the Synergistic Effect of the Cobalt/Nickel Sulfide Cocatalyst ", ACS Applied Energy Materials, 2020 Publication	1%
5	Ananta Rizki Fareza, Ferry Anggoro Ardy Nugroho, Fatwa Abdi, Vivi Fauzia. "Nanoscale Metal Oxides–2D Materials Heterostructures for Photoelectrochemical Water Splitting—A	<1%

Review", Journal of Materials Chemistry A, 2022
Publication

6	Submitted to University of Portsmouth Student Paper	<1%
7	Xin Li, Jiaguo Yu, Mietek Jaroniec, Xiaobo Chen. " Cocatalysts for Selective Photoreduction of CO into Solar Fuels ", Chemical Reviews, 2019 Publication	<1%
8	Miao Zhong, Takashi Hisatomi, Yongbo Kuang, Jiao Zhao et al. " Surface Modification of CoO Loaded BiVO Photoanodes with Ultrathin - Type NiO Layers for Improved Solar Water Oxidation ", Journal of the American Chemical Society, 2015 Publication	<1%
9	www.researchgate.net Internet Source	<1%
10	Quan Liu, Rong Mo, Xiaoli Li, Sui Yang, Jianxin Zhong, Hongxing Li. "Cobalt Phosphate Modified 3D TiO2/BiVO4 Composite Inverse Opals Photoanode for Enhanced Photoelectrochemical Water Splitting", Applied Surface Science, 2018 Publication	<1%

11	Mahesh P. Suryawanshi, Uma V. Ghorpade, Cui Ying Toe, Umesh P. Suryawanshi et al. "Earth-abundant photoelectrodes for water splitting and alternate oxidation reactions: Recent advances and future perspectives", Progress in Materials Science, 2023 Publication	<1 %
12	Submitted to University College London Student Paper	<1 %
13	Submitted to Majmaah University Student Paper	<1 %
14	Hardy Shuwanto, Hairus Abdullah, Dong-Hau Kuo. " Nanostructuring Bi-Doped α-Fe O Thin-Layer Photoanode to Advance the Water Oxidation Performance ", ACS Applied Energy Materials, 2022 Publication	<1 %
15	Prabhakarn Arunachalam, Haneen A. AlOraij, Mabrook S. Amer, Mahmoud Hezam, Maged N. Shaddad, Jagannathan Madhavan. "Activation effect of nickel phosphate co-catalysts on the photoelectrochemical water oxidation performance of TiO2 nanotubes", Journal of Saudi Chemical Society, 2022 Publication	<1 %
16	repository.wima.ac.id Internet Source	<1 %

17	mafiadoc.com Internet Source	<1 %
18	Submitted to Universiti Malaysia Terengganu UMT Student Paper	<1 %
19	Xing Cao, Peng Wen, Rui Ma, Ya Liu, Shichang Sun, Qing Ma, Peixin Zhang, Yejun Qiu. "Ni2P nanocrystals modification on Ta:α-Fe2O3 photoanode for efficient photoelectrochemical water splitting: In situ formation and synergistic catalysis of Ni2P@NiOOH cocatalyst", Chemical Engineering Journal, 2022 Publication	<1 %
20	www.helmholtz-berlin.de Internet Source	<1 %
21	depositonce.tu-berlin.de Internet Source	<1 %
22	www.nature.com Internet Source	<1 %
23	www.science.gov Internet Source	<1 %
24	Yi Wen Phuan, Wee-Jun Ong, Meng Nan Chong, Joey D. Ocon. "Prospects of electrochemically synthesized hematite photoanodes for photoelectrochemical water	<1 %

splitting: A review", Journal of Photochemistry and Photobiology C: Photochemistry Reviews, 2017
Publication

25	link.springer.com Internet Source	<1 %
26	purehost.bath.ac.uk Internet Source	<1 %
27	Submitted to Mugla University Student Paper	<1 %
28	Margaret A. Lumley, Kyoung-Shin Choi. " Investigation of Pristine and (Mo, W)-Doped Cu V O for Use as Photoanodes for Solar Water Splitting ", Chemistry of Materials, 2017 Publication	<1 %
29	"Photoelectrochemical Solar Fuel Production", Springer Science and Business Media LLC, 2016 Publication	<1 %
30	Cui Ying Toe, Shujie Zhou, Michael Gunawan, Xinxin Lu, Yun Hau Ng, Rose Amal. "Recent advances and the design criteria of metal sulfide photocathodes and photoanodes for photoelectrocatalysis", Journal of Materials Chemistry A, 2021 Publication	<1 %

Submitted to Monash University

31	Student Paper	<1%
32	acikbilim.yok.gov.tr Internet Source	<1%
33	d-nb.info Internet Source	<1%
34	academic.hep.com.cn Internet Source	<1%
35	www.jmst.org Internet Source	<1%
36	Hairus Abdullah, Riski Titian Ginting, Anita Christine Sembiring, Noto Susanto Gultom, Hardy Shuwanto, Dong-Hau Kuo. " One-pot preparation of multicomponent photocatalyst with (Zn, Co, Ni)(O, S)/Ga O nanocomposites to significantly enhance hydrogen production ", New Journal of Chemistry, 2021 Publication	<1%
37	Submitted to University of Macau Student Paper	<1%
38	mdpi-res.com Internet Source	<1%
39	onlinelibrary.wiley.com Internet Source	<1%
40	os.zhdk.cloud.switch.ch Internet Source	

		<1 %
41	"Graphene-based Energy Devices", Wiley, 2015 Publication	<1 %
42	Submitted to Imperial College of Science, Technology and Medicine Student Paper	<1 %
43	scholars.cityu.edu.hk Internet Source	<1 %
44	Theron J. Pappas. "Recent advances in micellar electrokinetic chromatography", Electrophoresis, 02/2005 Publication	<1 %
45	Xiaoqian Huang, Ruikang Zhang, Xiaoru Gao, Borong Yu, Yuanzhe Gao, Zhan-gang Han. "TiO2-rutile/anatase homojunction with enhanced charge separation for photoelectrochemical water splitting", International Journal of Hydrogen Energy, 2021 Publication	<1 %
46	Zhiwei Wang, Heng Zhu, Wenguang Tu, Xi Zhu, Yingfang Yao, Yong Zhou, Zhigang Zou. "Host/Guest Nanostructured Photoanodes Integrated with Targeted Enhancement	<1 %

Strategies for Photoelectrochemical Water Splitting", Advanced Science, 2021
Publication

47	dokumen.pub Internet Source	<1 %
48	Submitted to CSU, San Jose State University Student Paper	<1 %
49	Donghyeon Kang, Tae Woo Kim, Stephen R. Kubota, Allison C. Cardiel, Hyun Gil Cha, Kyoung-Shin Choi. "Electrochemical Synthesis of Photoelectrodes and Catalysts for Use in Solar Water Splitting", Chemical Reviews, 2015 Publication	<1 %
50	pubs.acs.org Internet Source	<1 %
51	ebin.pub Internet Source	<1 %
52	www.mdpi.com Internet Source	<1 %
53	Angang Song, Abdelkrim Chemseddine, Ibbi Yilmaz Ahmet, Peter Bogdanoff et al. " Evaluation of Copper Vanadate (β-Cu V O) as a Photoanode Material for Photoelectrochemical Water Oxidation ", Chemistry of Materials, 2020 Publication	<1 %

54	N.F. Khusnun, A. Arshad, A.A. Jalil, L. Firmansyah et al. "An avant-garde of carbon-doped photoanode materials on photo-electrochemical water splitting performance: A review", Journal of Electroanalytical Chemistry, 2022 Publication	<1 %
55	eprints.lib.hokudai.ac.jp Internet Source	<1 %
56	Joseph E. Yourey, Kayla J. Pyper, Joshua B. Kurtz, Bart M. Bartlett. " Chemical Stability of CuWO for Photoelectrochemical Water Oxidation ", The Journal of Physical Chemistry C, 2013 Publication	<1 %
57	Xuefeng Long, Lili Gao, Feng Li, Yiping Hu, Shenqi Wei, Chenglong Wang, Tong Wang, Jun Jin, Jiantai Ma. "Bamboo shoots shaped FeVO4 passivated ZnO nanorods photoanode for improved charge separation/transfer process towards efficient solar water splitting", Applied Catalysis B: Environmental, 2019 Publication	<1 %
58	Yubin Chen, Ya Liu, Feng Wang, Xiangjiu Guan, Liejin Guo. "Toward practical photoelectrochemical water splitting and CO2 reduction using earth-abundant materials", Journal of Energy Chemistry, 2021	<1 %

Publication

59	Yumin He, Thomas Hamann, Dunwei Wang. "Thin film photoelectrodes for solar water splitting", Chemical Society Reviews, 2019 Publication	<1 %
60	dr.ntu.edu.sg Internet Source	<1 %
61	oak.ulsan.ac.kr Internet Source	<1 %
62	www.rs.kagu.tus.ac.jp Internet Source	<1 %
63	Jin Hyun Kim, Jae Sung Lee. " Elaborately Modified BiVO Photoanodes for Solar Water Splitting ", Advanced Materials, 2019 Publication	<1 %
64	Sol A Lee, Seokhoon Choi, Changyeon Kim, Jin Wook Yang, Soo Young Kim, Ho Won Jang. "Si-Based Water Oxidation Photoanodes Conjugated with Earth-Abundant Transition Metal-Based Catalysts", ACS Materials Letters, 2019 Publication	<1 %
65	Jin Hyun Kim, Dharmesh Hansora, Pankaj Sharma, Ji-Wook Jang, Jae Sung Lee. "Toward practical solar hydrogen production – an artificial photosynthetic leaf-to-farm challenge", Chemical Society Reviews, 2019	<1 %

Publication

66	Joshua O. Olowoyo, Roelof J. Kriek. "Mono- and bimetallic oxides as photo-electrocatalysts for the oxygen evolution reaction – A review", Journal of Physics and Chemistry of Solids, 2022 Publication	<1 %
67	Siti Nurul Falaein Moridon, Khuzaimah Arifin, Rozan Mohammad Yunus, Lorna Jeffery Minggu, Mohammad B. Kassim. "Photocatalytic water splitting performance of TiO2 sensitized by metal chalcogenides: A review", Ceramics International, 2021 Publication	<1 %
68	Stephanie J. Boyd, Run Long, Niall J. English. "Electric Field Effects on Photoelectrochemical Water Splitting: Perspectives and Outlook", Energies, 2022 Publication	<1 %
69	Submitted to University of Durham Student Paper	<1 %
70	gyan.iitg.ernet.in Internet Source	<1 %
71	infoscience.epfl.ch Internet Source	<1 %
72	Dan Yin, Xingming Ning, Peiyao Du, Dongxu Zhang, Qi Zhang, Xiaoquan Lu. "Cascaded	<1 %

Multiple-Step Hole Transfer for Enhancing Photoelectrochemical Water Splitting", Applied Catalysis B: Environmental, 2021
Publication

73	Submitted to Khalifa University of Science Technology and Research Student Paper	<1 %
74	unsworks.unsw.edu.au Internet Source	<1 %
75	www.science.org Internet Source	<1 %
76	Qi Sun, Ting Cheng, Zhirong Liu, Limin Qi. "A cobalt silicate modified BiVO4 photoanode for efficient solar water oxidation", Applied Catalysis B: Environmental, 2020 Publication	<1 %
77	ro.uow.edu.au Internet Source	<1 %
78	Jeong Hun Kim, Hyo Eun Kim, Jin Hyun Kim, Jae Sung Lee. "Ferrites: Emerging light absorbers for solar water splitting", Journal of Materials Chemistry A, 2020 Publication	<1 %
79	Submitted to Savitribai Phule Pune University Student Paper	<1 %

80	Sushil Kumar Saraswat, Dylan D. Rodene, Ram B. Gupta. "Recent advancements in semiconductor materials for photoelectrochemical water splitting for hydrogen production using visible light", Renewable and Sustainable Energy Reviews, 2018 Publication	<1 %
81	Tianhao Li, Tao Hu, Liming Dai, Chang Ming Li. "Metal-free photo- and electro-catalysts for hydrogen evolution reaction", Journal of Materials Chemistry A, 2020 Publication	<1 %
82	repo.lib.tokushima-u.ac.jp Internet Source	<1 %
83	spiral.imperial.ac.uk Internet Source	<1 %
84	Submitted to Chulalongkorn University Student Paper	<1 %
85	Hengcong Tao, Qun Fan, Tao Ma, Shizhen Liu, Henry Gysling, John Texter, Fen Guo, Zhenyu Sun. "Two-dimensional materials for energy conversion and storage", Progress in Materials Science, 2020 Publication	<1 %
86	Jitendra N. Tiwari, Aditya Narayan Singh, Siraj Sultan, Kwang S. Kim. "Recent Advancement	<1 %

of p - and d - Block Elements, Single Atoms, and Graphene - Based Photoelectrochemical Electrodes for Water Splitting", Advanced Energy Materials, 2020
Publication

87	Yongcai Qiu, Zhenghui Pan, Haining Chen, Daiqi Ye, Lin Guo, Zhiyong Fan, Shihe Yang. "Current progress in developing metal oxide nanoarrays-based photoanodes for photoelectrochemical water splitting", Science Bulletin, 2019 Publication	<1 %
88	discovery.ucl.ac.uk Internet Source	<1 %
89	edoc.ub.uni-muenchen.de Internet Source	<1 %
90	kyutech.repo.nii.ac.jp Internet Source	<1 %
91	science.sciencemag.org Internet Source	<1 %
92	"Methods for Electrocatalysis", Springer Science and Business Media LLC, 2020 Publication	<1 %
93	Chunmei Ding, Jingying Shi, Zhiliang Wang, Can Li. "Photoelectrocatalytic Water Splitting: Significance of Cocatalysts, Electrolyte, and Interfaces", ACS Catalysis, 2016	<1 %

Publication

94 Hongwei Zhang, Ruitao Lv. "Defect engineering of two-dimensional materials for efficient electrocatalysis", Journal of Materiomics, 2018 <1%
Publication

95 Huanhuan Sun, Wei Hua, Yueying Li, Jian-Gan Wang. "Conformal coating of superhydrophilic metal-organic complex toward substantially improved photoelectrochemical water oxidation", Chemical Engineering Journal, 2022 <1%
Publication

96 Huichao He, Aizhen Liao, Wenlong Guo, Wenjun Luo, Yong Zhou, Zhigang Zou. "State-of-the-art progress in the use of ternary metal oxides as photoelectrode materials for water splitting and organic synthesis", Nano Today, 2019 <1%
Publication

97 Huimin Xu, Weiqiang Fan, Yong Zhao, Biyi Chen, Yang Gao, Xue Chen, Dongbo Xu, Weidong Shi. "Amorphous iron (III)-borate decorated electrochemically treated-BiVO4 photoanode for efficient photoelectrochemical water splitting", Chemical Engineering Journal, 2021 <1%
Publication

98	Jeong Hun Kim, Hyo Eun Kim, Jin Hyun Kim, Jae Sung Lee. "Ferrites: emerging light absorbers for solar water splitting", Journal of Materials Chemistry A, 2020 Publication	<1 %
99	Submitted to Kyungpook National University Student Paper	<1 %
100	Peng Wen, Feijing Su, Hui Li, Yinghui Sun et al. "A Ni2P nanocrystal cocatalyst enhanced TiO2 photoanode towards highly efficient photoelectrochemical water splitting", Chemical Engineering Journal, 2020 Publication	<1 %
101	Xiang Yin, Qiong Liu, Yahui Yang, Yang Liu, Keke Wang, Yaomin Li, Dongwei Li, Xiaoqing Qiu, Wenzhang Li, Jie Li. "An efficient tandem photoelectrochemical cell composed of FeOOH/TiO2/BiVO4 and Cu2O for self-driven solar water splitting", International Journal of Hydrogen Energy, 2018 Publication	<1 %
102	Xiaobo Chen, Shaohua Shen, Liejin Guo, Samuel S. Mao. "Semiconductor-based Photocatalytic Hydrogen Generation", Chemical Reviews, 2010 Publication	<1 %

103	Xiaogang Yang, Dunwei Wang. "Photocatalysis: From Fundamental Principles to Materials and Applications", ACS Applied Energy Materials, 2018 Publication	<1 %
104	Yuqi Fan, Guoliang Zhang, Huiming Zhou, Yang Qiu, Weiliang Wang, Feng Dang. "Construction of Quantum Well surface from an Nb Surface doped Core-shell La-SrTiO3 Nanocubes for Photocatalytic Hydrogen Production", Research Square Platform LLC, 2023 Publication	<1 %
105	Zhifeng Liu, Qinggong Song, Miao Zhou, Zhengang Guo, Jianhai Kang, Huiyu Yan. "Synergistic enhancement of charge management and surface reaction kinetics by spatially separated cocatalysts and p-n heterojunctions in Pt/CuWO4/Co3O4 photoanode", Chemical Engineering Journal, 2019 Publication	<1 %
106	chemistry-europe.onlinelibrary.wiley.com Internet Source	<1 %
107	d.lib.msu.edu Internet Source	<1 %
108	geb.uni-giessen.de Internet Source	

		<1%
109	keep.lib.asu.edu Internet Source	<1%
110	open.library.ubc.ca Internet Source	<1%
111	ore.exeter.ac.uk Internet Source	<1%
112	repository.ntu.edu.sg Internet Source	<1%
113	research-information.bris.ac.uk Internet Source	<1%
114	www.scribd.com Internet Source	<1%
115	Gaoliang Yang, Sijie Li, Xusheng Wang, Bing Ding et al. "A universal strategy boosting photoelectrochemical water oxidation by utilizing MXene nanosheets as hole transfer mediators", Applied Catalysis B: Environmental, 2021 Publication	<1%
116	Haifeng Zhang, Chuanwei Cheng. " Three-Dimensional FTO/TiO /BiVO Composite Inverse Opals Photoanode with Excellent Photoelectrochemical Performance ", ACS Energy Letters, 2017	<1%

Publication

117	Hongxing Li, Meisong Yin, Mengjie Huang, Xiongxiong Xue, Xianglin Li, Rong Mo. "Wide-pH-Compatible MoSx Co-catalyst Layer on TiO2 Nanowire Arrays Photoanode for Simultaneous Acceleration of Charge Carrier Separation and Catalytic Reactions", Chemical Engineering Journal, 2022 Publication	<1 %
118	Katz, Michael J., Shannon C. Riha, Nak Cheon Jeong, Alex B.F. Martinson, Omar K. Farha, and Joseph T. Hupp. "Toward solar fuels: Water splitting with sunlight and â€œrustâ€?", Coordination Chemistry Reviews, 2012. Publication	<1 %
119	Mayur A. Gaikwad, Umesh P. Suryawanshi, Uma V. Ghorpade, Jun Sung Jang, Mahesh P. Suryawanshi, Jin Hyeok Kim. " Emerging Surface, Bulk, and Interface Engineering Strategies on BiVO for Photoelectrochemical Water Splitting ", Small, 2021 Publication	<1 %
120	Ruifeng Chong, Zhenzhen Wang, Ming Fan, Li Wang, Zhixian Chang, Ling Zhang. "Hematite decorated with nanodot-like Cobalt (oxy)hydroxides for boosted photoelectrochemical water oxidation", Journal of Colloid and Interface Science, 2022 Publication	<1 %

121 Songcan Wang, Gang Liu, Lianzhou Wang. "Crystal Facet Engineering of Photoelectrodes for Photoelectrochemical Water Splitting", Chemical Reviews, 2019 <1%
Publication

122 Ananta R. Fareza, Ferry Anggoro Ardy Nugroho, Fatwa F. Abdi, Vivi Fauzia. "Nanoscale metal oxides–2D materials heterostructures for photoelectrochemical water splitting—a review", Journal of Materials Chemistry A, 2022 <1%
Publication

123 Bo Zhang, Zeyan Wang, Baibiao Huang, Xiaoyang Zhang, Xiaoyan Qin, Huiliang Li, Ying Dai, Yingjie Li. "Anisotropic Photoelectrochemical (PEC) Performances of ZnO Single-Crystalline Photoanode: Effect of Internal Electrostatic Fields on the Separation of Photogenerated Charge Carriers during PEC Water Splitting", Chemistry of Materials, 2016 <1%
Publication

124 Haijiao Lu, Julie Tournet, Kamran Dastafkan, Yun Liu, Yun Hau Ng, Siva Krishna Karuturi, Chuan Zhao, Zongyou Yin. "Noble-Metal-Free Multicomponent Nanointegration for Sustainable Energy Conversion", Chemical Reviews, 2021 <1%

Publication

125	In Kwon Jeong, Mahadeo A. Mahadik, Sa Rang Kim, Habib M. Pathan et al. "Transparent Zirconium-doped Hematite Nanocoral Photoanode via In Situ Diluted Hydrothermal Approach for Efficient Solar Water Splitting", Chemical Engineering Journal, 2020 Publication	<1 %
126	Mengke Cai, Xin Li, Hongyang Zhao, Cheng Liu, Yimin You, Feng Lin, Xin Tong, Zhiming M. Wang. " Decoration of BiVO Photoanodes with Near-Infrared Quantum Dots for Boosted Photoelectrochemical Water Oxidation ", ACS Applied Materials & Interfaces, 2021 Publication	<1 %
127	Pengfei Yue, Houde She, Liang Zhang, Bin Niu, Rui Lian, Jingwei Huang, Lei Wang, Qizhao Wang. "Super-hydrophilic CoAl-LDH on BiVO4 for enhanced photoelectrochemical water oxidation activity", Applied Catalysis B: Environmental, 2021 Publication	<1 %
128	Songcan Wang, Lianzhou Wang. "Recent progress of tungsten- and molybdenum-based semiconductor materials for solar-hydrogen production", Tungsten, 2019 Publication	<1 %

129	Zhang, Xinsheng, Huicheng Li, Shijun Wang, Fu-Ren F. Fan, and Allen J. Bard. "Improvement of Hematite as Photocatalyst by Doping with Tantalum", The Journal of Physical Chemistry C Publication	<1 %
130	livrepository.liverpool.ac.uk Internet Source	<1 %

Exclude quotes	Off	Exclude matches	Off
Exclude bibliography	On		